Probing the Role of *SORL1* and Endolysosomal Network Dysfunction in Alzheimer's Disease

Allison E Knupp

A dissertation

submitted in partial fulfillment of the

requirements for the degree of

Doctor of Philosophy

University of Washington

2021

Reading Committee:

Jessica Young, Chair

Daniel Promislow

Suman Jayadev

Program Authorized to Offer Degree:

Molecular Medicine and Mechanisms of Disease

University of Washington

Abstract

Probing the Role of *SORL1* and Endolysosomal Network Dysfunction in Alzheimer's Disease

Allison E Knupp

Chair of the Supervisory Committee:
Dr. Jessica Young, Assistant Professor
Department of Lab Medicine and Pathology

Alzheimer's disease (AD) is a progressive neurodegenerative disorder, and the most common cause of dementia among adults. There is currently no treatment that halts disease progression. There is ample pathological and biological evidence for endolysosomal network (ELN) dysfunction in AD, and emerging genetic studies repeatedly implicate ELN genes such as *SORL1* as associated with increased AD risk. The *SORL1* gene encodes the protein SORLA, a sorting receptor involved in retromer-related endosomal traffic. Many *SORL1* genetic variants increase AD risk, and rare loss-of-function truncation mutations have been found to be causal of AD. To model the causal loss-of-function mutations, we used CRISPR/Cas9 technology to deplete *SORL1* in human induced pluripotent stem cells (hiPSCs) to test the hypothesis that loss of *SORL1* (*SORL1* KO) contributes to AD pathogenesis by leading to dysfunction in ELN

trafficking. We additionally used CRISPR/Cas9 to insert AD-risk variants in the VPS10 domain of *SORL1* (*SORL1*^{Var}) in hiPSCs to test the hypothesis that these VPS10 variants result in loss of SORLA function and lead to ELN dysfunction. We report that loss of *SORL1* as well as *SORL1* VPS10 variants in hiPSC-derived neurons leads to early endosome enlargement, a cellular phenotype that is indicative of 'traffic jams' and is now considered a hallmark cytopathology AD. We further report trafficking defects in the recycling and degradative pathways of the ELN in *SORL1* KO neurons. Finally, we determine that retromer stabilizing small molecules reduce early endosome enlargement in both *SORL1* KO and *SORL1*^{Var} neurons. Collectively, and together with other recent observations, these findings suggest that *SORL1* is a key and broad regulator of ELN trafficking in neurons, a conclusion that has both pathogenic and therapeutic implications. Moreover, demonstrating a partial rescue of cellular phenotypes in *SORL1* deficient neurons will contribute to the development of new and precision treatments for AD.

TABLE OF CONTENTS

LIST OF FIGURES

ACKNOWLEDGEMENTS

First and foremost, I would like to thank my advisor, Dr. Jessica Young. I was so excited to work in your lab that I tried to start a rotation before the lab was even finished being set up. I'm so glad I was able to eventually start working with you. It has been incredibly fun to see the lab grow from just a few people to the current size. Your mentorship and training have been invaluable, and I'm grateful for all of your time and efforts to help me reach this stage in my career.

I thank my doctoral supervisory committee members, Dr. Dirk Keene, Dr. Suman Jayadev, Dr. Daniel Promislow, and Dr. Elizabeth Nance. You have all been incredibly supportive, especially during the more challenging portions of my PhD. Dr. Promislow, you served as my senior mentor and helped me to navigate my program. Dr. Keene, you helped me to participate in the collection of leptomeningeal tissues and gave me perspective on neuropathology techniques. Dr. Jayadev, you helped me attend clinic hours and see the human side of neurodegenerative research. Dr. Nance, you have been incredibly supportive and helpful as I began to think about the next stages of my career. Thank you all. Special thanks to Dr. Promislow, Dr. Jayadev, and Dr. Young for serving as my reading committee.

I thank all past and present members of Jessica's lab. You have been colleagues, mentors, and friends to me over the past five years, and I am incredibly grateful for all of you. Special gratitude to Refugio Martinez, Chizuru Kinoshito, Shannon Rose, Dr. Bonnie Berry, and Dr. Jaki Braggin. Thank you to Dr. Swati Mishra, who collaborated with me on all things, and who taught me so much about how good science is done.

Thank you to all the members of the M3D program, especially Dr. William Mahoney and Megan Barker for your guidance. Thank you also to the members of my cohort, Dr. Chelsea Fortin, Dr. Emily Kohlbrenner, and Michael Kiflezghi. I wouldn't have survived our first year without you. Thank you to Dr. Nick Crispe and his lab members, who took me in when I knew nothing about biology. Thank you for taking a chance on me, and for helping me get from neophyte to graduate student.

I owe so many thanks to my family for the love and encouragement you have always shown me. To my parents, Ralph and Andrea, and my siblings, Peter and Sarah, I'm so thankful for your perpetual support for my somewhat varied ventures. To my partner, Bob Sweeny, thank you for being you.

DEDICATION

For K and S, who make studying more fun.

CONTRIBUTIONS

Chapter 1: Portions of this chapter have been modified from the following publications:
D'Souza, G.X., Rose, S.E., Knupp, A., Nicholson, D.A., Keene, C.D., and Young, J.E. (2021). The Application of in vitro-derived Human Neurons in Neurodegenerative Disease Modeling. J Neurosci Res *99*, 124-140.
Szabo, M., Mishra, S., Knupp, A., and Young, J.E. (2021). The Role of AD Risk Genes in Endolysosomal Pathways. Neurobiology of Disease – *in review*

Chapter 2: This chapter has been published as the following work:
Knupp, A.*, Mishra, S.*, Martinez, R., Braggin, J.E., Szabo, M., Kinoshita, C., Hailey, D.W., Small, S.A., Jayadev, S., and Young, J.E. (2020). Depletion of the AD Risk Gene SORL1 Selectively Impairs Neuronal Endosomal Traffic Independent of Amyloidogenic APP Processing. Cell Rep *31*, 107719.

Chapter 3: This chapter has been submitted for publication as the following work:
Mishra, S.*, Knupp, A.*, Szabo, M., Kinoshita, C., Hailey, D.W., Wang, Y., and Young, J.E. (2021). The Alzheimer's Gene SORL1 is a Key Regulator of Endosomal Recycling in Human Neurons. Cellular and Molecular Life Sciences. – *in review*

Chapter 4: This chapter will be submitted for publication in Cell Reports Medicine.

Chapter 1. INTRODUCTION

1.1 ALZHEIMER'S DISEASE

1.1.1 *Alzheimer's Disease Prevalence*

Alzheimer's disease (AD) is a progressive neurodegenerative disorder, and the most common cause of dementia(Barker et al., 2002). There are currently approximately 5.8 million Americans living with AD, and that number is expected to more than double by 2050. The US healthcare costs associated with AD, including long-term and hospice care, are expected to increase from $305 billion in 2020 to $1.1 trillion in 2050(2020). Prevalence rates of AD increase with age, particularly over age 60, with a 15-fold increase in the rates of AD between individuals aged 60 and 85(Mayeux and Stern, 2012). With an aging US population, it is critical to address the social, economic, and healthcare burden associated with AD(Davidson and Schnaider Beeri, 2000).

Clinically, AD is characterized by an impairment of short-term memory interfering with daily activities, progressing to impairment of other cognitive functions such as language, judgement, and executive function(Cappa, 2018; Graham et al., 2017; Masters et al., 2015; Querfurth and LaFerla, 2010). Although several classes of medications are approved to treat AD symptoms, there are currently no treatments that substantially reverse or affect the progression of the disease, no reliable early diagnostic approaches for AD, and no effective preventative approaches(Cummings et al., 2019). The lack of effective therapies is, at least in part, related to the fact that biology of AD is only incompletely understood.

1.1.2 *Alzheimer's Disease Pathophysiology*

The hallmark neuropathological features of AD include extracellular plaques comprised of amyloid-β (Aβ) peptides and intracellular neurofibrillary tangles (NFTs) containing hyperphosphorylated tau proteins. Aβ peptides are formed during the proteolytic processing of the Amyloid Precursor Protein (APP). APP cleavage can be either amyloidogenic or non-amyloidogenic(Wilquet and De Strooper, 2004). During non-amyloidogenic processing, APP is exported from the *trans*-Golgi network (TGN) to the cell surface where it is cleaved by α-secretase enzymes. α-secretase cleavage prevents amyloidogenic processing. During amyloidogenic cleavage, full-length APP is endocytosed from the cell surface into the endolysosomal network (ELN)(Kinoshita et al., 2003). Within the ELN, APP is cleaved by the β- and γ-secretase complexes to produce various Aβ peptides. The two forms of Aβ thought to be most relevant to AD study are 40- and 42-amino acid length peptides, known as $A\beta_{40}$ and $A\beta_{42}$, respectively, although longer peptides are present and may show increasing toxicity.

Aβ peptides tend to aggregate, first accumulating into insoluble fibrils and then into neuritic or non-neuritic plaques. Neuritic plaques have a clear association with AD progression and are required for the post-mortem diagnosis of AD(Montine et al., 2012). Consisting of dystrophic neurites, microglia, and a dense core of $A\beta_{42}$ peptides, neuritic plaques are found in conjunction with neuronal injury, synaptic dysfunction, and glial inflammation(Masliah et al., 1993; Masliah et al., 1990; Terry et al., 1991). In addition to neuritic plaques, non-neuritic accumulations of Aβ also occur, including diffuse plaques, cotton-wool plaques, and amyloid lakes. Different types of plaques tend to accumulate in different brain regions(Dickson, 1997), but non-neuritic plaques are not considered diagnostic of AD(Braak and Braak, 1991).

Formation of intracellular NFTs of hyperphosphorylated tau protein is another hallmark of AD pathology. Tau is a microtubule binding protein containing 45 phosphorylation sites(Hanger et al., 2009). Controlled phosphorylation of tau is critical for normal binding to microtubules(Liu et al., 2007). During AD, tau becomes hyperphosphorylated, which interferes with microtubule binding. Hyperphosphorylated tau dissociates from microtubules and accumulates into NFTs(Mondragón-Rodríguez et al., 2010; Mondragón-Rodríguez et al., 2008). NFTs develop in a well-defined pattern through the brain, with stages of pathological progression correlating well with clinical progression and neurodegeneration(Braak and Braak, 1991; Hyman et al., 2012). NFTs can be observed in the entorhinal cortex in the earliest stages of disease, spreading to the hippocampus and amygdala as disease progresses, and ultimately reaching the cortex during late-stage disease(Braak and Braak, 1991).

While the presence of neuritic plaques and NFTs are required for the diagnosis of AD, the neuropathology that correlates best with cognitive impairment is synapse loss(Blennow et al., 1996; Terry et al., 1991; Yu and Lu, 2012). The loss of synapses is present in the early stages of AD(Masliah et al., 2001; Selkoe, 2002), seen in regions of the cortex and particularly in the hippocampus(Clare et al., 2010; Scheff et al., 1993). The number of synapses does decrease in aging brains, but AD exacerbates this loss(Bertoni-Freddari et al., 1990). The direct cause of synapse loss is unclear, and interactions of AD hallmarks Aβ and tau with synapses requires more investigation. Studies have identified the simultaneous presence of Aβ and tau in synapses, indicating a role for the pathologic proteins(Fein et al., 2008; Takahashi et al., 2010). Oligomeric forms of Aβ and tau have been shown to be toxic to synapses, but it is still unclear how the aggregate forms might interact(Guerrero-Muñoz et al., 2015; Tu et al., 2014; Walsh et al., 2002; Wang et al., 2017).

Widespread inflammatory responses, including activated microglia and astrocytosis, are also characteristic of the AD brain(Akiyama et al., 2000; Combs et al., 2000). Acute inflammation is an effective response against infection and injury, but the sustained immune response seen in AD can result in chronic neuroinflammation(Ferreira et al., 2014). GWAS have consistently identified inflammatory genes as risk factors(Lambert et al., 2013; Naj et al., 2011), and genetic studies have found that mutations in the gene triggering receptor expressed on myeloid cells 2 (*TREM2*) substantially increase AD risk(Guerreiro and Hardy, 2014; Jonsson et al., 2013). *TREM2* encodes a cell membrane receptor involved in signaling pathways required for the activation of microglia and other immune cells. Disruption to TREM2 function has been shown to result in aberrant immune response(Jay et al., 2015; Jiang et al., 2014). Inflammatory responses in AD are not thought to be causative in isolation, but neuroinflammation can exacerbate Aβ and tau pathologies(Zotova et al., 2010).

Ultimately in AD, pathologic proteins and loss of synapses combine to result in neurodegeneration. Progression of cognitive impairment accompanies a widespread shrinking of the cortex, indicative of neuronal death(Giraldo et al., 2014). Neurodegeneration in AD has been observed in the frontal, temporal, and parietal lobes of the brain as well as the entorhinal cortex and the hippocampus(Gómez-Isla et al., 1996; Simić et al., 1997; Whitehouse et al., 1981). The pattern of neuronal death in AD is distinct from that of normal aging, confirming that although advanced aging is a risk factor, AD is not simply an acceleration of brain aging(Mattson, 2004). AD hallmark proteins may contribute to neurodegeneration, with abnormal tau shown to result in neuronal death(Gendron and Petrucelli, 2009) and Aβ shown to induce apoptosis in neurons *in vitro*(Eckert et al., 2003; Mattson, 2000).

1.1.3 *Alzheimer's Disease Genetics*

Early-onset AD (EOAD) manifestations, characterized by onset of clinical symptoms before age 65, constitute roughly 1-5% of all AD cases(Bekris et al., 2010). Many EOAD cases arise from highly penetrant, autosomal dominant mutations in the *APP*, presenilin 1 (*PSEN1*), and presenilin 2 (*PSEN2*) genes(Goate et al., 1991; Levy-Lahad et al., 1995; Rogaev et al., 1995; Sherrington et al., 1995). *PSEN1* and *PSEN2* encode major components of the γ-secretase enzymatic complex and play a critical role in the cleavage of APP. Mutations in *APP* and *PSEN1* are typically fully penetrant, while mutations in *PSEN2* are roughly 95% penetrant(Goldman et al., 2011; Sherrington et al., 1996). Approximately 300 pathogenic mutations in these three genes have been identified, but novel mutations continue to be described(Giau et al., 2019).

Late-onset AD (LOAD) is characterized by age of onset after age 65, and accounts for roughly 95% of AD cases(Reitz et al., 2011). While the neuropathological features of EOAD and LOAD are similar, LOAD is far more genetically complex, with heritability estimated at approximately 80%(Gatz et al., 2006). The apolipoprotein E (*APOE*) gene accounts for roughly 25% of heritable AD risk, making it the largest genetic risk factor for LOAD(Gatz et al., 2006). Several large genome-wide association studies (GWAS) have been completed to identify remaining heritability, altogether identifying about 25 independent loci reaching genome-wide significance(Harold et al., 2009; Hollingworth et al., 2011; Lambert et al., 2013; Naj et al., 2011; Seshadri et al., 2010). LOAD risk genes fall into 4 pathways – APP processing, cholesterol metabolism, immune response, and endolysosomal network function(Kunkle et al., 2019).

1.2 THE ENDOLYSOSOMAL NETWORK

1.2.1 *Normal Endolysosomal Network Function*

The ELN consists of intracellular membranous organelles which interconvert in a dynamic fashion. Proteins associated with these organelles in the ELN can distinguish the main components such as early endosomes (EEs), recycling endosomes (REs), late endosomes (LEs), autophagosomes and lysosomes. These proteins are widely used as markers for discreet structures within the ELN, although the network itself is fluid and dynamic. The ELN actively participates in internalization of various macromolecules and fluid into the cell through a process called endocytosis, transport of these materials through endosomes and lysosomes, and release of selected cellular contents into the extracellular environment through a process called exocytosis. Additionally, the ELN is involved in the specialized degradative process, autophagy, wherein damaged cellular contents are degraded.

Endocytosis regulates several processes initiated at the plasma membrane including receptor mediated cell signaling and nutrient uptake. Depending on the cargo, specialized vesicles are formed at the plasma membrane of either a large size (>500nm in diameter) to internalize larger cargo or smaller size (<500 nm in diameter) to internalize fluid, solutes and other cargo(Kunkle et al., 2019; Swanson, 2008). Clathrin mediated endocytosis (CME) is a common type of endocytosis that internalizes a wide range of smaller sized (<200nm in diameter) cargo. This process starts with cargo recognition, which leads to membrane bending and the formation of specialized 'pits' called clathrin coated pits. Clathrin forms a complex lattice like structure around vesicles formed by membrane invaginations(Marsh and McMahon, 1999; Merrifield et al., 2005; Pearse, 1976; Ungewickell and Hinrichsen, 2007). Formation of these vesicles and the linking of cargo to the clathrin coat and intracellular cytosolic regulatory

machinery requires the recruitment of various cytosolic proteins including adaptor and scaffold proteins. Adaptor proteins can be either heterotetrameric such as the Adaptor protein 2 complex(AP2)(Kadlecova et al., 2017; Kelly et al., 2014) or monomeric such as Phosphatidylinositol Binding Clathrin assembly Protein (PICALM)(Miller et al., 2015). Scission of these clathrin coated pits from the plasma membrane is caused by a large GTPase, dynamin(van der Bliek et al., 1993) along with dynamin partners including Bin, amphiphysin and Rvs (BAR) domain proteins(Daumke et al., 2014; Takei et al., 1999). These vesicles then fuse with pre-existing EEs for subsequent intracellular trafficking(Choudhury et al., 2005; Ungewickell et al., 2004). Several clathrin independent pathways also exist(Mayor et al., 2014; Sandvig et al., 2018; Shafaq-Zadah et al., 2020).

After endocytosis, the compartment in the ELN that first receives cargo that has entered the cell is the EE(Huotari and Helenius, 2011). The EE is the sorting hub for cellular cargo and is marked by GTP-binding protein Rab5 and/or its effector protein, early endosome antigen 1 (EEA1)(Behnia and Munro, 2005; Zerial and McBride, 2001). Several other cytosolic proteins associate transiently with EE to execute downstream trafficking to other compartments of the ELN(Christoforidis et al., 1999; Lakadamyali et al., 2006; Miaczynska et al., 2004). After rapid sorting at the EE, cargo is either directed to LEs and lysosomes(Luzio et al., 2007; Poteryaev et al., 2010) for degradation or recycled back to the plasma membrane(Maxfield and McGraw, 2004). Recycling can occur either directly from the EE to the plasma membrane or via another specialized endosomal compartment called RE, marked by the GTPase Rab11(Pasqualato et al., 2004; Sonnichsen et al., 2000). Conversion of EE to downstream endosomal compartments in the ELN occurs through a process called endosomal maturation that involves a series of fusion events, dynamic association and dissociation of several Rab proteins and their effectors, and

additional regulatory cytosolic proteins and gradual acidification of the lumen(Huotari and Helenius, 2011). LEs are subcellular membrane bound organelles that transport selected cargo from EE into lysosomes(Rink et al., 2005), newly synthesized lysosomal hydrolases from the TGN into lysosomes, and selected cargo from LE to TGN(Zhang et al., 2009). Transport from LE and EE to the TGN occurs via the large multiprotein complex retromer(Rojas et al., 2008). LEs are typically marked by the GTPase Rab7 and biogenesis of these vesicles depends on activity of receptors of certain signaling pathways, suggesting that this process is subject to alterations depending on cellular activity(1992). LEs eventually mature to form the most acidic intracellular compartments of the ELN, lysosomes, which are marked by membrane proteins like Lysosomal-associated membrane protein 1 (LAMP1) and have a lumen composition comprised of enzymes active only at acidic pH, acid hydrolases(Maxfield and Yamashiro, 1987). Cathepsins, a group of proteases, are the most abundant lysosomal acid hydrolases and Cathepsin D is one of the most abundant aspartic proteases mainly within lysosomes(Mason, 1996). Continuous endocytic trafficking into lysosomes is crucial to maintain lysosome morphology, pH and intracellular localization(Bucci et al., 2000).

1.2.2 *Endolysosomal Network Dysfunction in Alzheimer's Disease*

Through coordination of these multiple complex intracellular pathways, the ELN maintains cellular homeostasis and dysfunction of this network can result in disease phenotypes in distinct cell types. Early reports of ELN dysfunction in AD were closely associated with the trafficking and cleavage of the amyloid precursor protein, APP. Studies showed that that APP localizes within vesicle-like structures in cells(Ferreira et al., 1993) and these vesicles and endocytic pathways were identified as locations where APP cleavage could occur, increasing Aβ peptides and plaque formation(Roher et al., 1988).

Early clinical studies suggested a pathogenic role for the ELN in AD. Schwagerl et al., measured the levels of Cathepsin D (Cat-D), a major lysosomal protease, in the cerebrospinal fluid (CSF) of patients with AD. Cat-D was presumed to enter the CSF following neuronal death and measured levels were approximately 4-times higher than healthy control levels, and also higher than the corresponding levels in patients with other neurodegenerative diseases such as Huntington's disease(Schwagerl et al., 1995). This study and others suggested that dysfunction of the lysosome could lead to neuronal cell death associated with various neurodegenerative diseases including AD(Nixon and Cataldo, 1995). Further work showed hippocampal and prefrontal cortex cells from AD patients contained 2-8-fold more hydrolase-positive vacuolar compartments than healthy control brains, suggestive of distinct physiologic differences in ELN components in AD that were unrelated to normal aging(Cataldo et al., 1996). In addition to lysosomal defects, enlarged EEs are also markers of ELN dysfunction, indicative of delayed maturation or a block in the endocytic pathway(Kaur and Lakkaraju, 2018). Elegant work in the late 1990s and early 2000s demonstrated that enlarged EEs preceded canonical AD pathology in patient brains, indicating that ELN dysfunction occurs early in the course of disease(Cataldo et al., 1997; Cataldo et al., 2004; Cataldo et al., 2000).

Further studies have shown alterations in multiple genes that regulate endosomal pathways in both autosomal dominant EOAD and in LOAD. In EOAD, mutations in the *APP*, *PSEN1*, and *PSEN2* genes disrupt various components of the ELN. EOAD mutations in *APP* lead to enlarged EEs, can alter interactions between APP and BACE1 in endocytic compartments, affect intracellular sorting and ultimately increase amyloidogenic processing. *PSEN1/2* mutations disrupt lysosome function, alter autophagy, and also result in enlarged EEs(Bhalla et al., 2012; Das et al., 2016; Fedeli et al., 2019; Hung and Livesey, 2018; Kwart et

al., 2019). With respect to LOAD, GWAS have consistently implicated endo-lysosomal loci with increased genetic risk for disease development. Loss of expression of the LOAD risk gene Sortilin-related receptor 1 (*SORL1*) also leads to enlarged EEs and lysosomes(Hung et al., 2021; Knupp et al., 2020).

The early endosome serves as a hub in which internalized cargo can be retrogradely transported to the trans-Golgi, recycled back to the cell surface or degraded as endosomes mature into late endosomes and lysosomes(Mayle et al., 2012). As such, disruptions to EEs may result in alterations in multiple downstream ELN pathways. Trafficking of substrates out of the early endosome to late endosomes and, subsequently, lysosomes is important for protein degradation and has been shown to be disrupted in hiPSC-neurons lacking *SORL1* expression(Hung et al., 2021; Knupp et al., 2020). PSEN deficiency and mutations have been linked to impaired lysosomal acidification(Lee et al., 2010), calcium dysregulation(McBrayer and Nixon, 2013) and altered acidic vesicle distribution(Bezprozvanny, 2012). Lysosome function can also be affected by lysosome size, which has been shown to be altered in AD and in cellular models of AD(Hung et al., 2021; Hwang et al., 2019).

The recycling pathway is a process by which neurons ensure reuse of receptors, maintain membrane protein and lipid composition and regulate activation of several signaling pathways. This pathway is known to regulate crucial neuronal functions including synaptic plasticity and neurotrophic signaling (Dittman and Ryan, 2009; Itofusa and Kamiguchi, 2011; Kennedy and Ehlers, 2006; Winckler and Mellman, 2010). Specifically, Rab11, the GTPase that labels recycling endosomes has been shown to influence synaptic activity and neurite growth (Sann et al., 2009; Siri et al., 2020; Takano et al., 2012; Villarroel-Campos et al., 2016). Rab11 has been identified as a regulator of Aβ production(Udayar et al., 2013), and increased colocalization of

APP and Rab11 is associated with elevated Ab production(Kyriazis et al., 2008). Additionally, retromer-dependent recycling is critical for the insertion of glutamate receptors at synapses(Temkin et al., 2017), which is a key component of synaptic plasticity. The loss of cell surface glutamate receptors in AD brains results in synaptic dysfunction and ultimately synaptic loss(Selkoe, 2002). Thus, ELN trafficking and recycling has been referred to as a "hub" that can reconcile multiple cellular pathologies in AD(Small and Petsko, 2020).

1.3 SORL1

1.3.1 *SORL1 Functions*

The Sortilin-related receptor 1 (*SORL1)* gene encodes the protein SORLA, one of five mammalian sorting receptors that contain a vacuolar protein sorting domain (Jacobsen et al., 2001; Jacobsen et al., 1996; Willnow et al., 2008; Yamazaki et al., 1996). SORLA is a 250kDa transmembrane protein originally identified in a screen for novel lipoprotein receptors expressed in mammalian brains(Jacobsen et al., 1996; Yamazaki et al., 1996). Expression of SORLA is abundant in neurons in various brain regions, including the cortex, hippocampus, and cerebellum and the protein primarily localizes to intracellular vesicles in the neuronal soma(Motoi et al., 1999). Early biochemical characterization revealed a direct interaction between SORLA and APP and characterized SORLA as a sorting receptor that protected APP from amyloidogenic processing(Andersen et al., 2005). SORLA has been also been implicated in targeting Aβ to lysosomes for degradation(Caglayan et al., 2014).

SORLA has a variety of ligands beyond APP and Aβ, and can act as a receptor or co-receptor for cell signaling cascades. As it is expressed in a variety of cell types in addition to neurons, SORLA is involved in many cellular processes(Talbot et al., 2018). SORLA serves as an

adaptor protein for the retromer complex, playing a critical role in retrograde sorting and recycling of various cargoes(Andersen et al., 2016; Fjorback et al., 2012). As a regulator of lipoproteins and lipolytic activity, SORLA has been identified as a risk factor for atherosclerosis and obesity (Klinger et al., 2011; Nilsson et al., 2008; Schmidt et al., 2017). SORLA is also implicated in inflammatory processes, particularly in the regulation of IL-6 cytokine family signaling and turnover(Larsen and Petersen, 2017). Importantly for synaptic function, SORLA is involved neurotrophin signaling as a sorting receptor for tyrosine kinase-B (TRKB). TRKB belongs to the tyrosine kinase family of neurotrophin receptors(Huang and Reichardt, 2001) and regulates neuronal survival and synaptic health through its neurotrophin ligand, BDNF (Patapoutian and Reichardt, 2001).

1.3.2 *SORL1 and Alzheimer's Disease*

Prior to genetic associations with AD, early studies described a 2.5-fold decrease in SORLA expression in the cortex and hippocampus of LOAD brains(Dodson et al., 2006; Scherzer et al., 2004). Following this finding, a candidate gene study implicated two haplotypes in *SORL1* that were associated with increased AD in several population groups(Rogaeva et al., 2007), indicating that *SORL1* might be considered an AD risk gene. A large GWAS in 2013 associated SORL1 as a susceptibility locus in LOAD and this association has been consistently replicated(Lambert et al., 2013; Miyashita et al., 2013; Raghavan et al., 2018). *SORL1* has also been shown to be associated with EOAD, with exome sequencing studies identified rare coding variants in *SORL1* present in families with early-onset AD without known mutations in *APP* or *PSEN1/2*(Holstege et al., 2017; Pottier et al., 2012). *SORL1* is a large gene and this in-depth analysis has also found variants that occur in controls; however, the highly pathogenic frameshift

variants that lead to premature stop codons and therefore haploinsufficiency of *SORL1* appear to only occur in in AD cases(Holstege et al., 2017; Raghavan et al., 2018).

Along with genetic studies, functional analyses have continued to indicate the important role *SORL1* plays in AD pathogenesis. SORLA has been reported to traffic Aβ peptides to lysosomes for degradation(Caglayan et al., 2014), and manipulating SORLA expression in non-neuronal and neuronal cells directly impacts APP processing to Aβ peptides(Rogaeva et al., 2007; Young et al., 2015). In addition to a direct role in APP processing, SORLA traffics receptors for the neurotrophins BDNF and GDNF (Geng et al., 2011; Glerup et al., 2013; Rohe et al., 2013) and SORLA expression may impact synaptic function. Synapsins are a family of proteins that are involved with the regulation of neurotransmitter release at synapses, and thus are essential in the processes of endo- and exocytosis. Deletion of SORLA in mice resulted in an accumulation of phosphorylated synapsins in various regions of the brain, indicating that SORLA may have a direct effect on the degradation of synapsins, which, in turn, could impact on synaptic vesicle endocytosis(Hartl et al., 2016). Additionally, Huang and colleagues used SORLA transgenic mice to demonstrate an interaction with the ephrin receptor EphA4, which is important for synaptic structure and function(Huang et al., 2017). Aberrant EphA4 activation by Ab has been described in AD(Fu et al., 2007; Vargas et al., 2018) and SORLA association with EphA4 was show to suppress synaptotoxic activation of this receptor(Huang et al., 2017). Taken together, the above studies clearly suggest that the SORL1 gene and SORLA protein may have a direct role in ELN function and in AD pathogenesis and may have the potential to lead to future diagnostic or therapeutic approaches in AD.

1.4 HUMAN INDUCED PLURIPOTENT STEM CELL MODELS OF DISEASE

1.4.1 *Generating hiPSC Models*

The development of safe and effective treatments for age-associated neurodegenerative disorders is an on-going challenge. Key to the development of such therapies is the appropriate selection of laboratory models in which to investigate disease mechanisms and test candidate interventions. Models that incorporate the complexity of human genetics, include disease-relevant cellular phenotypes, and can be utilized in therapeutic screens represent powerful tools in understanding and treating neurodegenerative disorders such as AD.

The generation of hiPSCs first requires the introduction of exogenous transcription factors into fully differentiated cells, thus reverting the cells back to an embryonic-like state(Mahmoudi and Brunet, 2012). This technology was pioneered by Takahashi and Yamanaka who demonstrated that expression of four transcription factors (OCT4, SOX2, KLF4, and c-MYC, termed the "Yamanaka factors") could successfully reprogram mouse and human fibroblasts into pluripotent cells with a gene expression profile, morphology and growth profile similar to that of embryonic stem cells (ESCs)(Takahashi et al., 2007; Takahashi and Yamanaka, 2006). Ensuing protocols included the additional transcription factors NANOG and LIN28(Yu et al., 2007). Current protocols for generating hiPSCs largely use non-integrating methods to ensure that the reprogramming factors are not permanently established in the host genome. hiPSC technology has rapidly progressed with hiPSCs being derived from somatic cell sources as diverse as keratinocytes from hair(Linta et al., 2012), CD34+ cells from peripheral blood(Loh et al., 2009) and renal proximal epithelial cells from urine(Zhou et al., 2011). hiPSCs have also been established from postmortem tissue including dura mater(Bliss et al., 2012; Sproul et al., 2014) and leptomeninges(Rose et al., 2018). As the field has expanded, multiple protocols have

been developed to differentiate central nervous system cell types, including various neuron subtypes, astrocytes, oligodendrocytes, and microglia, from hiPSCs using small molecule-based methods and transcription factor-based methods(Abud et al., 2017; Ehrlich et al., 2017; Ladewig et al., 2012; Perriot et al., 2018), and this remains a very active area of ongoing research.

1.4.2 *hiPSC Models of Neurodegenerative Diseases*

hiPSCs are an attractive *in vitro* model for neurodegenerative diseases because of their human patient-specific origin, expandability, and ability to differentiate into diverse human cell types(Shi et al., 2017). This approach is invaluable for studies exploring the mechanistic aspects of human neurons, as it is challenging to isolate and expand human primary neurons from the brain. hiPSC-derived neurons (hiPSC-Ns) have been used to study multiple neurodegenerative diseases, including AD, Parkinson's disease (PD), and Amyotrophic Lateral Sclerosis (ALS)(Berry et al., 2018; Penney et al., 2020; Zhang et al., 2020). Such hiPSC models have helped elucidate the pathogenesis of sporadic forms of neurodegenerative diseases and contributed to drug discovery, with compounds identified using hiPSC-N models of AD(Bright et al., 2015) and ALS(Wainger et al., 2014) progressing to phase II clinical trials.

An ongoing challenge in neurodegenerative disease modeling is the ability to understand selective vulnerability, in which a specific neuronal subtype is more affected than others. Refinements in neuronal differentiation protocols have made significant advances in producing distinct neuronal subtypes such as CA3 hippocampal neurons(Sarkar et al., 2018), cortical interneurons(Nestor et al., 2015), medium spiny neurons (MSNs)(Stanslowsky et al., 2016), dopaminergic neurons(Mahajani et al., 2019; Theka et al., 2013), motor neurons(Hester et al., 2011; Shimojo et al., 2015), and Purkinje neurons(Watson et al., 2018). Furthermore, studies that transplant hiPSC-Ns into slice cultures show that the transplanted cells take on the specific

properties of the region where they were transplanted, such as CA1 or the dentate gyrus(Hiragi et al., 2017). Large-scale single cell transcriptome studies of the human brain, such as those done by Hodge and colleagues(Hodge et al., 2019), provide data about specific neuronal subtypes and will certainly influence hiPSC differentiation protocols to further refine *in vitro* cell types.

hiPSCs have great utility as a tool to generate neurons to model neurodegenerative diseases; however, as with any model there are important limitations to consider. The generation of hiPSCs can be expensive and labor-intensive(Nicholas et al., 2013; Schlachetzki et al., 2013). hiPSCs also have potential for tumorigenicity(Miura et al., 2009) and aberrant genetic and epigenetic modifications(Gore et al., 2011; Lister et al., 2011). While many cell types of the CNS can be differentiated from hiPSCs, including neurons, astrocytes, oligodendrocytes, and microglia, protocols vary widely in their ease and efficiency; many differentiation protocols can take weeks to months to generate the cell type of interest(Espuny-Camacho et al., 2013; Krencik et al., 2011; Nicholas et al., 2013; Wang et al., 2013).

The strongest risk factor for most neurodegenerative diseases is age(Niccoli and Partridge, 2012), and modeling age-related neurodegenerative disorders using hiPSCs presents a unique set of challenges. hiPSC-Ns are fetal in nature and gene expression profiles are characteristic of an early embryonic stage(Israel et al., 2012). Despite this, phenotypes classically associated with age-related neurodegenerative disease have been consistently reported in experiments using hiPSC-Ns. Recent work demonstrates that hiPSC-derived neural cells show *APOE* genotype-dependent phenotypes consistent with AD pathophysiological changes, including tau phosphorylation, endosome enlargement, and impaired Aβ clearance in hiPSC-derived neurons, astrocytes, and microglia(Lin et al., 2018; Wang et al., 2018). This work highlights the utility of using hiPSC-derived cells to understand cell type-specific mechanisms,

especially those that may have a genetic driver. Aging is a multifactorial process driven by genetics and environment and affects diverse cellular pathways(López-Otín et al., 2013; Rodríguez-Rodero et al., 2011). Similarly, the progressive dysfunction of neurons in age-associated neurodegenerative diseases is also multifactorial and takes decades to develop. Because reprogramming protocols appear to reverse many of the cellular and molecular hallmarks of aging, hiPSCs may not effectively model all aspects of neurodegenerative diseases(Lo Sardo et al., 2017; Mertens et al., 2015; Studer et al., 2015). If and how cells age *in vitro* is not well understood and has prompted an intriguing line of research to introduce the effects of aging into hiPSC-derived cellular models of neurodegenerative disease(Miller et al., 2013; Tagliafierro et al., 2019).

Finally, while simple monogenetic diseases can often be modeled using a single cell type with a defined phenotype, modeling multifactorial neurodegenerative diseases is more challenging. In more complex diseases, factors contribute to development of the phenotype and pathology that often cannot be modelled in a single cell type. To more closely replicate the environment in the brain, there may be value in coculturing patient-derived hiPSC-Ns with other cell types. With the development of protocols to generate patient-specific microglia(Abud et al., 2017) and patient-specific astrocytes(Caiazzo et al., 2015), these cells could be cocultured together with patient-specific hiPSC-Ns in a three-dimensional culture to capture the spatiotemporal context of the brain environment. This 3D culture system could either be an engineered system, in which cells are cultured on a supporting material such as a biodegradable scaffold(Kim et al., 2015; Soman et al., 2012; Zhang et al., 2014); or a structure-free system, whereby the different cell types form self-organizing, discrete structures for example, spheroids or organoids(Lancaster et al., 2013; Qian et al., 2016; Raja et al., 2016).

1.5 REFERENCES

(1992). Research in Medical Education. Proceedings of the 31st annual conference. New Orleans, Louisiana, November 1992. Acad Med *67*, S1-88.

(2020). 2020 Alzheimer's disease facts and figures. Alzheimer's & Dementia *16*, 391-460.

Abud, E.M., Ramirez, R.N., Martinez, E.S., Healy, L.M., Nguyen, C.H.H., Newman, S.A., Yeromin, A.V., Scarfone, V.M., Marsh, S.E., Fimbres, C.*, et al.* (2017). iPSC-Derived Human Microglia-like Cells to Study Neurological Diseases. Neuron *94*, 278-293.e279.

Akiyama, H., Arai, T., Kondo, H., Tanno, E., Haga, C., and Ikeda, K. (2000). Cell mediators of inflammation in the Alzheimer disease brain. Alzheimer Dis Assoc Disord *14 Suppl 1*, S47-53.

Andersen, O.M., Reiche, J., Schmidt, V., Gotthardt, M., Spoelgen, R., Behlke, J., von Arnim, C.A., Breiderhoff, T., Jansen, P., Wu, X.*, et al.* (2005). Neuronal sorting protein-related receptor sorLA/LR11 regulates processing of the amyloid precursor protein. Proc Natl Acad Sci U S A *102*, 13461-13466.

Andersen, O.M., Rudolph, I.M., and Willnow, T.E. (2016). Risk factor SORL1: from genetic association to functional validation in Alzheimer's disease. Acta Neuropathol *132*, 653-665.

Barker, W.W., Luis, C.A., Kashuba, A., Luis, M., Harwood, D.G., Loewenstein, D., Waters, C., Jimison, P., Shepherd, E., Sevush, S.*, et al.* (2002). Relative Frequencies of Alzheimer Disease, Lewy Body, Vascular and Frontotemporal Dementia, and Hippocampal Sclerosis in the State of Florida Brain Bank. Alzheimer Disease & Associated Disorders *16*, 203-212.

Behnia, R., and Munro, S. (2005). Organelle identity and the signposts for membrane traffic. Nature *438*, 597-604.

Bekris, L.M., Yu, C.E., Bird, T.D., and Tsuang, D.W. (2010). Genetics of Alzheimer disease. J Geriatr Psychiatry Neurol *23*, 213-227.

Berry, B.J., Smith, A.S.T., Young, J.E., and Mack, D.L. (2018). Advances and Current Challenges Associated with the Use of Human Induced Pluripotent Stem Cells in Modeling Neurodegenerative Disease. Cells Tissues Organs *205*, 331-349.

Bertoni-Freddari, C., Fattoretti, P., Casoli, T., Meier-Ruge, W., and Ulrich, J. (1990). Morphological adaptive response of the synaptic junctional zones in the human dentate gyrus during aging and Alzheimer's disease. Brain Res *517*, 69-75.

Bezprozvanny, I. (2012). Presenilins: a novel link between intracellular calcium signaling and lysosomal function? J Cell Biol *198*, 7-10.

Bhalla, A., Vetanovetz, C.P., Morel, E., Chamoun, Z., Di Paolo, G., and Small, S.A. (2012). The location and trafficking routes of the neuronal retromer and its role in amyloid precursor protein transport. Neurobiol Dis *47*, 126-134.

Blennow, K., Bogdanovic, N., Alafuzoff, I., Ekman, R., and Davidsson, P. (1996). Synaptic pathology in Alzheimer's disease: relation to severity of dementia, but not to senile plaques, neurofibrillary tangles, or the ApoE4 allele. J Neural Transm (Vienna) *103*, 603-618.

Bliss, L.A., Sams, M.R., Deep-Soboslay, A., Ren-Patterson, R., Jaffe, A.E., Chenoweth, J.G., Jaishankar, A., Kleinman, J.E., and Hyde, T.M. (2012). Use of postmortem human dura mater and scalp for deriving human fibroblast cultures. PLoS One *7*, e45282.

Braak, H., and Braak, E. (1991). Neuropathological stageing of Alzheimer-related changes. Acta Neuropathol *82*, 239-259.

Bright, J., Hussain, S., Dang, V., Wright, S., Cooper, B., Byun, T., Ramos, C., Singh, A., Parry, G., Stagliano, N.*, et al.* (2015). Human secreted tau increases amyloid-beta production. Neurobiol Aging *36*, 693-709.

Bucci, C., Thomsen, P., Nicoziani, P., McCarthy, J., and van Deurs, B. (2000). Rab7: a key to lysosome biogenesis. Mol Biol Cell *11*, 467-480.
Caglayan, S., Takagi-Niidome, S., Liao, F., Carlo, A.S., Schmidt, V., Burgert, T., Kitago, Y., Fuchtbauer, E.M., Fuchtbauer, A., Holtzman, D.M.*, et al.* (2014). Lysosomal sorting of amyloid-beta by the SORLA receptor is impaired by a familial Alzheimer's disease mutation. Sci Transl Med *6*, 223ra220.
Caiazzo, M., Giannelli, S., Valente, P., Lignani, G., Carissimo, A., Sessa, A., Colasante, G., Bartolomeo, R., Massimino, L., Ferroni, S.*, et al.* (2015). Direct conversion of fibroblasts into functional astrocytes by defined transcription factors. Stem Cell Reports *4*, 25-36.
Cappa, S.F. (2018). The Quest for an Alzheimer Therapy. Front Neurol *9*, 108.
Cataldo, A.M., Barnett, J.L., Pieroni, C., and Nixon, R.A. (1997). Increased neuronal endocytosis and protease delivery to early endosomes in sporadic Alzheimer's disease: neuropathologic evidence for a mechanism of increased beta-amyloidogenesis. J Neurosci *17*, 6142-6151.
Cataldo, A.M., Hamilton, D.J., Barnett, J.L., Paskevich, P.A., and Nixon, R.A. (1996). Properties of the endosomal-lysosomal system in the human central nervous system: disturbances mark most neurons in populations at risk to degenerate in Alzheimer's disease. J Neurosci *16*, 186-199.
Cataldo, A.M., Petanceska, S., Terio, N.B., Peterhoff, C.M., Durham, R., Mercken, M., Mehta, P.D., Buxbaum, J., Haroutunian, V., and Nixon, R.A. (2004). Abeta localization in abnormal endosomes: association with earliest Abeta elevations in AD and Down syndrome. Neurobiol Aging *25*, 1263-1272.
Cataldo, A.M., Peterhoff, C.M., Troncoso, J.C., Gomez-Isla, T., Hyman, B.T., and Nixon, R.A. (2000). Endocytic pathway abnormalities precede amyloid beta deposition in sporadic Alzheimer's disease and Down syndrome: differential effects of APOE genotype and presenilin mutations. Am J Pathol *157*, 277-286.
Choudhury, R., Diao, A., Zhang, F., Eisenberg, E., Saint-Pol, A., Williams, C., Konstantakopoulos, A., Lucocq, J., Johannes, L., Rabouille, C.*, et al.* (2005). Lowe syndrome protein OCRL1 interacts with clathrin and regulates protein trafficking between endosomes and the trans-Golgi network. Mol Biol Cell *16*, 3467-3479.
Christoforidis, S., Miaczynska, M., Ashman, K., Wilm, M., Zhao, L., Yip, S.C., Waterfield, M.D., Backer, J.M., and Zerial, M. (1999). Phosphatidylinositol-3-OH kinases are Rab5 effectors. Nat Cell Biol *1*, 249-252.
Clare, R., King, V.G., Wirenfeldt, M., and Vinters, H.V. (2010). Synapse loss in dementias. J Neurosci Res *88*, 2083-2090.
Combs, C.K., Johnson, D.E., Karlo, J.C., Cannady, S.B., and Landreth, G.E. (2000). Inflammatory mechanisms in Alzheimer's disease: inhibition of beta-amyloid-stimulated proinflammatory responses and neurotoxicity by PPARgamma agonists. J Neurosci *20*, 558-567.
Cummings, J.L., Tong, G., and Ballard, C. (2019). Treatment Combinations for Alzheimer's Disease: Current and Future Pharmacotherapy Options. J Alzheimers Dis *67*, 779-794.
Das, U., Wang, L., Ganguly, A., Saikia, J.M., Wagner, S.L., Koo, E.H., and Roy, S. (2016). Visualizing APP and BACE-1 approximation in neurons yields insight into the amyloidogenic pathway. Nat Neurosci *19*, 55-64.
Daumke, O., Roux, A., and Haucke, V. (2014). BAR domain scaffolds in dynamin-mediated membrane fission. Cell *156*, 882-892.
Davidson, M., and Schnaider Beeri, M. (2000). Cost of Alzheimer's disease. Dialogues Clin Neurosci *2*, 157-161.

Dickson, D.W. (1997). The pathogenesis of senile plaques. J Neuropathol Exp Neurol *56*, 321-339.
Dittman, J., and Ryan, T.A. (2009). Molecular circuitry of endocytosis at nerve terminals. Annu Rev Cell Dev Biol *25*, 133-160.
Dodson, S.E., Gearing, M., Lippa, C.F., Montine, T.J., Levey, A.I., and Lah, J.J. (2006). LR11/SorLA expression is reduced in sporadic Alzheimer disease but not in familial Alzheimer disease. J Neuropathol Exp Neurol *65*, 866-872.
Eckert, A., Marques, C.A., Keil, U., Schüssel, K., and Müller, W.E. (2003). Increased apoptotic cell death in sporadic and genetic Alzheimer's disease. Ann N Y Acad Sci *1010*, 604-609.
Ehrlich, M., Mozafari, S., Glatza, M., Starost, L., Velychko, S., Hallmann, A.L., Cui, Q.L., Schambach, A., Kim, K.P., Bachelin, C.*, et al.* (2017). Rapid and efficient generation of oligodendrocytes from human induced pluripotent stem cells using transcription factors. Proc Natl Acad Sci U S A *114*, E2243-e2252.
Espuny-Camacho, I., Michelsen, K.A., Gall, D., Linaro, D., Hasche, A., Bonnefont, J., Bali, C., Orduz, D., Bilheu, A., Herpoel, A.*, et al.* (2013). Pyramidal neurons derived from human pluripotent stem cells integrate efficiently into mouse brain circuits in vivo. Neuron *77*, 440-456.
Fedeli, C., Filadi, R., Rossi, A., Mammucari, C., and Pizzo, P. (2019). PSEN2 (presenilin 2) mutants linked to familial Alzheimer disease impair autophagy by altering Ca(2+) homeostasis. Autophagy *15*, 2044-2062.
Fein, J.A., Sokolow, S., Miller, C.A., Vinters, H.V., Yang, F., Cole, G.M., and Gylys, K.H. (2008). Co-localization of amyloid beta and tau pathology in Alzheimer's disease synaptosomes. Am J Pathol *172*, 1683-1692.
Ferreira, A., Caceres, A., and Kosik, K.S. (1993). Intraneuronal compartments of the amyloid precursor protein. J Neurosci *13*, 3112-3123.
Ferreira, S.T., Clarke, J.R., Bomfim, T.R., and De Felice, F.G. (2014). Inflammation, defective insulin signaling, and neuronal dysfunction in Alzheimer's disease. Alzheimers Dement *10*, S76-83.
Fjorback, A.W., Seaman, M., Gustafsen, C., Mehmedbasic, A., Gokool, S., Wu, C., Militz, D., Schmidt, V., Madsen, P., Nyengaard, J.R.*, et al.* (2012). Retromer binds the FANSHY sorting motif in SorLA to regulate amyloid precursor protein sorting and processing. J Neurosci *32*, 1467-1480.
Fu, W.Y., Chen, Y., Sahin, M., Zhao, X.S., Shi, L., Bikoff, J.B., Lai, K.O., Yung, W.H., Fu, A.K., Greenberg, M.E.*, et al.* (2007). Cdk5 regulates EphA4-mediated dendritic spine retraction through an ephexin1-dependent mechanism. Nat Neurosci *10*, 67-76.
Gatz, M., Reynolds, C.A., Fratiglioni, L., Johansson, B., Mortimer, J.A., Berg, S., Fiske, A., and Pedersen, N.L. (2006). Role of genes and environments for explaining Alzheimer disease. Arch Gen Psychiatry *63*, 168-174.
Gendron, T.F., and Petrucelli, L. (2009). The role of tau in neurodegeneration. Mol Neurodegener *4*, 13.
Geng, Z., Xu, F.Y., Huang, S.H., and Chen, Z.Y. (2011). Sorting protein-related receptor SorLA controls regulated secretion of glial cell line-derived neurotrophic factor. J Biol Chem *286*, 41871-41882.
Giau, V.V., Bagyinszky, E., Youn, Y.C., An, S.S.A., and Kim, S. (2019). APP, PSEN1, and PSEN2 Mutations in Asian Patients with Early-Onset Alzheimer Disease. Int J Mol Sci *20*.

Giraldo, E., Lloret, A., Fuchsberger, T., and Viña, J. (2014). Aβ and tau toxicities in Alzheimer's are linked via oxidative stress-induced p38 activation: protective role of vitamin E. Redox Biol *2*, 873-877.
Glerup, S., Lume, M., Olsen, D., Nyengaard, J.R., Vaegter, C.B., Gustafsen, C., Christensen, E.I., Kjolby, M., Hay-Schmidt, A., Bender, D.*, et al.* (2013). SorLA controls neurotrophic activity by sorting of GDNF and its receptors GFRalpha1 and RET. Cell Rep *3*, 186-199.
Goate, A., Chartier-Harlin, M.C., Mullan, M., Brown, J., Crawford, F., Fidani, L., Giuffra, L., Haynes, A., Irving, N., James, L.*, et al.* (1991). Segregation of a missense mutation in the amyloid precursor protein gene with familial Alzheimer's disease. Nature *349*, 704-706.
Goldman, J.S., Hahn, S.E., Catania, J.W., LaRusse-Eckert, S., Butson, M.B., Rumbaugh, M., Strecker, M.N., Roberts, J.S., Burke, W., Mayeux, R.*, et al.* (2011). Genetic counseling and testing for Alzheimer disease: joint practice guidelines of the American College of Medical Genetics and the National Society of Genetic Counselors. Genet Med *13*, 597-605.
Gómez-Isla, T., Price, J.L., McKeel, D.W., Jr., Morris, J.C., Growdon, J.H., and Hyman, B.T. (1996). Profound loss of layer II entorhinal cortex neurons occurs in very mild Alzheimer's disease. J Neurosci *16*, 4491-4500.
Gore, A., Li, Z., Fung, H.L., Young, J.E., Agarwal, S., Antosiewicz-Bourget, J., Canto, I., Giorgetti, A., Israel, M.A., Kiskinis, E.*, et al.* (2011). Somatic coding mutations in human induced pluripotent stem cells. Nature *471*, 63-67.
Graham, W.V., Bonito-Oliva, A., and Sakmar, T.P. (2017). Update on Alzheimer's Disease Therapy and Prevention Strategies. Annu Rev Med *68*, 413-430.
Guerreiro, R., and Hardy, J. (2014). Genetics of Alzheimer's disease. Neurotherapeutics *11*, 732-737.
Guerrero-Muñoz, M.J., Gerson, J., and Castillo-Carranza, D.L. (2015). Tau Oligomers: The Toxic Player at Synapses in Alzheimer's Disease. Front Cell Neurosci *9*, 464.
Hanger, D.P., Anderton, B.H., and Noble, W. (2009). Tau phosphorylation: the therapeutic challenge for neurodegenerative disease. Trends Mol Med *15*, 112-119.
Harold, D., Abraham, R., Hollingworth, P., Sims, R., Gerrish, A., Hamshere, M.L., Pahwa, J.S., Moskvina, V., Dowzell, K., Williams, A.*, et al.* (2009). Genome-wide association study identifies variants at CLU and PICALM associated with Alzheimer's disease. Nat Genet *41*, 1088-1093.
Hartl, D., Nebrich, G., Klein, O., Stephanowitz, H., Krause, E., and Rohe, M. (2016). SORLA regulates calpain-dependent degradation of synapsin. Alzheimers Dement *12*, 952-963.
Hester, M.E., Murtha, M.J., Song, S., Rao, M., Miranda, C.J., Meyer, K., Tian, J., Boulting, G., Schaffer, D.V., Zhu, M.X.*, et al.* (2011). Rapid and efficient generation of functional motor neurons from human pluripotent stem cells using gene delivered transcription factor codes. Mol Ther *19*, 1905-1912.
Hiragi, T., Andoh, M., Araki, T., Shirakawa, T., Ono, T., Koyama, R., and Ikegaya, Y. (2017). Differentiation of Human Induced Pluripotent Stem Cell (hiPSC)-Derived Neurons in Mouse Hippocampal Slice Cultures. Front Cell Neurosci *11*, 143.
Hodge, R.D., Bakken, T.E., Miller, J.A., Smith, K.A., Barkan, E.R., Graybuck, L.T., Close, J.L., Long, B., Johansen, N., Penn, O.*, et al.* (2019). Conserved cell types with divergent features in human versus mouse cortex. Nature *573*, 61-68.
Hollingworth, P., Harold, D., Sims, R., Gerrish, A., Lambert, J.C., Carrasquillo, M.M., Abraham, R., Hamshere, M.L., Pahwa, J.S., Moskvina, V.*, et al.* (2011). Common variants at ABCA7,

MS4A6A/MS4A4E, EPHA1, CD33 and CD2AP are associated with Alzheimer's disease. Nat Genet *43*, 429-435.
Holstege, H., van der Lee, S.J., Hulsman, M., Wong, T.H., van Rooij, J.G., Weiss, M., Louwersheimer, E., Wolters, F.J., Amin, N., Uitterlinden, A.G.*, et al.* (2017). Characterization of pathogenic SORL1 genetic variants for association with Alzheimer's disease: a clinical interpretation strategy. Eur J Hum Genet *25*, 973-981.
Huang, E.J., and Reichardt, L.F. (2001). Neurotrophins: roles in neuronal development and function. Annu Rev Neurosci *24*, 677-736.
Huang, T.Y., Zhao, Y., Jiang, L.L., Li, X., Liu, Y., Sun, Y., Pina-Crespo, J.C., Zhu, B., Masliah, E., Willnow, T.E.*, et al.* (2017). SORLA attenuates EphA4 signaling and amyloid beta-induced neurodegeneration. J Exp Med *214*, 3669-3685.
Hung, C., Tuck, E., Stubbs, V., van der Lee, S.J., Aalfs, C., van Spaendonk, R., Scheltens, P., Hardy, J., Holstege, H., and Livesey, F.J. (2021). SORL1 deficiency in human excitatory neurons causes APP-dependent defects in the endolysosome-autophagy network. Cell Rep *35*, 109259.
Hung, C.O.Y., and Livesey, F.J. (2018). Altered gamma-Secretase Processing of APP Disrupts Lysosome and Autophagosome Function in Monogenic Alzheimer's Disease. Cell Rep *25*, 3647-3660 e3642.
Huotari, J., and Helenius, A. (2011). Endosome maturation. EMBO J *30*, 3481-3500.
Hwang, J., Estick, C.M., Ikonne, U.S., Butler, D., Pait, M.C., Elliott, L.H., Ruiz, S., Smith, K., Rentschler, K.M., Mundell, C.*, et al.* (2019). The Role of Lysosomes in a Broad Disease-Modifying Approach Evaluated across Transgenic Mouse Models of Alzheimer's Disease and Parkinson's Disease and Models of Mild Cognitive Impairment. Int J Mol Sci *20*.
Hyman, B.T., Phelps, C.H., Beach, T.G., Bigio, E.H., Cairns, N.J., Carrillo, M.C., Dickson, D.W., Duyckaerts, C., Frosch, M.P., Masliah, E.*, et al.* (2012). National Institute on Aging-Alzheimer's Association guidelines for the neuropathologic assessment of Alzheimer's disease. Alzheimers Dement *8*, 1-13.
Israel, M.A., Yuan, S.H., Bardy, C., Reyna, S.M., Mu, Y., Herrera, C., Hefferan, M.P., Van Gorp, S., Nazor, K.L., Boscolo, F.S.*, et al.* (2012). Probing sporadic and familial Alzheimer's disease using induced pluripotent stem cells. Nature *482*, 216-220.
Itofusa, R., and Kamiguchi, H. (2011). Polarizing membrane dynamics and adhesion for growth cone navigation. Mol Cell Neurosci *48*, 332-338.
Jacobsen, L., Madsen, P., Jacobsen, C., Nielsen, M.S., Gliemann, J., and Petersen, C.M. (2001). Activation and functional characterization of the mosaic receptor SorLA/LR11. J Biol Chem *276*, 22788-22796.
Jacobsen, L., Madsen, P., Moestrup, S.K., Lund, A.H., Tommerup, N., Nykjaer, A., Sottrup-Jensen, L., Gliemann, J., and Petersen, C.M. (1996). Molecular characterization of a novel human hybrid-type receptor that binds the alpha2-macroglobulin receptor-associated protein. J Biol Chem *271*, 31379-31383.
Jay, T.R., Miller, C.M., Cheng, P.J., Graham, L.C., Bemiller, S., Broihier, M.L., Xu, G., Margevicius, D., Karlo, J.C., Sousa, G.L.*, et al.* (2015). TREM2 deficiency eliminates TREM2+ inflammatory macrophages and ameliorates pathology in Alzheimer's disease mouse models. J Exp Med *212*, 287-295.
Jiang, T., Yu, J.T., Zhu, X.C., Tan, M.S., Gu, L.Z., Zhang, Y.D., and Tan, L. (2014). Triggering receptor expressed on myeloid cells 2 knockdown exacerbates aging-related neuroinflammation

and cognitive deficiency in senescence-accelerated mouse prone 8 mice. Neurobiol Aging *35*, 1243-1251.
Jonsson, T., Stefansson, H., Steinberg, S., Jonsdottir, I., Jonsson, P.V., Snaedal, J., Bjornsson, S., Huttenlocher, J., Levey, A.I., Lah, J.J.*, et al.* (2013). Variant of TREM2 associated with the risk of Alzheimer's disease. N Engl J Med *368*, 107-116.
Kadlecova, Z., Spielman, S.J., Loerke, D., Mohanakrishnan, A., Reed, D.K., and Schmid, S.L. (2017). Regulation of clathrin-mediated endocytosis by hierarchical allosteric activation of AP2. J Cell Biol *216*, 167-179.
Kaur, G., and Lakkaraju, A. (2018). Early Endosome Morphology in Health and Disease. Adv Exp Med Biol *1074*, 335-343.
Kelly, B.T., Graham, S.C., Liska, N., Dannhauser, P.N., Honing, S., Ungewickell, E.J., and Owen, D.J. (2014). Clathrin adaptors. AP2 controls clathrin polymerization with a membrane-activated switch. Science *345*, 459-463.
Kennedy, M.J., and Ehlers, M.D. (2006). Organelles and trafficking machinery for postsynaptic plasticity. Annu Rev Neurosci *29*, 325-362.
Kim, Y.H., Choi, S.H., D'Avanzo, C., Hebisch, M., Sliwinski, C., Bylykbashi, E., Washicosky, K.J., Klee, J.B., Brüstle, O., Tanzi, R.E.*, et al.* (2015). A 3D human neural cell culture system for modeling Alzheimer's disease. Nat Protoc *10*, 985-1006.
Kinoshita, A., Fukumoto, H., Shah, T., Whelan, C.M., Irizarry, M.C., and Hyman, B.T. (2003). Demonstration by FRET of BACE interaction with the amyloid precursor protein at the cell surface and in early endosomes. J Cell Sci *116*, 3339-3346.
Klinger, S.C., Glerup, S., Raarup, M.K., Mari, M.C., Nyegaard, M., Koster, G., Prabakaran, T., Nilsson, S.K., Kjaergaard, M.M., Bakke, O.*, et al.* (2011). SorLA regulates the activity of lipoprotein lipase by intracellular trafficking. J Cell Sci *124*, 1095-1105.
Knupp, A., Mishra, S., Martinez, R., Braggin, J.E., Szabo, M., Kinoshita, C., Hailey, D.W., Small, S.A., Jayadev, S., and Young, J.E. (2020). Depletion of the AD Risk Gene SORL1 Selectively Impairs Neuronal Endosomal Traffic Independent of Amyloidogenic APP Processing. Cell Rep *31*, 107719.
Krencik, R., Weick, J.P., Liu, Y., Zhang, Z.J., and Zhang, S.C. (2011). Specification of transplantable astroglial subtypes from human pluripotent stem cells. Nat Biotechnol *29*, 528-534.
Kunkle, B.W., Grenier-Boley, B., Sims, R., Bis, J.C., Damotte, V., Naj, A.C., Boland, A., Vronskaya, M., van der Lee, S.J., Amlie-Wolf, A.*, et al.* (2019). Genetic meta-analysis of diagnosed Alzheimer's disease identifies new risk loci and implicates Aβ, tau, immunity and lipid processing. Nat Genet *51*, 414-430.
Kwart, D., Gregg, A., Scheckel, C., Murphy, E.A., Paquet, D., Duffield, M., Fak, J., Olsen, O., Darnell, R.B., and Tessier-Lavigne, M. (2019). A Large Panel of Isogenic APP and PSEN1 Mutant Human iPSC Neurons Reveals Shared Endosomal Abnormalities Mediated by APP beta-CTFs, Not Abeta. Neuron *104*, 1022.
Kyriazis, G.A., Wei, Z., Vandermey, M., Jo, D.G., Xin, O., Mattson, M.P., and Chan, S.L. (2008). Numb endocytic adapter proteins regulate the transport and processing of the amyloid precursor protein in an isoform-dependent manner: implications for Alzheimer disease pathogenesis. J Biol Chem *283*, 25492-25502.
Ladewig, J., Mertens, J., Kesavan, J., Doerr, J., Poppe, D., Glaue, F., Herms, S., Wernet, P., Kögler, G., Müller, F.J.*, et al.* (2012). Small molecules enable highly efficient neuronal conversion of human fibroblasts. Nat Methods *9*, 575-578.

Lakadamyali, M., Rust, M.J., and Zhuang, X. (2006). Ligands for clathrin-mediated endocytosis are differentially sorted into distinct populations of early endosomes. Cell *124*, 997-1009.
Lambert, J.C., Ibrahim-Verbaas, C.A., Harold, D., Naj, A.C., Sims, R., Bellenguez, C., DeStafano, A.L., Bis, J.C., Beecham, G.W., Grenier-Boley, B.*, et al.* (2013). Meta-analysis of 74,046 individuals identifies 11 new susceptibility loci for Alzheimer's disease. Nat Genet *45*, 1452-1458.
Lancaster, M.A., Renner, M., Martin, C.A., Wenzel, D., Bicknell, L.S., Hurles, M.E., Homfray, T., Penninger, J.M., Jackson, A.P., and Knoblich, J.A. (2013). Cerebral organoids model human brain development and microcephaly. Nature *501*, 373-379.
Larsen, J.V., and Petersen, C.M. (2017). SorLA and CLC:CLF-1-dependent Downregulation of CNTFRα as Demonstrated by Western Blotting, Inhibition of Lysosomal Enzymes, and Immunocytochemistry. J Vis Exp.
Lee, J.H., Yu, W.H., Kumar, A., Lee, S., Mohan, P.S., Peterhoff, C.M., Wolfe, D.M., Martinez-Vicente, M., Massey, A.C., Sovak, G.*, et al.* (2010). Lysosomal proteolysis and autophagy require presenilin 1 and are disrupted by Alzheimer-related PS1 mutations. Cell *141*, 1146-1158.
Levy-Lahad, E., Wijsman, E.M., Nemens, E., Anderson, L., Goddard, K.A., Weber, J.L., Bird, T.D., and Schellenberg, G.D. (1995). A familial Alzheimer's disease locus on chromosome 1. Science *269*, 970-973.
Lin, Y.T., Seo, J., Gao, F., Feldman, H.M., Wen, H.L., Penney, J., Cam, H.P., Gjoneska, E., Raja, W.K., Cheng, J.*, et al.* (2018). APOE4 Causes Widespread Molecular and Cellular Alterations Associated with Alzheimer's Disease Phenotypes in Human iPSC-Derived Brain Cell Types. Neuron.
Linta, L., Stockmann, M., Kleinhans, K.N., Böckers, A., Storch, A., Zaehres, H., Lin, Q., Barbi, G., Böckers, T.M., Kleger, A.*, et al.* (2012). Rat embryonic fibroblasts improve reprogramming of human keratinocytes into induced pluripotent stem cells. Stem Cells Dev *21*, 965-976.
Lister, R., Pelizzola, M., Kida, Y.S., Hawkins, R.D., Nery, J.R., Hon, G., Antosiewicz-Bourget, J., O'Malley, R., Castanon, R., Klugman, S.*, et al.* (2011). Hotspots of aberrant epigenomic reprogramming in human induced pluripotent stem cells. Nature *471*, 68-73.
Liu, Q., Xie, F., Rolston, R., Moreira, P.I., Nunomura, A., Zhu, X., Smith, M.A., and Perry, G. (2007). Prevention and treatment of Alzheimer disease and aging: antioxidants. Mini Rev Med Chem *7*, 171-180.
Lo Sardo, V., Ferguson, W., Erikson, G.A., Topol, E.J., Baldwin, K.K., and Torkamani, A. (2017). Influence of donor age on induced pluripotent stem cells. Nat Biotechnol *35*, 69-74.
Loh, Y.H., Agarwal, S., Park, I.H., Urbach, A., Huo, H., Heffner, G.C., Kim, K., Miller, J.D., Ng, K., and Daley, G.Q. (2009). Generation of induced pluripotent stem cells from human blood. Blood *113*, 5476-5479.
López-Otín, C., Blasco, M.A., Partridge, L., Serrano, M., and Kroemer, G. (2013). The hallmarks of aging. Cell *153*, 1194-1217.
Luzio, J.P., Pryor, P.R., and Bright, N.A. (2007). Lysosomes: fusion and function. Nat Rev Mol Cell Biol *8*, 622-632.
Mahajani, S., Raina, A., Fokken, C., Kügler, S., and Bähr, M. (2019). Homogenous generation of dopaminergic neurons from multiple hiPSC lines by transient expression of transcription factors. Cell Death Dis *10*, 898.
Mahmoudi, S., and Brunet, A. (2012). Aging and reprogramming: a two-way street. Curr Opin Cell Biol *24*, 744-756.
Marsh, M., and McMahon, H.T. (1999). The structural era of endocytosis. Science *285*, 215-220.

Masliah, E., Mallory, M., Alford, M., DeTeresa, R., Hansen, L.A., McKeel, D.W., Jr., and Morris, J.C. (2001). Altered expression of synaptic proteins occurs early during progression of Alzheimer's disease. Neurology *56*, 127-129.
Masliah, E., Miller, A., and Terry, R.D. (1993). The synaptic organization of the neocortex in Alzheimer's disease. Med Hypotheses *41*, 334-340.
Masliah, E., Terry, R.D., Mallory, M., Alford, M., and Hansen, L.A. (1990). Diffuse plaques do not accentuate synapse loss in Alzheimer's disease. Am J Pathol *137*, 1293-1297.
Mason, R.W. (1996). Lysosomal metabolism of proteins. Subcell Biochem *27*, 159-190.
Masters, C.L., Bateman, R., Blennow, K., Rowe, C.C., Sperling, R.A., and Cummings, J.L. (2015). Alzheimer's disease. Nat Rev Dis Primers *1*, 15056.
Mattson, M.P. (2000). Risk Factors and Mechanisms of Alzheimer's Disease Pathogenesis: Obviously and Obviously Not. J Alzheimers Dis *2*, 109-112.
Mattson, M.P. (2004). Pathways towards and away from Alzheimer's disease. Nature *430*, 631-639.
Maxfield, F.R., and McGraw, T.E. (2004). Endocytic recycling. Nat Rev Mol Cell Biol *5*, 121-132.
Maxfield, F.R., and Yamashiro, D.J. (1987). Endosome acidification and the pathways of receptor-mediated endocytosis. Adv Exp Med Biol *225*, 189-198.
Mayeux, R., and Stern, Y. (2012). Epidemiology of Alzheimer disease. Cold Spring Harb Perspect Med *2*.
Mayle, K.M., Le, A.M., and Kamei, D.T. (2012). The intracellular trafficking pathway of transferrin. Biochim Biophys Acta *1820*, 264-281.
Mayor, S., Parton, R.G., and Donaldson, J.G. (2014). Clathrin-independent pathways of endocytosis. Cold Spring Harb Perspect Biol *6*.
McBrayer, M., and Nixon, R.A. (2013). Lysosome and calcium dysregulation in Alzheimer's disease: partners in crime. Biochem Soc Trans *41*, 1495-1502.
Merrifield, C.J., Perrais, D., and Zenisek, D. (2005). Coupling between clathrin-coated-pit invagination, cortactin recruitment, and membrane scission observed in live cells. Cell *121*, 593-606.
Mertens, J., Paquola, A.C.M., Ku, M., Hatch, E., Böhnke, L., Ladjevardi, S., McGrath, S., Campbell, B., Lee, H., Herdy, J.R.*, et al.* (2015). Directly Reprogrammed Human Neurons Retain Aging-Associated Transcriptomic Signatures and Reveal Age-Related Nucleocytoplasmic Defects. Cell Stem Cell *17*, 705-718.
Miaczynska, M., Christoforidis, S., Giner, A., Shevchenko, A., Uttenweiler-Joseph, S., Habermann, B., Wilm, M., Parton, R.G., and Zerial, M. (2004). APPL proteins link Rab5 to nuclear signal transduction via an endosomal compartment. Cell *116*, 445-456.
Miller, J.D., Ganat, Y.M., Kishinevsky, S., Bowman, R.L., Liu, B., Tu, E.Y., Mandal, P.K., Vera, E., Shim, J.W., Kriks, S.*, et al.* (2013). Human iPSC-based modeling of late-onset disease via progerin-induced aging. Cell Stem Cell *13*, 691-705.
Miller, S.E., Mathiasen, S., Bright, N.A., Pierre, F., Kelly, B.T., Kladt, N., Schauss, A., Merrifield, C.J., Stamou, D., Honing, S.*, et al.* (2015). CALM regulates clathrin-coated vesicle size and maturation by directly sensing and driving membrane curvature. Dev Cell *33*, 163-175.
Miura, K., Okada, Y., Aoi, T., Okada, A., Takahashi, K., Okita, K., Nakagawa, M., Koyanagi, M., Tanabe, K., Ohnuki, M.*, et al.* (2009). Variation in the safety of induced pluripotent stem cell lines. Nat Biotechnol *27*, 743-745.

Miyashita, A., Koike, A., Jun, G., Wang, L.S., Takahashi, S., Matsubara, E., Kawarabayashi, T., Shoji, M., Tomita, N., Arai, H.*, et al.* (2013). SORL1 is genetically associated with late-onset Alzheimer's disease in Japanese, Koreans and Caucasians. PLoS One *8*, e58618.
Mondragón-Rodríguez, S., Basurto-Islas, G., Lee, H.G., Perry, G., Zhu, X., Castellani, R.J., and Smith, M.A. (2010). Causes versus effects: the increasing complexities of Alzheimer's disease pathogenesis. Expert Rev Neurother *10*, 683-691.
Mondragón-Rodríguez, S., Basurto-Islas, G., Santa-Maria, I., Mena, R., Binder, L.I., Avila, J., Smith, M.A., Perry, G., and García-Sierra, F. (2008). Cleavage and conformational changes of tau protein follow phosphorylation during Alzheimer's disease. Int J Exp Pathol *89*, 81-90.
Montine, T.J., Phelps, C.H., Beach, T.G., Bigio, E.H., Cairns, N.J., Dickson, D.W., Duyckaerts, C., Frosch, M.P., Masliah, E., Mirra, S.S.*, et al.* (2012). National Institute on Aging-Alzheimer's Association guidelines for the neuropathologic assessment of Alzheimer's disease: a practical approach. Acta Neuropathol *123*, 1-11.
Motoi, Y., Aizawa, T., Haga, S., Nakamura, S., Namba, Y., and Ikeda, K. (1999). Neuronal localization of a novel mosaic apolipoprotein E receptor, LR11, in rat and human brain. Brain Res *833*, 209-215.
Naj, A.C., Jun, G., Beecham, G.W., Wang, L.S., Vardarajan, B.N., Buros, J., Gallins, P.J., Buxbaum, J.D., Jarvik, G.P., Crane, P.K.*, et al.* (2011). Common variants at MS4A4/MS4A6E, CD2AP, CD33 and EPHA1 are associated with late-onset Alzheimer's disease. Nat Genet *43*, 436-441.
Nestor, M.W., Jacob, S., Sun, B., Prè, D., Sproul, A.A., Hong, S.I., Woodard, C., Zimmer, M., Chinchalongporn, V., Arancio, O.*, et al.* (2015). Characterization of a subpopulation of developing cortical interneurons from human iPSCs within serum-free embryoid bodies. Am J Physiol Cell Physiol *308*, C209-219.
Niccoli, T., and Partridge, L. (2012). Ageing as a risk factor for disease. Curr Biol *22*, R741-752.
Nicholas, C.R., Chen, J., Tang, Y., Southwell, D.G., Chalmers, N., Vogt, D., Arnold, C.M., Chen, Y.J., Stanley, E.G., Elefanty, A.G.*, et al.* (2013). Functional maturation of hPSC-derived forebrain interneurons requires an extended timeline and mimics human neural development. Cell Stem Cell *12*, 573-586.
Nilsson, K., Gustafson, L., and Hultberg, B. (2008). Plasma homocysteine and vascular disease in elderly patients with mental illness. Clin Chem Lab Med *46*, 1556-1561.
Nixon, R.A., and Cataldo, A.M. (1995). The endosomal-lysosomal system of neurons: new roles. Trends Neurosci *18*, 489-496.
Pasqualato, S., Senic-Matuglia, F., Renault, L., Goud, B., Salamero, J., and Cherfils, J. (2004). The structural GDP/GTP cycle of Rab11 reveals a novel interface involved in the dynamics of recycling endosomes. J Biol Chem *279*, 11480-11488.
Patapoutian, A., and Reichardt, L.F. (2001). Trk receptors: mediators of neurotrophin action. Curr Opin Neurobiol *11*, 272-280.
Pearse, B.M. (1976). Clathrin: a unique protein associated with intracellular transfer of membrane by coated vesicles. Proc Natl Acad Sci U S A *73*, 1255-1259.
Penney, J., Ralvenius, W.T., and Tsai, L.H. (2020). Modeling Alzheimer's disease with iPSC-derived brain cells. Mol Psychiatry *25*, 148-167.
Perriot, S., Mathias, A., Perriard, G., Canales, M., Jonkmans, N., Merienne, N., Meunier, C., El Kassar, L., Perrier, A.L., Laplaud, D.A.*, et al.* (2018). Human Induced Pluripotent Stem Cell-Derived Astrocytes Are Differentially Activated by Multiple Sclerosis-Associated Cytokines. Stem Cell Reports *11*, 1199-1210.

Poteryaev, D., Datta, S., Ackema, K., Zerial, M., and Spang, A. (2010). Identification of the switch in early-to-late endosome transition. Cell *141*, 497-508.
Pottier, C., Hannequin, D., Coutant, S., Rovelet-Lecrux, A., Wallon, D., Rousseau, S., Legallic, S., Paquet, C., Bombois, S., Pariente, J.*, et al.* (2012). High frequency of potentially pathogenic SORL1 mutations in autosomal dominant early-onset Alzheimer disease. Mol Psychiatry *17*, 875-879.
Qian, X., Nguyen, H.N., Song, M.M., Hadiono, C., Ogden, S.C., Hammack, C., Yao, B., Hamersky, G.R., Jacob, F., Zhong, C.*, et al.* (2016). Brain-Region-Specific Organoids Using Mini-bioreactors for Modeling ZIKV Exposure. Cell *165*, 1238-1254.
Querfurth, H.W., and LaFerla, F.M. (2010). Alzheimer's disease. N Engl J Med *362*, 329-344.
Raghavan, N.S., Brickman, A.M., Andrews, H., Manly, J.J., Schupf, N., Lantigua, R., Wolock, C.J., Kamalakaran, S., Petrovski, S., Tosto, G.*, et al.* (2018). Whole-exome sequencing in 20,197 persons for rare variants in Alzheimer's disease. Ann Clin Transl Neurol *5*, 832-842.
Raja, W.K., Mungenast, A.E., Lin, Y.T., Ko, T., Abdurrob, F., Seo, J., and Tsai, L.H. (2016). Self-Organizing 3D Human Neural Tissue Derived from Induced Pluripotent Stem Cells Recapitulate Alzheimer's Disease Phenotypes. PLoS One *11*, e0161969.
Reitz, C., Cheng, R., Rogaeva, E., Lee, J.H., Tokuhiro, S., Zou, F., Bettens, K., Sleegers, K., Tan, E.K., Kimura, R.*, et al.* (2011). Meta-analysis of the association between variants in SORL1 and Alzheimer disease. Arch Neurol *68*, 99-106.
Rink, J., Ghigo, E., Kalaidzidis, Y., and Zerial, M. (2005). Rab conversion as a mechanism of progression from early to late endosomes. Cell *122*, 735-749.
Rodríguez-Rodero, S., Fernández-Morera, J.L., Menéndez-Torre, E., Calvanese, V., Fernández, A.F., and Fraga, M.F. (2011). Aging genetics and aging. Aging Dis *2*, 186-195.
Rogaev, E.I., Sherrington, R., Rogaeva, E.A., Levesque, G., Ikeda, M., Liang, Y., Chi, H., Lin, C., Holman, K., Tsuda, T.*, et al.* (1995). Familial Alzheimer's disease in kindreds with missense mutations in a gene on chromosome 1 related to the Alzheimer's disease type 3 gene. Nature *376*, 775-778.
Rogaeva, E., Meng, Y., Lee, J.H., Gu, Y., Kawarai, T., Zou, F., Katayama, T., Baldwin, C.T., Cheng, R., Hasegawa, H.*, et al.* (2007). The neuronal sortilin-related receptor SORL1 is genetically associated with Alzheimer disease. Nat Genet *39*, 168-177.
Rohe, M., Hartl, D., Fjorback, A.N., Klose, J., and Willnow, T.E. (2013). SORLA-mediated trafficking of TrkB enhances the response of neurons to BDNF. PLoS One *8*, e72164.
Roher, A., Gray, E.G., and Paula-Barbosa, M. (1988). Alzheimer's disease: coated vesicles, coated pits and the amyloid-related cell. Proc R Soc Lond B Biol Sci *232*, 367-373.
Rojas, R., van Vlijmen, T., Mardones, G.A., Prabhu, Y., Rojas, A.L., Mohammed, S., Heck, A.J., Raposo, G., van der Sluijs, P., and Bonifacino, J.S. (2008). Regulation of retromer recruitment to endosomes by sequential action of Rab5 and Rab7. J Cell Biol *183*, 513-526.
Rose, S.E., Frankowski, H., Knupp, A., Berry, B.J., Martinez, R., Dinh, S.Q., Bruner, L.T., Willis, S.L., Crane, P.K., Larson, E.B.*, et al.* (2018). Leptomeninges-Derived Induced Pluripotent Stem Cells and Directly Converted Neurons From Autopsy Cases With Varying Neuropathologic Backgrounds. Journal of Neuropathology & Experimental Neurology, nly013-nly013.
Sandvig, K., Kavaliauskiene, S., and Skotland, T. (2018). Clathrin-independent endocytosis: an increasing degree of complexity. Histochem Cell Biol *150*, 107-118.
Sann, S., Wang, Z., Brown, H., and Jin, Y. (2009). Roles of endosomal trafficking in neurite outgrowth and guidance. Trends Cell Biol *19*, 317-324.

Sarkar, A., Mei, A., Paquola, A.C.M., Stern, S., Bardy, C., Klug, J.R., Kim, S., Neshat, N., Kim, H.J., Ku, M.*, et al.* (2018). Efficient Generation of CA3 Neurons from Human Pluripotent Stem Cells Enables Modeling of Hippocampal Connectivity In Vitro. Cell Stem Cell *22*, 684-697.e689.
Scheff, S.W., Sparks, L., and Price, D.A. (1993). Quantitative assessment of synaptic density in the entorhinal cortex in Alzheimer's disease. Ann Neurol *34*, 356-361.
Scherzer, C.R., Offe, K., Gearing, M., Rees, H.D., Fang, G., Heilman, C.J., Schaller, C., Bujo, H., Levey, A.I., and Lah, J.J. (2004). Loss of apolipoprotein E receptor LR11 in Alzheimer disease. Arch Neurol *61*, 1200-1205.
Schlachetzki, J.C., Saliba, S.W., and Oliveira, A.C. (2013). Studying neurodegenerative diseases in culture models. Braz J Psychiatry *35 Suppl 2*, S92-100.
Schmidt, V., Subkhangulova, A., and Willnow, T.E. (2017). Sorting receptor SORLA: cellular mechanisms and implications for disease. Cell Mol Life Sci *74*, 1475-1483.
Schwagerl, A.L., Mohan, P.S., Cataldo, A.M., Vonsattel, J.P., Kowall, N.W., and Nixon, R.A. (1995). Elevated levels of the endosomal-lysosomal proteinase cathepsin D in cerebrospinal fluid in Alzheimer disease. J Neurochem *64*, 443-446.
Selkoe, D.J. (2002). Alzheimer's disease is a synaptic failure. Science *298*, 789-791.
Seshadri, S., Fitzpatrick, A.L., Ikram, M.A., DeStefano, A.L., Gudnason, V., Boada, M., Bis, J.C., Smith, A.V., Carassquillo, M.M., Lambert, J.C.*, et al.* (2010). Genome-wide analysis of genetic loci associated with Alzheimer disease. Jama *303*, 1832-1840.
Shafaq-Zadah, M., Dransart, E., and Johannes, L. (2020). Clathrin-independent endocytosis, retrograde trafficking, and cell polarity. Curr Opin Cell Biol *65*, 112-121.
Sherrington, R., Froelich, S., Sorbi, S., Campion, D., Chi, H., Rogaeva, E.A., Levesque, G., Rogaev, E.I., Lin, C., Liang, Y.*, et al.* (1996). Alzheimer's disease associated with mutations in presenilin 2 is rare and variably penetrant. Hum Mol Genet *5*, 985-988.
Sherrington, R., Rogaev, E.I., Liang, Y., Rogaeva, E.A., Levesque, G., Ikeda, M., Chi, H., Lin, C., Li, G., Holman, K.*, et al.* (1995). Cloning of a gene bearing missense mutations in early-onset familial Alzheimer's disease. Nature *375*, 754-760.
Shi, Y., Inoue, H., Wu, J.C., and Yamanaka, S. (2017). Induced pluripotent stem cell technology: a decade of progress. Nat Rev Drug Discov *16*, 115-130.
Shimojo, D., Onodera, K., Doi-Torii, Y., Ishihara, Y., Hattori, C., Miwa, Y., Tanaka, S., Okada, R., Ohyama, M., Shoji, M.*, et al.* (2015). Rapid, efficient, and simple motor neuron differentiation from human pluripotent stem cells. Mol Brain *8*, 79.
Simić, G., Kostović, I., Winblad, B., and Bogdanović, N. (1997). Volume and number of neurons of the human hippocampal formation in normal aging and Alzheimer's disease. J Comp Neurol *379*, 482-494.
Siri, S.O., Rozés-Salvador, V., de la Villarmois, E.A., Ghersi, M.S., Quassollo, G., Pérez, M.F., and Conde, C. (2020). Decrease of Rab11 prevents the correct dendritic arborization, synaptic plasticity and spatial memory formation. Biochim Biophys Acta Mol Cell Res *1867*, 118735.
Small, S.A., and Petsko, G.A. (2020). Endosomal recycling reconciles the Alzheimer's disease paradox. Sci Transl Med *12*.
Soman, P., Tobe, B.T.D., Lee, J.W., Winquist, A.M., Singec, I., Vecchio, K.S., Snyder, E.Y., and Chen, S. (2012). Three-dimensional scaffolding to investigate neuronal derivatives of human embryonic stem cells. Biomed Microdevices *14*, 829-838.

Sonnichsen, B., De Renzis, S., Nielsen, E., Rietdorf, J., and Zerial, M. (2000). Distinct membrane domains on endosomes in the recycling pathway visualized by multicolor imaging of Rab4, Rab5, and Rab11. J Cell Biol *149*, 901-914.
Sproul, A.A., Vensand, L.B., Dusenberry, C.R., Jacob, S., Vonsattel, J.P., Paull, D.J., Shelanski, M.L., Crary, J.F., and Noggle, S.A. (2014). Generation of iPSC lines from archived non-cryoprotected biobanked dura mater. Acta Neuropathol Commun *2*, 4.
Stanslowsky, N., Reinhardt, P., Glass, H., Kalmbach, N., Naujock, M., Hensel, N., Lübben, V., Pal, A., Venneri, A., Lupo, F.*, et al.* (2016). Neuronal Dysfunction in iPSC-Derived Medium Spiny Neurons from Chorea-Acanthocytosis Patients Is Reversed by Src Kinase Inhibition and F-Actin Stabilization. J Neurosci *36*, 12027-12043.
Studer, L., Vera, E., and Cornacchia, D. (2015). Programming and Reprogramming Cellular Age in the Era of Induced Pluripotency. Cell Stem Cell *16*, 591-600.
Swanson, J.A. (2008). Shaping cups into phagosomes and macropinosomes. Nat Rev Mol Cell Biol *9*, 639-649.
Tagliafierro, L., Zamora, M.E., and Chiba-Falek, O. (2019). Multiplication of the SNCA locus exacerbates neuronal nuclear aging. Hum Mol Genet *28*, 407-421.
Takahashi, K., Tanabe, K., Ohnuki, M., Narita, M., Ichisaka, T., Tomoda, K., and Yamanaka, S. (2007). Induction of pluripotent stem cells from adult human fibroblasts by defined factors. Cell *131*, 861-872.
Takahashi, K., and Yamanaka, S. (2006). Induction of pluripotent stem cells from mouse embryonic and adult fibroblast cultures by defined factors. Cell *126*, 663-676.
Takahashi, M., Bujo, H., Jiang, M., Noike, H., Saito, Y., and Shirai, K. (2010). Enhanced circulating soluble LR11 in patients with coronary organic stenosis. Atherosclerosis *210*, 581-584.
Takano, T., Tomomura, M., Yoshioka, N., Tsutsumi, K., Terasawa, Y., Saito, T., Kawano, H., Kamiguchi, H., Fukuda, M., and Hisanaga, S. (2012). LMTK1/AATYK1 is a novel regulator of axonal outgrowth that acts via Rab11 in a Cdk5-dependent manner. J Neurosci *32*, 6587-6599.
Takei, K., Slepnev, V.I., Haucke, V., and De Camilli, P. (1999). Functional partnership between amphiphysin and dynamin in clathrin-mediated endocytosis. Nat Cell Biol *1*, 33-39.
Talbot, H., Saada, S., Naves, T., Gallet, P.F., Fauchais, A.L., and Jauberteau, M.O. (2018). Regulatory Roles of Sortilin and SorLA in Immune-Related Processes. Front Pharmacol *9*, 1507.
Temkin, P., Morishita, W., Goswami, D., Arendt, K., Chen, L., and Malenka, R. (2017). The Retromer Supports AMPA Receptor Trafficking During LTP. Neuron *94*, 74-82.e75.
Terry, R.D., Masliah, E., Salmon, D.P., Butters, N., DeTeresa, R., Hill, R., Hansen, L.A., and Katzman, R. (1991). Physical basis of cognitive alterations in Alzheimer's disease: synapse loss is the major correlate of cognitive impairment. Ann Neurol *30*, 572-580.
Theka, I., Caiazzo, M., Dvoretskova, E., Leo, D., Ungaro, F., Curreli, S., Managò, F., Dell'Anno, M.T., Pezzoli, G., Gainetdinov, R.R.*, et al.* (2013). Rapid generation of functional dopaminergic neurons from human induced pluripotent stem cells through a single-step procedure using cell lineage transcription factors. Stem Cells Transl Med *2*, 473-479.
Tu, S., Okamoto, S., Lipton, S.A., and Xu, H. (2014). Oligomeric Aβ-induced synaptic dysfunction in Alzheimer's disease. Mol Neurodegener *9*, 48.
Udayar, V., Buggia-Prévot, V., Guerreiro, R.L., Siegel, G., Rambabu, N., Soohoo, A.L., Ponnusamy, M., Siegenthaler, B., Bali, J., Simons, M.*, et al.* (2013). A paired RNAi and RabGAP overexpression screen identifies Rab11 as a regulator of β-amyloid production. Cell Rep *5*, 1536-1551.

Ungewickell, A., Ward, M.E., Ungewickell, E., and Majerus, P.W. (2004). The inositol polyphosphate 5-phosphatase Ocrl associates with endosomes that are partially coated with clathrin. Proc Natl Acad Sci U S A *101*, 13501-13506.
Ungewickell, E.J., and Hinrichsen, L. (2007). Endocytosis: clathrin-mediated membrane budding. Curr Opin Cell Biol *19*, 417-425.
van der Bliek, A.M., Redelmeier, T.E., Damke, H., Tisdale, E.J., Meyerowitz, E.M., and Schmid, S.L. (1993). Mutations in human dynamin block an intermediate stage in coated vesicle formation. J Cell Biol *122*, 553-563.
Vargas, L.M., Cerpa, W., Munoz, F.J., Zanlungo, S., and Alvarez, A.R. (2018). Amyloid-beta oligomers synaptotoxicity: The emerging role of EphA4/c-Abl signaling in Alzheimer's disease. Biochim Biophys Acta Mol Basis Dis *1864*, 1148-1159.
Villarroel-Campos, D., Bronfman, F.C., and Gonzalez-Billault, C. (2016). Rab GTPase signaling in neurite outgrowth and axon specification. Cytoskeleton (Hoboken) *73*, 498-507.
Wainger, B.J., Kiskinis, E., Mellin, C., Wiskow, O., Han, S.S., Sandoe, J., Perez, N.P., Williams, L.A., Lee, S., Boulting, G.*, et al.* (2014). Intrinsic membrane hyperexcitability of amyotrophic lateral sclerosis patient-derived motor neurons. Cell Rep *7*, 1-11.
Walsh, D.M., Klyubin, I., Fadeeva, J.V., Cullen, W.K., Anwyl, R., Wolfe, M.S., Rowan, M.J., and Selkoe, D.J. (2002). Naturally secreted oligomers of amyloid beta protein potently inhibit hippocampal long-term potentiation in vivo. Nature *416*, 535-539.
Wang, C., Najm, R., Xu, Q., Jeong, D.E., Walker, D., Balestra, M.E., Yoon, S.Y., Yuan, H., Li, G., Miller, Z.A.*, et al.* (2018). Gain of toxic apolipoprotein E4 effects in human iPSC-derived neurons is ameliorated by a small-molecule structure corrector. Nat Med *24*, 647-657.
Wang, Y., Liu, J., Tan, X., Li, G., Gao, Y., Liu, X., Zhang, L., and Li, Y. (2013). Induced pluripotent stem cells from human hair follicle mesenchymal stem cells. Stem Cell Rev Rep *9*, 451-460.
Wang, Z., Jackson, R.J., Hong, W., Taylor, W.M., Corbett, G.T., Moreno, A., Liu, W., Li, S., Frosch, M.P., Slutsky, I.*, et al.* (2017). Human Brain-Derived Aβ Oligomers Bind to Synapses and Disrupt Synaptic Activity in a Manner That Requires APP. J Neurosci *37*, 11947-11966.
Watson, L.M., Wong, M.M.K., Vowles, J., Cowley, S.A., and Becker, E.B.E. (2018). A Simplified Method for Generating Purkinje Cells from Human-Induced Pluripotent Stem Cells. Cerebellum *17*, 419-427.
Whitehouse, P.J., Price, D.L., Clark, A.W., Coyle, J.T., and DeLong, M.R. (1981). Alzheimer disease: evidence for selective loss of cholinergic neurons in the nucleus basalis. Ann Neurol *10*, 122-126.
Willnow, T.E., Petersen, C.M., and Nykjaer, A. (2008). VPS10P-domain receptors - regulators of neuronal viability and function. Nat Rev Neurosci *9*, 899-909.
Wilquet, V., and De Strooper, B. (2004). Amyloid-beta precursor protein processing in neurodegeneration. Curr Opin Neurobiol *14*, 582-588.
Winckler, B., and Mellman, I. (2010). Trafficking guidance receptors. Cold Spring Harb Perspect Biol *2*, a001826.
Yamazaki, H., Bujo, H., Kusunoki, J., Seimiya, K., Kanaki, T., Morisaki, N., Schneider, W.J., and Saito, Y. (1996). Elements of neural adhesion molecules and a yeast vacuolar protein sorting receptor are present in a novel mammalian low density lipoprotein receptor family member. J Biol Chem *271*, 24761-24768.
Young, J.E., Boulanger-Weill, J., Williams, D.A., Woodruff, G., Buen, F., Revilla, A.C., Herrera, C., Israel, M.A., Yuan, S.H., Edland, S.D.*, et al.* (2015). Elucidating molecular

phenotypes caused by the SORL1 Alzheimer's disease genetic risk factor using human induced pluripotent stem cells. Cell Stem Cell *16*, 373-385.
Yu, J., Vodyanik, M.A., Smuga-Otto, K., Antosiewicz-Bourget, J., Frane, J.L., Tian, S., Nie, J., Jonsdottir, G.A., Ruotti, V., Stewart, R.*, et al.* (2007). Induced pluripotent stem cell lines derived from human somatic cells. Science *318*, 1917-1920.
Yu, W., and Lu, B. (2012). Synapses and dendritic spines as pathogenic targets in Alzheimer's disease. Neural Plast *2012*, 247150.
Zerial, M., and McBride, H. (2001). Rab proteins as membrane organizers. Nat Rev Mol Cell Biol *2*, 107-117.
Zhang, D., Pekkanen-Mattila, M., Shahsavani, M., Falk, A., Teixeira, A.I., and Herland, A. (2014). A 3D Alzheimer's disease culture model and the induction of P21-activated kinase mediated sensing in iPSC derived neurons. Biomaterials *35*, 1420-1428.
Zhang, M., Chen, L., Wang, S., and Wang, T. (2009). Rab7: roles in membrane trafficking and disease. Biosci Rep *29*, 193-209.
Zhang, X., Hu, D., Shang, Y., and Qi, X. (2020). Using induced pluripotent stem cell neuronal models to study neurodegenerative diseases. Biochim Biophys Acta Mol Basis Dis *1866*, 165431.
Zhou, T., Benda, C., Duzinger, S., Huang, Y., Li, X., Li, Y., Guo, X., Cao, G., Chen, S., Hao, L.*, et al.* (2011). Generation of induced pluripotent stem cells from urine. J Am Soc Nephrol *22*, 1221-1228.
Zotova, E., Nicoll, J.A., Kalaria, R., Holmes, C., and Boche, D. (2010). Inflammation in Alzheimer's disease: relevance to pathogenesis and therapy. Alzheimers Res Ther *2*, 1.

Chapter 2. DEPLETION OF THE AD RISK GENE *SORL1* SELECTIVELY IMPAIRS NEURONAL ENDOSOMAL TRAFFIC INDEPENDENT OF AMYLOIDOGENIC APP PROCESSING

2.1 INTRODUCTION

Alzheimer's disease (AD) is the most common neurodegenerative disorder in the elderly affecting nearly 40 million people worldwide(2019) and there is no treatment that alters disease progression. Recent therapeutic designs have focused on the main neuropathologic hallmarks of AD, accumulations of amyloid beta (Aβ) in senile plaques and abnormally phosphorylated tau protein in neurofibrillary tangles. The nearly universal failures of these trials to date, the vast majority of which have focused on removing or modulating Aβ, argues that other cellular pathways should be mechanistically studied for therapeutic development. Both genetics and pathology point to endosomal abnormalities and dysfunction as an early pathway in AD pathogenesis(Cataldo et al., 2000; Karch and Goate, 2015; Offe et al., 2006; Rogaeva et al., 2007). In particular, the *SORL1* gene, which encodes the sorting protein SORLA, is highly relevant, being associated with both late-onset and early-onset forms of AD(Bettens et al., 2008; Holstege et al., 2017; Pottier et al., 2012; Reitz et al., 2011; Rogaeva et al., 2007). SORLA, first identified as a neuronal sorting receptor(Andersen et al., 2005; Hermans-Borgmeyer et al., 1998), is expressed in nearly all central nervous system (CNS) cell types(Zhang et al., 2014) and has multiple roles in endocytic sorting(Dumanis et al., 2015; Glerup et al., 2013; Herskowitz et al., 2012; Klinger et al., 2011; Nielsen et al., 2007), retromer-dependent retrograde trafficking(Fjorback et al., 2012), and amyloid precursor protein (APP) processing

regulation(Andersen et al., 2005; Mehmedbasic et al., 2015; Rogaeva et al., 2007; Young et al., 2015). SORLA expression decreases in sporadic AD (SAD)(Dodson et al., 2006; Ma et al., 2009; Sager et al., 2007), and protein coding variants identified in early-onset AD families may lead to functional defects in the sorting of Aβ in cells(Caglayan et al., 2014). Rare loss-of-function truncation mutations have been found to be causal of late-onset AD(Holstege et al., 2017; Raghavan et al., 2018). We previously evaluated *SORL1* activity in human induced pluripotent stem cell (hiPSC)-derived neurons from AD patients and controls and demonstrated that *SORL1* expression induction with neurotrophic factors and its subsequent effect on neuronal Aβ peptides can be impacted by the presence of AD-associated risk variants(Young et al., 2015).

Due to its role as a sorting receptor and because it may be decreased in AD, we hypothesized that *SORL1* deficiency would impact endosome pathology and, by default, trafficking of cargo in the endo-lysosomal network. To evaluate this hypothesis, we generated *SORL1* deficient hiPSC lines using CRISPR/Cas9 genomic editing. We examined endosomal size in two cell types differentiated from these hiPSCs-- neurons and microglia. We also tested whether inhibiting amyloidogenic processing of APP by inhibiting BACE modulated endosome enlargement in hiPSC-derived neurons. In this study, we report that loss of *SORL1* by itself induces enlarged endosomes in hiPSC-derived neurons and this phenotype is not altered by BACE inhibition. We also observe that *SORL1* deficiency alters APP localization within the neuronal endosomal network. Interestingly, *SORL1* loss does not induce endosome enlargement in hiPSC-derived microglial-like cells, suggesting cell-type specific differences in this early AD cytopathology. Taken together, our data suggest that loss of the known AD risk gene *SORL1* induces early AD cytopathology in neurons and that, while it impacts trafficking of APP, the endosomal pathology occurs in an amyloid-independent manner. We observe important

endosome pathology differences in two CNS cell types, underscoring the complexity of this cellular pathway in the brain.

2.2 RESULTS

2.2.1 *Loss of SORL1 in hiPSC-Derived Neurons Results in Enlarged Early Endosomes*

We hypothesized that depletion of *SORL1* in human neurons would allow us to investigate early features of AD that may involve endosomal network dysfunction. We established isogenic *SORL1* KO and WT hiPSC lines using CRIPSR/Cas9 technology. We targeted exon 6 of the *SORL1* gene, inducing indels that disrupted the reading frame, leading to complete loss of SORLA protein (*SORL1* KO) (**Figure 2.3**). In neurons differentiated from the *SORL1* KO hiPSC lines, we quantified staining of endogenous EEA1 and Rab5 (markers of early endosome morphology) using confocal microscopy. We observed significantly increased fluorescence intensity from EEA1+ puncta (**Figure 2.1A-B**) and Rab5+ puncta (**Figure 2.5C)** in *SORL1* KO neurons. Western blot analysis showed no change in total EEA1 protein between WT and *SORL1* KO neurons **(Figure 2.4)**, suggesting that the increased fluorescence intensity is due to enlarged or fused early endosomes**.** We quantified endosome size and binned populations based on $\geq$0.5 mm^2 or <0.5 mm^2 area distributions (**Figure 2.1C**). We observed significantly more endosomes $\geq$0.5 mm^2 (**Figure 2.1C**), and a significant increase in the mean EEA1+ puncta area in *SORL1* KO neurons (**Figure 2.1D-E**). Interestingly, we also noticed significantly enlarged endosomes in neural progenitor cells (NPCs) from the *SORL1* KO lines (**Figure 2.5A**) suggesting that loss of *SORL1* impacts endosome morphology early in the neural lineage, after hiPSCs are driven to neuroectoderm. Finally, we also tested an shRNA against *SORL1* in WT neurons and again observed significantly enlarged endosomes (**Figure 2.5B**), suggesting that an acute reduction of *SORL1* expression also leads to this phenotype.

2.2.2 *Enlarged Early Endosomes in the Context of SORL1 Depletion Occur Independent of Amyloidogenic APP Processing*

Recent work has shown that neurons with introduced familial AD (FAD) mutations also show enlarged endosome morphology that is FAD gene-dose dependent(Kwart et al., 2019). In Kwart et al.'s study, endosome enlargement was dependent on b-secretase processing of APP. To test whether amyloidogenic processing of APP also contributed to early endosome enlargement in the context of *SORL1* loss, we treated *SORL1* KO and isogenic WT neurons with a BACE inhibitor (BACEi), effectively reducing Aβ peptide levels in our neurons (**Figure 2.2G-H**). There was no difference in endosome size nor EEA1 intensity in WT cells treated with BACEi compared to DMSO (Vehicle control) (**Figure 2.1F-J.)** Interestingly, in BACEi treated *SORL1* KO neurons we observed an even stronger increase in mean EEA1 intensity (**Figure 2.1F,G**) and no amelioration of early endosome enlargement compared to *SORL1* KO cells treated with DMSO (**Figure 2.1H,I,J)**. These data suggest the mechanism by which loss of *SORL1* expression induces endosome enlargement is independent of amyloidogenic APP processing and differs from how FAD mutations impact the endosomal network.

2.2.3 *Enlarged Early Endosomes in SORL1 Deficient Cells are Present in hiPSC-Derived Neurons, But Not Microglial-Like Cells*

AD-associated risk genes and their biological pathways may function differently between unique CNS cell types. Indeed, recent work using hiPSC-derived, gene-edited cells demonstrates that the strongest AD genetic risk factor, *APOE ε4*, impacts different cellular AD phenotypes in a cell type-specific manner(Lin et al., 2018; Wang et al., 2018). Microglia, the innate immune cells of the CNS, also express *SORL1*(Zhang et al., 2014) but the role of *SORL1* in microglia is

undefined and functionality of the endosomal network is likely very different in these highly phagocytic cells compared with neurons, which are professional secretory cells. We differentiated *SORL1* KO hiPSCs to microglial-like cells using a previously published protocol(McQuade et al., 2018) (**Figure 2.6**) and analyzed endogenous EEA1 staining using similar protocols as used with hiPSC-derived neurons and NPCs. Surprisingly, we did not observe differences in EEA1 fluorescence intensity (**Figure 2.1K,L**) or puncta size (**Figure 2.1M,N)** when we compared WT and *SORL1* KO microglial-like cells. Microglia are derived from mesoderm/hematopoietic lineages while NPCs and neurons are derived from neural ectoderm. Our findings suggest that the endosomal trafficking and sorting functions of *SORL1* may depend on cell lineage and that *SORL1*-dependent early endosome pathology is specific to neuronal cells.

2.2.4 *Loss of SORL1 in hiPSC-Derived Neurons Alters APP Trafficking and Processing in the Endosomal Network*

Enlarged endosomes are indicative of endosomal traffic jams and may delay the proper maturation and progression of vesicles and cargo for processing and degradation(Kaur and Lakkaraju, 2018). One well-characterized cargo of *SORL1*-dependent trafficking is APP(Fjorback et al., 2012). We quantified the localization of APP in various compartments of the endo-lysosomal network in *SORL1* deficient neurons using confocal microscopy. We observed an increase in colocalization of APP with EEA1 (**Figure 2.2A-B**) and a decrease in colocalization of APP with TGN38, a marker for the trans-Golgi network (TGN) (**Figure 2.2C-D**), demonstrating reduced retrograde transport of APP in the absence of *SORL1*. We also observed decreased colocalization of APP with Rab7, a marker of maturing endosomes (**Figure 2.2E-F**), suggesting that in the context of *SORL1* deficiency, vesicles with APP cargo are either

not maturing into late endosomes/lysosomes, or that the trafficking of APP itself to these compartments is impaired. Although the enlarged endosome morphology we observe is amyloid independent, downstream amyloidogenic cleavage of APP occurs in acidic early endosomes(Small and Gandy, 2006), where we document increased localization of APP. Previous studies have shown that molecules that enhance retrograde trafficking away from the early endosome towards the Golgi or back to the plasma membrane reduce amyloidogenic cleavage and decrease colocalization of APP with early endosomal markers(Mecozzi et al., 2014; Young et al., 2018). The impact of *SORL1* expression on APP processing has been previously described by us and others in studies showing knock-down of *SORL1* increases Aβ peptides in non-neuronal cells(Rogaeva et al., 2007) and in hiPSC-derived neurons(Young et al., 2015). We confirmed that *SORL1* KO neurons have increased Aβ peptides released into the culture media, and that both $A\beta_{1-40}$ and $A\beta_{1-42}$ species were equally increased, without inducing a significant change in the Aβ 42:40 ratio (**Figure 2.2G-I**). We did not observe a change in APP holoprotein expression in *SORL1* KO neurons (**Figure 2.4).** While BACEi significantly reduced Aβ levels in all cell lines (**Figure 2.2G,H**), there were still detectable Aβ peptides in the neuronal media, showing an incomplete inhibition of BACE. In concordance with an increase of APP in early endosomes in the absence of *SORL1* (**Figure 2.2A**), there were still significantly higher levels of Aβ peptides secreted into the culture media in the *SORL1* KO neurons, even in the presence of BACEi (**Figure 2.2G**). In order to further confirm that our BACEi treatment was effective, we measured sAPPβ by ELISA assay and β-C-terminal fragments (βCTFs) levels by Western blot in WT and *SORL1* KO neurons in either BACEi conditions or DMSO controls. We observed a significant reduction in sAPPβ levels and in βCTFs upon application of the BACEi in both WT and *SORL1* KO neurons (**Figure 2.2J,K,M)**. We did not observe a significant increase in βCTFs

in *SORL1* KO neurons in control conditions (**Figure 2.2K)**. Together, these data support our hypothesis that, in *SORL1* deficient conditions, the enlarged endosome phenotype is independent of amyloidogenic cleavage of APP. Interestingly, we observed an increase in αCTFs in WT neurons under BACEi conditions, suggesting that α cleavage may be exacerbated under these conditions as α and β secretase have been shown to have competitive activity(Netzer et al., 2017; Skovronsky et al., 2000). We did not observe an increase in αCTFs in *SORL1* KO neurons (**Figure 2.2L)**. These data are consistent with the observation that loss of *SORL1* retains APP in the early endosome, where it is unavailable for α cleavage.

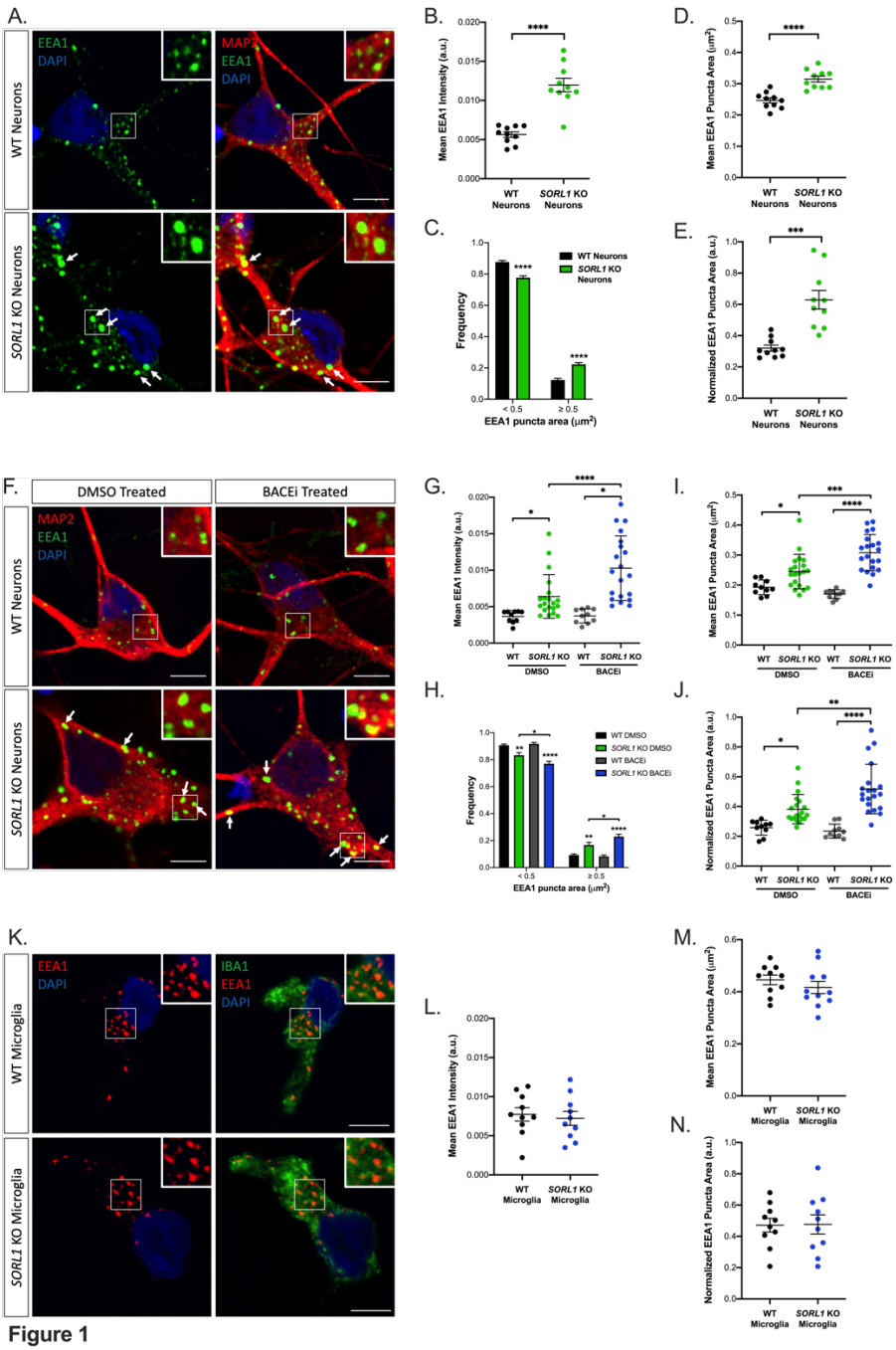

Figure 2.1. **Depletion of *SORL1* leads to enlarged early endosomes in hiPSC-derived neurons but not microglial-like cells, independent of amyloidogenic APP processing. (A)** Representative immunofluorescence images of WT and *SORL1* KO neurons stained with EEA1 (green), MAP2 (red), and DAPI (blue). White boxes indicate regions of interest (ROIs) magnified in insets. Arrows indicate enlarged EEA1+ puncta. Scale bars are 5 μm. **(B)**Quantification of immunofluorescence images demonstrates increased EEA1+ puncta fluorescence intensity in

SORL1 KO neurons compared to WT. n=10 images (18-22 cells). **(C)**Size distribution of EEA1+ puncta in *SORL1* KO neurons compared to WT demonstrates increased frequency of EEA1+ puncta $\geq$0.5 μm^2 in *SORL1* KO neurons. n=10 images (18-22 cells) **(D)**Quantification of mean EEA1+ puncta area in WT compared with *SORL1* KO neurons demonstrates increased mean EEA1+ puncta area in *SORL1* KO neurons compared to WT. n=10 images (18-22 cells). **(E)**Normalization of mean EEA1+ puncta area by cell area in WT compared with *SORL1* KO neurons. n=10 images (18-22 cells). **(F)**Representative immunofluorescence images of WT and SORL1 KO neurons treated with either DMSO or BACEi for 72 hours. Neurons were stained with EEA1 (green), MAP2 (red), and DAPI (blue). White boxes indicate regions of interest (ROIs) magnified in insets. Arrows indicate enlarged EEA1+ puncta. Scale bars are 5μm. **(G)**Quantification of immunofluorescence images demonstrates increased mean EEA1+ puncta intensity in BACEi treated *SORL1* KO neurons compared to DMSO treated controls. n=10-20 images (42-58 cells). **(H)**Size distribution of EEA1+ puncta in *SORL1* KO neurons compared to WT neurons with and without BACEi treatment. n=10-20 images (42-58 cells). **(I)**Quantification of immunofluorescence images demonstrates enlarged EEA1+ puncta area in BACEi treated *SORL1* KO neurons compared to DMSO treated controls. n=10-20 images (42-58 cells). **(J)**Normalization of mean EEA1+ puncta area by cell area in BACEi treated WT and *SORL1* KO neurons. n=10 images (18-22 cells). **(K)**Representative immunofluorescence images of WT and *SORL1* KO microglial-like cells stained with EEA1 (red), Iba1 (green), and DAPI (blue). White boxes indicate regions of interest (ROIs) magnified in insets. Scale bars are 5 μm. **(L)**Quantification of immunofluorescence images demonstrates no significant change in mean EEA1+ puncta intensity in *SORL1* KO microglial-like cells compared to WT. n=10 images (10-14 cells). **(M)**Quantification of immunofluorescence images demonstrates no significant change in EEA1+ puncta area in *SORL1* KO microglial-like cells compared to WT. n=10 images (10-14 cells). **(N)**Normalization of mean EEA1+ puncta area by cell area in WT compared with *SORL1* KO microglial-like cells. n=10 images (18-22 cells). All experiments represent two isogenic clones of each genotype (four total). All values represent mean +/- SEM. Normally distributed data (B, C, D, E, H, L, M, N) were analyzed by parametric statistical tests. Non-normally distributed data (G, I, J) were analyzed by non-parametric statistical tests. *p<.05, **p<.01, ***p<.001, ****p<.0001 by two-tailed unpaired t-test (B, D, E, L, M, N); by two-way ANOVA (C, H); or by Kruskal-Wallis test (G, I, J)**.**

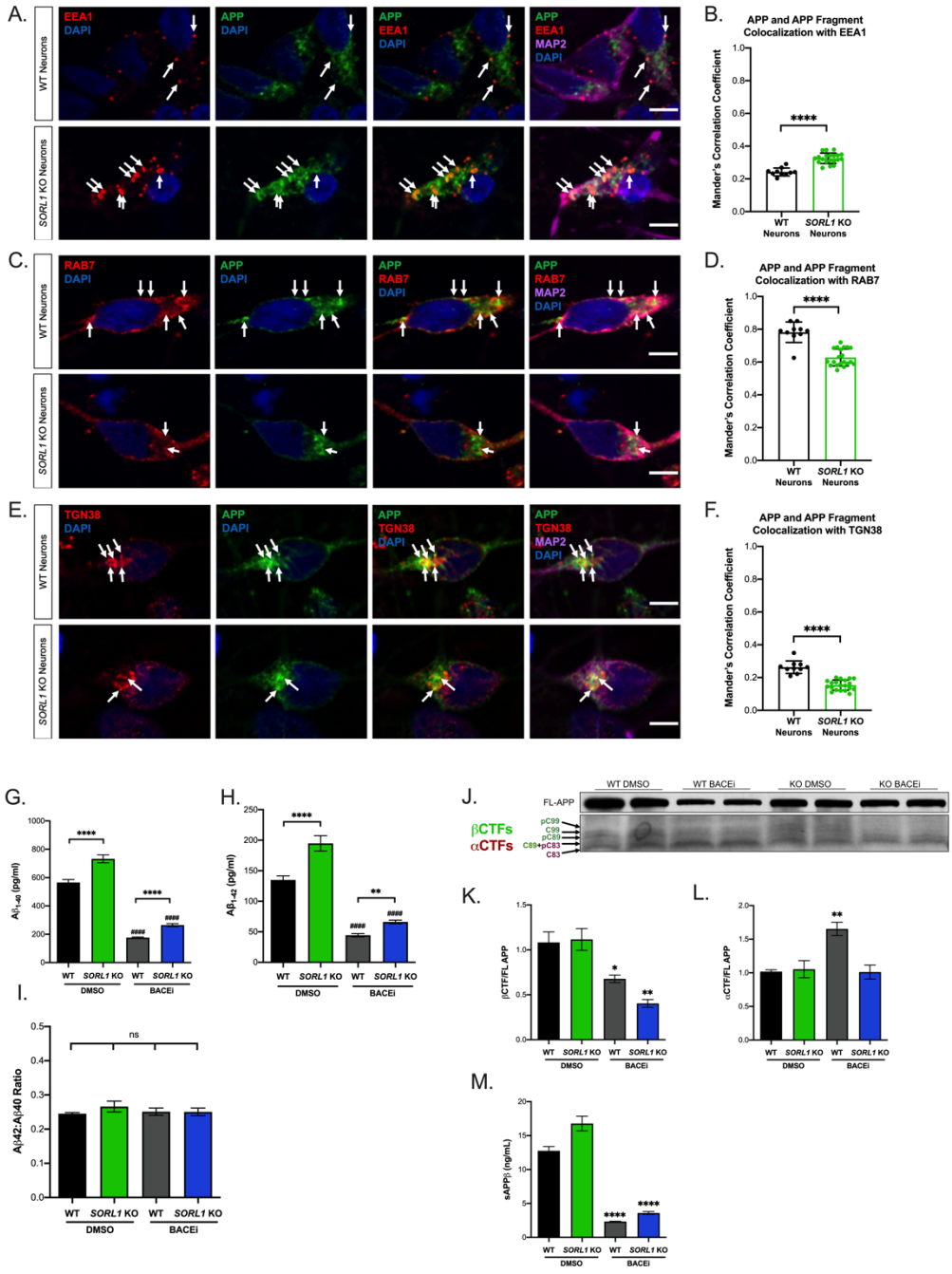

Figure 2.2. ***SORL1*** **depletion in hiPSC-derived neurons alters APP localization in the endosomal network and increases amyloidogenic processing of APP. (A)***SORL1* depletion results in APP accumulation in EEA1+ early endosomes. Representative immunofluorescence images of WT and *SORL1* KO neurons stained with EEA1 (red), APP C-terminal antibody (green), MAP2 (far-red) and DAPI (blue). Arrows indicate colocalization of EEA1+ puncta with APP and APP fragments. Scale bars are 5 µm. **(B)**Quantification of colocalization of EEA1 with APP, n=10-

20 images. **(C)***SORL1* KO neurons show reduced colocalization of APP and APP fragments with Rab7+ puncta. Representative immunofluorescence images of WT and *SORL1* KO neurons stained with Rab7 (red), APP C-terminal antibody (green), MAP2 (far-red), and DAPI (blue). Arrows indicate colocalization of Rab7+ puncta with APP and APP fragments. Scale bars are 5 μm. **(D)**Quantification of colocalization of Rab7 with APP, n=10-20 images. **(E)***SORL1* KO neurons show reduced colocalization of APP and APP fragments with TGN38+ puncta. Representative immunofluorescence images of WT and *SORL1* KO neurons stained with TGN38 (red), APP C-terminal antibody (green), MAP2 (far-red), and DAPI (blue). Arrows indicate colocalization of TGN38+ puncta with APP and APP fragments. Scale bars are 5 μm. **(F)**Quantification of colocalization of TGN38 with APP, n=10-20 images. **(G-H)***SORL1* KO neurons secrete higher levels of $A\beta_{1-40}$ and $A\beta_{1-42}$ peptides than WT cells, indicated by asterisks (*). BACEi significantly reduces these peptides in both genotypes compared to DMSO controls, indicated by hashmarks (#). In the presence of BACEi, *SORL1* KO neurons still secrete increased levels of $A\beta_{1-40}$ and $A\beta_{1-42}$ peptides, indicated by asterisks (*). n=2 biological replicates per genotype, 3-6 technical replicates. **(I)**Neither *SORL1* KO nor treatment with BACEi changes the ratio of $A\beta_{1-42}$:$A\beta_{1-40}$ peptides. n=2 biological replicates per genotype, 3-6 technical replicates. **(J)**Representative Western blot of full length (FL) APP and APP CTFs in WT and *SORL1* KO cell lines treated with BACEi or DMSO control. n=2 biological replicates. **(K)** βCTFs of APP are significantly reduced in BACEi treated neurons as determined by Western blot. n=2 biological replicates. **(L)**αCTFs of APP are significantly higher in WT neurons treated with BACEi but unchanged in *SORL1* KO neurons treated with BACEi, as determined by Western blot. n=2 biological replicates. **(M)**sAPPβ fragments are significantly reduced in WT and *SORL1* KO neurons with BACEi treatment, as determined by ELISA assay. n=2 biological replicates per genotype, 3-6 technical replicates. All experiments represent two isogenic clones of each genotype (Four total). All values represent mean +/- SD. All normally distributed data were analyzed by parametric statistical tests. *p<.05, **p<.01, ***p<.001, ****p<.0001 by two-tailed, unpaired t-test (B, D, F); by two-way ANOVA (G, H), or by one-way ANOVA (K, L, M)

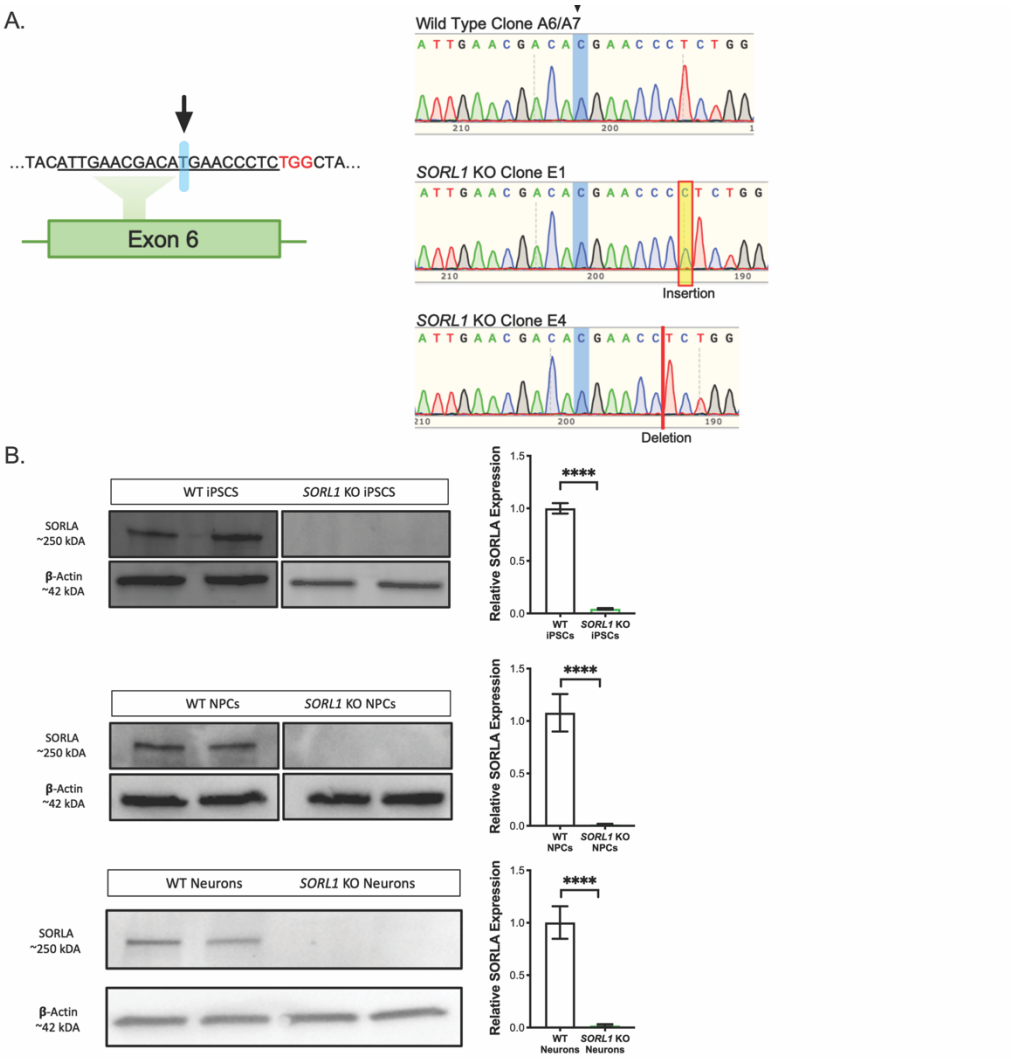

Figure 2.3. ***SORL1* KO gene editing and validation. (A)**Schematic drawing representing CRISPR/Cas9 depletion of *SORL1* in hiPSCs. The gRNA (underlined) was targeted to exon 6 in the *SORL1* coding sequence. The light blue shading, marked by arrowheads, indicates a synonymous SNP present in the donor hiPSC line that differs from the reference genome. The two KO clones used in this study show an insertion (clone E1) and a deletion (clone E4) three bases upstream from the PAM site that lead to a frameshift and premature stop codon. **(B)**Representative Western blots and quantitation show reduction of SORLA protein levels to nearly zero in the KO hiPSCs, NPCs, and neurons. Quantification for all cell types includes two biological replicates (clones) per genotype, n=6 biological replicates. All values represent mean +/- SD. All normally distributed data were analyzed by two-tailed unpaired t-test. *p<.05, **p<.01, ***p<.001, ****p<.0001

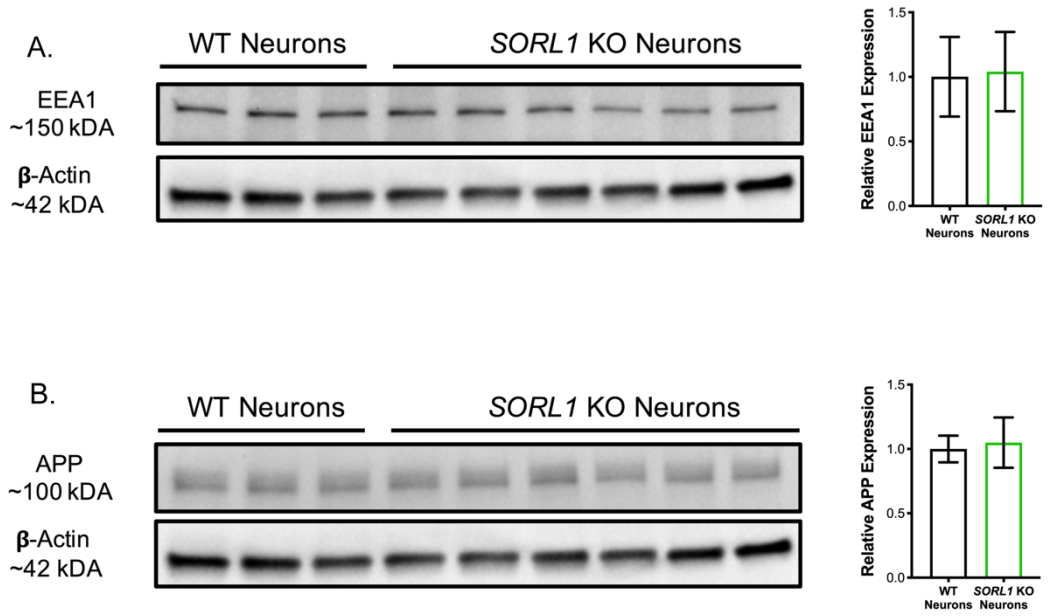

Figure 2.4. ***SORL1*** **depletion in hiPSC-derived neurons does not alter EEA1 or APP expression.** **(A)**WT and *SORL1* KO neurons show no significant difference in EEA1 protein expression as measured by Western blot. **(B)**WT and *SORL1* KO neurons show no significant difference in full-length APP expression as measured by Western blot. Quantification includes two biological replicates (clones) per genotype, n=3-6 biological replicates. All values represent mean +/- SD. All normally distributed data were analyzed by two-tailed unpaired t-test. *p<.05, **p<.01, ***p<.001, ****p<.0001

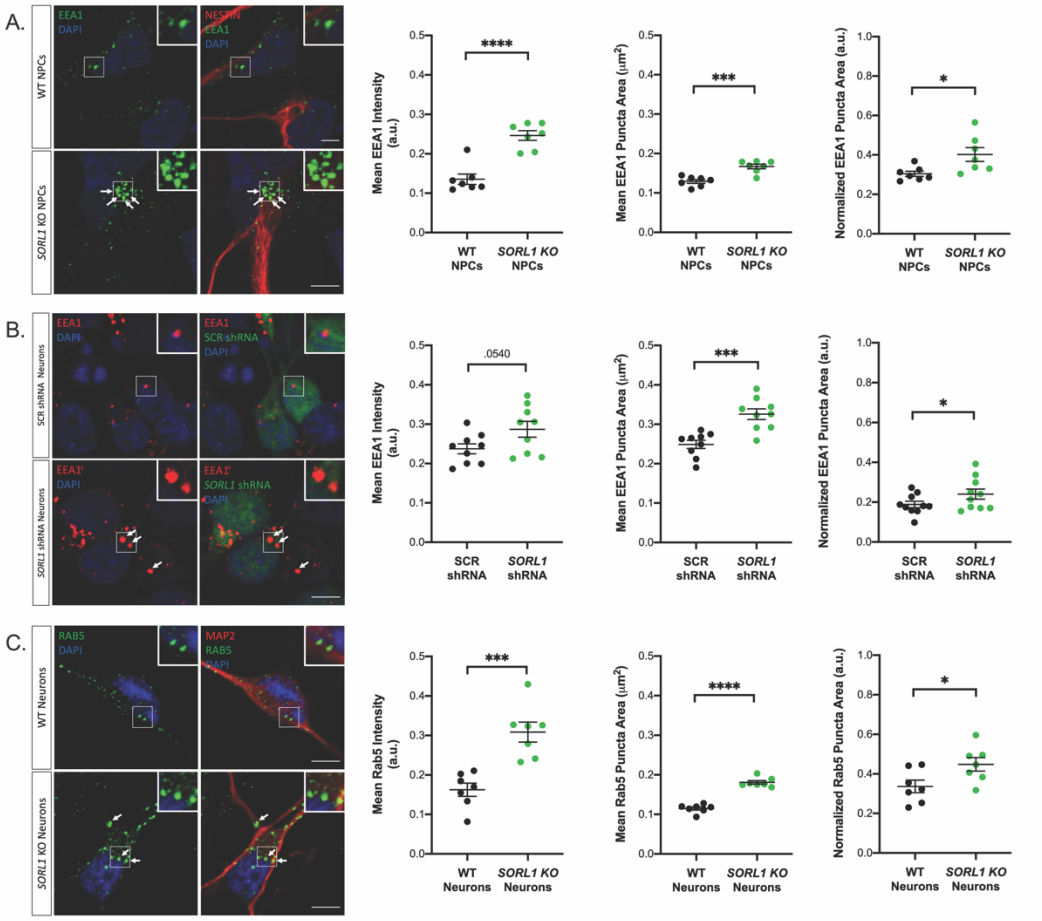

Figure 2.5. ***SORL1*** **depletion leads to enlarged early endosomes.** **(A)**Representative immunofluorescence images and quantitation of enlarged EEA1+ early endosomes in *SORL1* KO and isogenic WT NPCs. NPCs were stained with EEA1 (green), Nestin (red), and DAPI (blue). Two biological replicates (clones) per genotype, n=7 images (24-26 cells). **(B)**Representative immunofluorescence images and quantitation of enlarged EEA1+ early endosomes in WT hiPSC-derived neurons treated with a *SORL1* shRNA. Neurons were stained with EEA1 (red), scrambled (SCR) and *SORL1* shRNA (green), and DAPI (blue). n=9 images (36-48 cells). **(C)** Representative immunofluorescence images and quantitation of enlarged Rab5+ early endosomes in *SORL1* KO and isogenic WT hiPSC-derived neurons. Neurons were stained with Rab5 (green), MAP2 (red), and DAPI (blue). Two biological replicates (clones) per genotype, n=7 images (22-26 cells). All values represent mean +/- SEM. All normally distributed data were analyzed by two-tailed unpaired t-test. *p<.05, **p<.01, ***p<.001, ****p<.0001

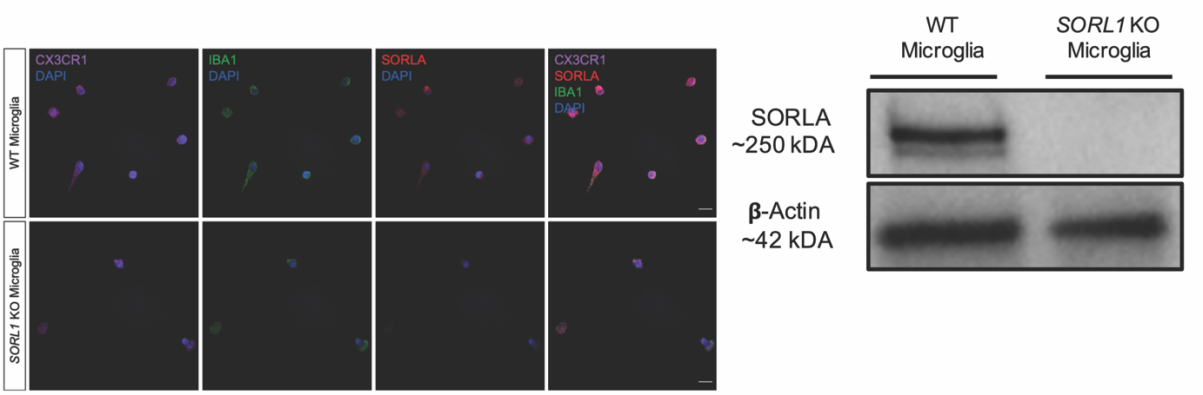

Figure 2.6. ***SORL1* KO microglia-like cells express microglia markers.** Representative immunofluorescence images and Western blot of *SORL1* KO and isogenic WT microglial-like cells differentiated from hiPSCs. Microglia-like cells show expression of microglial markers IBA1 (green) and CX3CR1 (far red). *SORL1* KO microglia-like cells show no SORLA staining (red) and no SORLA expression by Western blot. Scale bars are 20μm.

2.3 DISCUSSION

Endosome enlargement is an early cytopathology in AD(Cataldo et al., 2000) and abnormalities in the endolysosomal network are prevalent throughout human neurodegenerative disorders(Vagnozzi and Pratico, 2019). Multiple genetic studies also identify risk loci in or near genes involved in endosomal trafficking(Van Acker et al., 2019). This points to protein trafficking as an important, and potentially modifiable, pathway for AD and related disorders. As defects in the endosomal network are an early event in AD pathogenesis, this is an important target whose modulation may impact downstream pathologies. Indeed, our previous work has shown that molecules that enhance endosomal trafficking pathways affect Aβ and tau independently, supporting the premise that trafficking dysfunction is an early driver of AD (Young et al., 2018). In this study, we used hiPSC and CRISPR/Cas9 technology to ask whether loss of an established AD risk gene, *SORL1*, induces early endosome pathology in neurons and other cell types affected in AD. We document significantly enlarged endosomes in hiPSC-derived neurons lacking *SORL1*, demonstrating that loss of this sorting receptor is sufficient to induce this pathology in neurons (**Figure 2.1A-E**).

Endosome dysfunction is seen prior to Aβ accumulation in AD brains(Cataldo et al., 2000) and previous studies have established that the APP βCTFs are toxic and can themselves cause endosomal enlargement(Kim et al., 2016; Kwart et al., 2019; Xu et al., 2016). Recently, in a large cohort of FAD hiPSC-derived neurons, endosome enlargement due to FAD mutations was rescued by BACEi treatment(Kwart et al., 2019). In our study, BACEi treatment reduced Aβ peptides but did not ameliorate, and in fact exacerbated, endosomal size increases induced by loss of *SORL1* in hiPSC-derived neurons (**Figure 2.1F-J**). This suggests endosomal homeostasis may require a delicate balance of cargo, and that endosome pathology is a global event in AD

pathogenesis impacted by many different factors, which likely differ between early and late onset forms of the disease.

The genetic mutations causing FAD (in *APP* or *PSEN* genes) affect APP processing. In contrast, genetic studies of SAD have identified approximately two dozen associated candidate genes, a group of which converge around vesicular trafficking and endocytosis pathways. Among these, *SORL1* is common and truncation mutations causing loss-of-function of the SORLA protein are shown to be causal for late-onset AD(Holstege et al., 2017; Raghavan et al., 2018) making *SORL1* depletion a reliable approach for studying this pathway. Taken together with other recent findings(Kwart et al., 2019), our study establishes that two causative pathways in AD—APP cleavage and endosomal trafficking— independently cause AD's hallmark cytopathology.

Enlarged early endosomes were first reported in neurons in post-mortem brain(Cataldo et al., 2000) and models using hiPSCs with FAD mutations or from SAD patients have also shown endosome enlargement in neurons(Israel et al., 2012; Lin et al., 2018; Raja et al., 2016). In addition to neurons, microglia are also highly reliant on the endosomal network for the trafficking of internalized substrates(Sole-Domenech et al., 2016). We differentiated microglial-like cells from our *SORL1* deficient hiPSCs and performed the same analysis as with hiPSC-derived neurons. Interestingly, we did not observe significant endosome enlargement in *SORL1* deficient microglial-like cells (**Figure 2.1K-N**). These data demonstrate that loss of *SORL1* impacts microglial-like cells differently than neuronal cells, emphasizing important differences in cell-type specific responses to insults involving the endosomal network. For example, recent work reported that loss of the endosomal adaptor protein TOM1 in microglia led to reduced microglial branching and impaired phagocytosis, while in neurons it resulted in upregulation of

inflammatory signaling genes(Martini et al., 2019). Due to the vastly different roles microglia and neurons play in the CNS, future work on analyzing the functionality of endosomal trafficking, in addition to endosome size, in *SORL1* deficient microglial-like cells is warranted.

In neurons, one of the best-characterized cargos of *SORL1* is APP. The protein SORLA directly binds APP(Andersen et al., 2006) and serves as an adaptor molecule, via VPS26, in retromer-dependent retrograde trafficking of APP(Fjorback et al., 2012). We observed that loss of *SORL1* alters APP trafficking in the endosomal network, leading to increased colocalization of APP in early endosomes and a decrease in its localization in late endosomes and the TGN (**Figure 2.2A-F)**. Thus, we confirm in human neurons that *SORL1* functions as a retromer-receptor that traffics APP out of endosomes, and that by increasing the resident time of APP in endosomal membranes *SORL1* deficiency accelerates amyloidogenic APP cleavage. We also observe decreased APP localization in Rab7+ late endosomes/lysosomes, which suggests a defect in either endosomal maturation or trafficking of APP towards degradative compartments. Interestingly, in *SORL1* KO neurons the βCTF of APP is not significantly increased compared to WT (**Figure 2.2J**, **K**). We also document even more significant reduction of βCTFs under BACEi conditions in *SORL1* KO cells. Together, these data indicate that the enlarged endosome phenotype we observe is independent of amyloidogenic processing of APP and is directly tied to the loss of an endosomal sorting receptor. We do observe an increase in Aβ peptides in *SORL1* deficient neurons, as has been seen in other models(Andersen et al., 2005; Rogaeva et al., 2007). Therefore, it is plausible that the increase in Aβ peptides in *SORL1* KO neurons may be due, in part, to reduced trafficking of Aβ or APP to lysosomes. Indeed, previous studies have demonstrated that the VPS10 region of *SORL1* is important for trafficking Aβ to lysosomes for degradation(Caglayan et al., 2014)

Taken together, our work confirms the importance of *SORL1* in modulating processing APP and suggests that it may have a broader role in regulating endosomal network function. Our data support the idea that endosome pathology is an upstream event from amyloidogenic APP cleavage and Aβ generation and suggest that further disruptions of endosomal cargo processing or homeostasis (such as BACE inhibition) can enhance traffic jams or delay maturation in the absence of *SORL1*. Finally, our work demonstrates that hiPSC-derived neuronal models are valuable tools for dissecting early pathogenic events in AD and may help to clarify the molecular mechanisms that underlie therapeutic failures.

2.4 METHODS

2.4.1 *CRISPR/Cas9 Genome Editing*

All genome editing was performed in the previously published and characterized CV background human induced pluripotent stem cell line(Young et al., 2015). This cell line is male and has a *APOE ε3/ ε4* genotype(Levy et al., 2007). Genome edited lines were generated using published protocols(Young et al., 2018). Briefly, guide RNAs (gRNAs) to *SORL1* were generated using the Zhang Lab CRISPR Design website at MIT (crispr.mit.edu) and selected to minimize off-target effects. gRNAs were cloned into vector px458 that co-expresses the Cas9 nuclease and GFP, and hiPSCs were electroporated with the plasmid. Electroporated hiPSCs were FACS sorted for GFP, plated in 10 cm plates at a clonal density (~1x10^4 cells/plate), and allowed to grow for roughly 2 weeks. Colonies were picked into 96 well plates and split into two identical sets. One set was analyzed for sequence information by Sanger sequencing and one set was expanded for cell line generation. Four clones were chosen for experiments reported in this publication. Two wild-type clones, designated clone A6 and clone A7, and two *SORL1* KO

clones, designated clone E1 and clone E4, were selected. Sequencing data for all cell lines was confirmed by measuring protein expression using western blot techniques (**Figure 2.3B**). All four clones were shown to have normal karyotypes. Authentication: Sequencing data confirms CV cell lines by presence of a SNP unique to this genetic background (**Figure 2.3A)**. All cell lines are routinely karyotyped by Diagnostic Cytogenetics, Inc. (Seattle, WA), and tested for mycoplasma (MycoAlert).

2.4.2 *CRISPR/Cas9 gRNA, ssODN, and Primer Sequences*

gRNA: ATTGAACGACATGAACCCTC

ssODN:

GGGAATTGATCCCTATGACAAACCAAATACCATCTACATTGAACGACATGAACCCTC

TGGCTACTCCACGTCTTCCGAAGTACAGATTTCTTCCAGTCCCGGGAAAACCAGGAA

G

Forward primer: ctctatcctgagtcaaggagtaac

Reverse primer: ccttccaattcctgtgtatgc

PCR amplifies 458 bp sequence

2.4.3 *Western Blotting*

Cell lysates were run on 4-20% Mini-PROTEAN TGX Precast Protein Gels (#4561096; BioRad) or 16.5% Criterion™ Tris-Tricine Gel (#3450063; BioRad) and transferred to PVDF membranes. Membranes were probed with antibodies to Sortilin-related receptor 1 (SORLA) at 1:1000 (BD 611860 and abcam ab190684), β-actin (ACTB) at 1:2000 (EMD Millipore Corp MAB1501), early endosome antigen 1 (EEA1) at 1:5000 (BD 610456), and amyloid precursor protein (APP) at 1:500 (Invitrogen 14-9749-80) and APPY188 (Ab32136 Rabbit Y188; Abcam)

at 1:1000. Imaging was performed with a BioRad ChemiDoc system and quantification was performed using ImageJ software.

2.4.4 *hiPSC Neuronal Differentiation*

All cell lines were maintained at 37C in a 5% CO_2 incubator. hiPSCs were differentiated to neurons using previously described dual-SMAD inhibition techniques(Rose et al., 2018). Briefly, hiPSCs were plated on Matrigel (Growth factor reduced basement membrane matrix; # 356231; Corning) coated 6-well plates at a density of 3.5 million cells per well and fed with Basal Neural Maintenance Media (1:1 DMEM/F12 (#11039047 Life Technologies) + glutamine media/neurobasal media (#21103049, Gibco), 0.5% N2 supplement (# 17502-048; Thermo Fisher Scientific,) 1% B27 supplement (# 17504-044; Thermo Fisher Scientific), 0.5% GlutaMax (# 35050061; Thermo Fisher Scientific), 0.5% insulin-transferrin-selenium (#41400045; Thermo Fisher Scientific), 0.5% NEAA (# 11140050; Thermo Fisher Scientific), 0.2% β-mercaptoethanol (#21985023, Life Technologies) + 10 μM SB-431542 + 0.5 μM LDN-193189 (#1062443, Biogems). Cells were fed daily for seven days. On day eight, cells were incubated with Versene (#15640066, Gibco), gently dissociated using cell scrapers, and split 1:3. On day nine media was switched to Basal Neural Maintenance Media + 20 ng/mL FGF (R&D Systems, Minneapolis, MN) and fed daily. On day sixteen, cells were passaged 1:3. Cells were fed until approximately day twenty-three. At this time, cells were FACS sorted to obtain the CD184/CD24 (#557145/561646 BD Pharmingen) positive, CD44/CD271 (#555479/557196 BD Pharmingen) negative neural precursor cell (NPC) population(Yuan et al., 2011). Following sorting, NPCs were expanded for neural differentiation. For cortical neuronal differentiation, NPCs were plated out in 10 cm plates at a density of 6 million cells/plate. After 24 hours, cells were switched to Neural Differentiation media (DMEM-F12 + glutamine, 0.5% N2 supplement,

1% B27 supplement, 0.5% GlutaMax) + 0.02 μg/mL brain-derived neurotrophic factor (#450-02 PeproTech) + 0.02 μg/mL glial-cell-derived neurotrophic factor (#450-10 PeproTech) + 0.5 mM dbcAMP (#D0260 Sigma Aldrich). Media was refreshed twice a week for three weeks. After three weeks, neurons were selected for CD184/CD44 negative population by magnetic-activated cell sorting and plated for experiments.

2.4.5 *Purification of Neurons*

Following three weeks of differentiation, cells were dissociated with Accutase (#AT104-500 Innovative Cell Tech) and resuspended in IMAG solution (PBS + 0.5% bovine serum albumin [Sigma Aldrich] + 2 mM ethylenediaminetetraacetic acid [ThermoFisher]). Following a modification of Yuan et al., 2011(Yuan et al., 2011), cells were incubated with PE-conjugated mouse anti-Human CD44 and mouse anti-Human CD184 antibodies (BD Pharmingen) at a concentration of 5 μL/10 million cells. Following antibody incubation, cells were washed with IMAG solution and incubated with anti-PE magnetic beads (BD Pharmingen) at a concentration of 25 μL/10 million cells. Bead-antibody complexes were pulled down using a rare earth magnet, supernatants were selected, washed, and plated at an appropriate density.

2.4.6 *hiPSC Microglial-like Cells Differentiation*

SORL1 KO and WT hiPSCs were differentiated into microglial-like cells as previously described(McQuade et al., 2018). Briefly, hiPSCs were plated in mTESR™ 1 medium (STEMCELL Technologies) supplemented with ROCK Inhibitor (Y-27632; Apex Bio) on Matrigel (Growth factor reduced basement membrane matrix; # 356231; Corning) coated 6 well plates (#657160; CELLSTAR) at a dilution of 1:30. To begin hematopoietic progenitor differentiation, these cells were passaged to get a density of ~100 colonies (~150 cells per colony

of iPSCs) per well of a 6 well plate. On day 0, mTESR™ 1 medium was replaced with STEMdiff™ Hematopoietic Supplement A medium from the STEMdiff™ Hematopoietic kit (# 05310; STEMCELL technologies). On day 3, when colonies became flattened, medium was replaced with STEMdiff™ Hematopoietic Supplement B medium from the STEMdiff™ Hematopoietic kit (# 05310; STEMCELL technologies). Cells remained in this medium for 7 additional days. By day 10, non-adherent hematopoietic progenitor cells (HPCs) coming off from the flattened colonies were harvested by removing medium. Any remaining HPCs/floating cells were collected by gentle PBS washes. At this point, HPCs were either frozen using Bambanker cell freezing medium (#BBH01; Bulldog-Bio) or plated at a density of 0.2 M cells per well of a Matrigel coated (1:60 dilution) 6 well plate in microglia differentiation medium for 25 days. Microglia differentiation medium comprised of DMEM-F12 (#11039047; Thermo Fisher Scientific), Insulin-transferrin-selenite (#41400045; Thermo Fisher Scientific), B27 (# 17504-044; Thermo Fisher Scientific), N2 (# 17502-048; Thermo Fisher Scientific), glutamax (# 35050061; Thermo Fisher Scientific), non-essential amino acids (# 11140050; Thermo Fisher Scientific), monothioglycerol (# M1753; Sigma), Insulin (# I2643; Sigma) freshly supplemented with TGF-β (#130-108-969, Miltenyl) , IL-34 (# 200-34; Peprotech) and M-CSF (#PHC9501; Thermo Fisher Scientific). On day 25, this medium was supplemented with CD200 (#C311; Novoprotein) and CX3CL1 (#300-31; Peprotech) for maturation of microglial-like cells. Cells remained in this medium for 3 days. On day 28, microglial-like cell differentiation was complete, and these cells were plated in laminin (#L2020; Sigma) coated coverslips (12mm diameter, #1760-012; cglifesciences) in a 24 well plate for immunocytochemistry with appropriate antibodies.

2.4.7 *Amyloid Beta and sAPP Measurements*

Aβ peptides and phosphorylated tau were measured as previously described (Young 2015). Briefly, purified neurons were seeded at a density of 200,000 cells/well of a 96-well plate and maintained in culture for 5 days. Medium and lysates were harvested from triplicate wells. To measure secreted Aβ peptides, media was run on an Aβ Triplex ELISA plate (Meso Scale Discovery #151200E-2). To measure sAPPβ, media was run on a sAPPα/sAPPβ ELISA plate (Meso Scale Discovery #K15120E-1).

2.4.8 *Immunocytochemistry*

Purified neurons were seeded at a density of 500,000 cells per well of a 24-well plate on glass coverslips coated with Matrigel. After 5 days in culture, cells were fixed in 4% paraformaldehyde (PFA, Alfa Aesar, Reston, VA) for 15 minutes. Cells were incubated in blocking buffer containing 2.5% bovine serum albumin and 0.1% Triton X-100 (Sigma Aldrich, St Louis, MO) for 30 minutes at room temperature then incubated in a primary antibody dilution in blocking buffer for 2 hours at room temperature. Cells were washed 3x with PBS + 0.1% Triton X-100 and incubated with a secondary antibody dilution in blocking buffer for 1 hour at room temperature. Cells were washed 3x in PBS and mounted on glass slides with ProLong Gold Antifade mountant (ThermoFisher, Waltham, MA). The following primary antibodies were used: Ras-related protein Rab-5A (RAB5A) at 1:500 (Synaptic Systems 108 011); early endosome antigen 1 (EEA1) at 1:500 (BD 610456); amyloid precursor protein (APP) at 1:250 (Abcam ab32136); microtubule-associated protein 2 (MAP2) at 1:1000 (Abcam ab92434); Nestin (NES) at 1:1000 (Santa Cruz Biotechnology sc23927); Trans-Golgi network integral membrane protein

(TGN38) at 1:250 (Santa Cruz sc-166594); Ras-related protein Rab-7a (Rab7) at 1:1000 (Abcam ab50533); DAPI at 1 μg/mL final (Alfa Aesar).

2.4.9 *Confocal Microscopy and Image Processing*

All microscopy and image processing were performed under blinded conditions. Confocal z-stacks were obtained using a Nikon A1R confocal microscope with x63 and x100 plan apochromat oil immersion objectives. Image processing was performed using ImageJ software(Schindelin et al., 2012). For endosome analysis, 10-20 fields were analyzed for a total of 10-58 cells. Maximum intensity projections of confocal stacks were generated, and background was subtracted using the rolling ball algorithm. Endosome channels were enhanced using contrast limited adaptive histogram equalization algorithms (CLAHE) and masked using cell body stains. Size and intensity measurements were performed using CellProfiler software(McQuin et al., 2018). Individual puncta were identified using automated segmentation algorithms. Mean intensity of each puncta was measured and has been presented as a mean value over all puncta per field. Similarly, pixel area of each puncta was measured and has been presented as a mean area over all puncta per field. Finally, mean puncta area normalized by total cell area calculated from cell body stains is also presented. For colocalization analysis, a minimum of 10 fields of confocal z-stacks were captured using the x100 plan apochromat oil immersion objective. Median filtering was used to remove noise from images and manual thresholding was applied to all images. The colocalization of APP with endocytic markers was quantified using JACOP plugin (Bolte and Cordelieres, 2006) in Image J and presented as Mander's correlation coefficient.

2.4.10 *BACE1 Inhibition*

Purified neurons derived from SORL1 KO and WT hiPSCs were plated on a matrigel coated 96 well plate at a density of $2x10^5$ cells per well. After 5 days, cells were treated with either 25 nM β-secretase inhibitor (BACEi; LY2886721; # HY-13240; MedChemExpress) or DMSO (as a vehicle control) for 72h. All experiments were performed after 72 hours of drug treatment. At this point, medium from DMSO or BACEi treated neurons was harvested for quantification of $A\beta_{1-40}$, $A\beta_{1-42}$, and sAPPβ peptides secreted by neurons by ELISA. Additionally, cell lysates were harvested for determining protein levels of β-C terminal fragment (βCTF) of amyloid precursor protein (APP) by western blot.

2.4.11 *SORL1 shRNA Design and Transfection*

Sequences for *SORL1* shRNA and a scrambled (SCR) shRNA were designed previously(Young et al., 2015) and cloned into the pSICOR-GFP plasmid(Ventura et al., 2004). Plasmids were packaged into lentivirus using HEK293FT cells. Virus was purified using PEG-it. Following differentiation and purification of neurons, 5µl of purified virus was added to cells for 72 hours. Knockdown of *SORL1* was confirmed by western blot.

2.4.12 *Quantification and Statistical Analysis*

We used two independent clones of homozygous knockout cell lines and two independent clones of isogenic WT cell lines (cells that underwent the CRISPR/Cas9 transfection and sub-cloning process, but in which editing events did not occur). For all imaging experiments the data was analyzed in a blinded manner. Experimental data was tested for normal distributions using the Shapiro-Wilk normality test. Normally distributed data was analyzed using parametric two-tailed unpaired t-tests, one-way ANOVA tests, or two-way ANOVA tests. Non-normally

distributed data was analyzed by non-parametric Kruskal-Wallis tests. Significance was defined as a value of $p>0.05$. All statistical analysis was completed using GraphPad Prism software. Statistical details of individual experiments, including biological and technical replicate information, can be found in figure legends.

2.5 REFERENCES

(2019). Alzheimer's Association Report: 2019 Alzheimer's disease facts and figures. Alzheimer's & Dementia *15*, 321-387.
Andersen, O.M., Reiche, J., Schmidt, V., Gotthardt, M., Spoelgen, R., Behlke, J., von Arnim, C.A., Breiderhoff, T., Jansen, P., Wu, X.*, et al.* (2005). Neuronal sorting protein-related receptor sorLA/LR11 regulates processing of the amyloid precursor protein. Proc Natl Acad Sci U S A *102*, 13461-13466.
Andersen, O.M., Schmidt, V., Spoelgen, R., Gliemann, J., Behlke, J., Galatis, D., McKinstry, W.J., Parker, M.W., Masters, C.L., Hyman, B.T.*, et al.* (2006). Molecular dissection of the interaction between amyloid precursor protein and its neuronal trafficking receptor SorLA/LR11. Biochemistry *45*, 2618-2628.
Bettens, K., Browers, N., Engelborghs, S., De Deyn, P., Van Broeckhoven, C., and Sleegers, K. (2008). SORL1 is genetically associated with increased risk for late-onset Alzheimer disease in the Belgian population. Human Mutation *29*, 769-770.
Bolte, S., and Cordelieres, F.P. (2006). A guided tour into subcellular colocalization analysis in light microscopy. J Microsc *224*, 213-232.
Caglayan, S., Takagi-Niidome, S., Liao, F., Carlo, A.S., Schmidt, V., Burgert, T., Kitago, Y., Fuchtbauer, E.M., Fuchtbauer, A., Holtzman, D.M.*, et al.* (2014). Lysosomal sorting of amyloid-beta by the SORLA receptor is impaired by a familial Alzheimer's disease mutation. Sci Transl Med *6*, 223ra220.
Cataldo, A.M., Peterhoff, C.M., Troncoso, J.C., Gomez-Isla, T., Hyman, B.T., and Nixon, R.A. (2000). Endocytic pathway abnormalities precede amyloid beta deposition in sporadic Alzheimer's disease and Down syndrome: differential effects of APOE genotype and presenilin mutations. Am J Pathol *157*, 277-286.
Dodson, S.E., Gearing, M., Lippa, C.F., Montine, T.J., Levey, A.I., and Lah, J.J. (2006). LR11/SorLA expression is reduced in sporadic Alzheimer disease but not in familial Alzheimer disease. J Neuropathol Exp Neurol *65*, 866-872.
Dumanis, S.B., Burgert, T., Caglayan, S., Fuchtbauer, A., Fuchtbauer, E.M., Schmidt, V., and Willnow, T.E. (2015). Distinct Functions for Anterograde and Retrograde Sorting of SORLA in Amyloidogenic Processes in the Brain. J Neurosci *35*, 12703-12713.
Fjorback, A.W., Seaman, M., Gustafsen, C., Mehmedbasic, A., Gokool, S., Wu, C., Militz, D., Schmidt, V., Madsen, P., Nyengaard, J.R.*, et al.* (2012). Retromer binds the FANSHY sorting motif in SorLA to regulate amyloid precursor protein sorting and processing. J Neurosci *32*, 1467-1480.
Glerup, S., Lume, M., Olsen, D., Nyengaard, J.R., Vaegter, C.B., Gustafsen, C., Christensen, E.I., Kjolby, M., Hay-Schmidt, A., Bender, D.*, et al.* (2013). SorLA controls neurotrophic activity by sorting of GDNF and its receptors GFRalpha1 and RET. Cell Rep *3*, 186-199.
Hermans-Borgmeyer, I., Hampe, W., Schinke, B., Methner, A., Nykjaer, A., Susens, U., Fenger, U., Herbarth, B., and Schaller, H.C. (1998). Unique expression pattern of a novel mosaic receptor in the developing cerebral cortex. Mech Dev *70*, 65-76.
Herskowitz, J.H., Offe, K., Deshpande, A., Kahn, R.A., Levey, A.I., and Lah, J.J. (2012). GGA1-mediated endocytic traffic of LR11/SorLA alters APP intracellular distribution and amyloid-beta production. Mol Biol Cell *23*, 2645-2657.
Holstege, H., van der Lee, S.J., Hulsman, M., Wong, T.H., van Rooij, J.G., Weiss, M., Louwersheimer, E., Wolters, F.J., Amin, N., Uitterlinden, A.G.*, et al.* (2017). Characterization of

pathogenic SORL1 genetic variants for association with Alzheimer's disease: a clinical interpretation strategy. Eur J Hum Genet *25*, 973-981.
Israel, M.A., Yuan, S.H., Bardy, C., Reyna, S.M., Mu, Y., Herrera, C., Hefferan, M.P., Van Gorp, S., Nazor, K.L., Boscolo, F.S.*, et al.* (2012). Probing sporadic and familial Alzheimer's disease using induced pluripotent stem cells. Nature *482*, 216-220.
Karch, C.M., and Goate, A.M. (2015). Alzheimer's disease risk genes and mechanisms of disease pathogenesis. Biol Psychiatry *77*, 43-51.
Kaur, G., and Lakkaraju, A. (2018). Early Endosome Morphology in Health and Disease. Adv Exp Med Biol *1074*, 335-343.
Kim, S., Sato, Y., Mohan, P.S., Peterhoff, C., Pensalfini, A., Rigoglioso, A., Jiang, Y., and Nixon, R.A. (2016). Evidence that the rab5 effector APPL1 mediates APP-betaCTF-induced dysfunction of endosomes in Down syndrome and Alzheimer's disease. Molecular psychiatry *21*, 707-716.
Klinger, S.C., Glerup, S., Raarup, M.K., Mari, M.C., Nyegaard, M., Koster, G., Prabakaran, T., Nilsson, S.K., Kjaergaard, M.M., Bakke, O.*, et al.* (2011). SorLA regulates the activity of lipoprotein lipase by intracellular trafficking. J Cell Sci *124*, 1095-1105.
Kwart, D., Gregg, A., Scheckel, C., Murphy, E.A., Paquet, D., Duffield, M., Fak, J., Olsen, O., Darnell, R.B., and Tessier-Lavigne, M. (2019). A Large Panel of Isogenic APP and PSEN1 Mutant Human iPSC Neurons Reveals Shared Endosomal Abnormalities Mediated by APP beta-CTFs, Not Abeta. Neuron *104*, 1022.
Levy, S., Sutton, G., Ng, P.C., Feuk, L., Halpern, A.L., Walenz, B.P., Axelrod, N., Huang, J., Kirkness, E.F., Denisov, G.*, et al.* (2007). The diploid genome sequence of an individual human. PLoS Biol *5*, e254.
Lin, Y.T., Seo, J., Gao, F., Feldman, H.M., Wen, H.L., Penney, J., Cam, H.P., Gjoneska, E., Raja, W.K., Cheng, J.*, et al.* (2018). APOE4 Causes Widespread Molecular and Cellular Alterations Associated with Alzheimer's Disease Phenotypes in Human iPSC-Derived Brain Cell Types. Neuron.
Ma, Q.L., Galasko, D.R., Ringman, J.M., Vinters, H.V., Edland, S.D., Pomakian, J., Ubeda, O.J., Rosario, E.R., Teter, B., Frautschy, S.A.*, et al.* (2009). Reduction of SorLA/LR11, a sorting protein limiting beta-amyloid production, in Alzheimer disease cerebrospinal fluid. Arch Neurol *66*, 448-457.
Martini, A.C., Gomez-Arboledas, A., Forner, S., Rodriguez-Ortiz, C.J., McQuade, A., Danhash, E., Phan, J., Javonillo, D., Ha, J.V., Tram, M.*, et al.* (2019). Amyloid-beta impairs TOM1-mediated IL-1R1 signaling. Proc Natl Acad Sci U S A *116*, 21198-21206.
McQuade, A., Coburn, M., Tu, C.H., Hasselmann, J., Davtyan, H., and Blurton-Jones, M. (2018). Development and validation of a simplified method to generate human microglia from pluripotent stem cells. Mol Neurodegener *13*, 67.
McQuin, C., Goodman, A., Chernyshev, V., Kamentsky, L., Cimini, B.A., Karhohs, K.W., Doan, M., Ding, L., Rafelski, S.M., Thirstrup, D.*, et al.* (2018). CellProfiler 3.0: Next-generation image processing for biology. PLoS Biol *16*, e2005970.
Mecozzi, V.J., Berman, D.E., Simoes, S., Vetanovetz, C., Awal, M.R., Patel, V.M., Schneider, R.T., Petsko, G.A., Ringe, D., and Small, S.A. (2014). Pharmacological chaperones stabilize retromer to limit APP processing. Nature chemical biology *10*, 443-449.
Mehmedbasic, A., Christensen, S.K., Nilsson, J., Ruetschi, U., Gustafsen, C., Poulsen, A.S., Rasmussen, R.W., Fjorback, A.N., Larson, G., and Andersen, O.M. (2015). SorLA complement-

type repeat domains protect the amyloid precursor protein against processing. J Biol Chem *290*, 3359-3376.
Netzer, W.J., Bettayeb, K., Sinha, S.C., Flajolet, M., Greengard, P., and Bustos, V. (2017). Gleevec shifts APP processing from a beta-cleavage to a nonamyloidogenic cleavage. Proc Natl Acad Sci U S A *114*, 1389-1394.
Nielsen, M.S., Gustafsen, C., Madsen, P., Nyengaard, J.R., Hermey, G., Bakke, O., Mari, M., Schu, P., Pohlmann, R., Dennes, A.*, et al.* (2007). Sorting by the cytoplasmic domain of the amyloid precursor protein binding receptor SorLA. Mol Cell Biol *27*, 6842-6851.
Offe, K., Dodson, S.E., Shoemaker, J.T., Fritz, J.J., Gearing, M., Levey, A.I., and Lah, J.J. (2006). The lipoprotein receptor LR11 regulates amyloid beta production and amyloid precursor protein traffic in endosomal compartments. J Neurosci *26*, 1596-1603.
Pottier, C., Hannequin, D., Coutant, S., Rovelet-Lecrux, A., Wallon, D., Rousseau, S., Legallic, S., Paquet, C., Bombois, S., Pariente, J.*, et al.* (2012). High frequency of potentially pathogenic SORL1 mutations in autosomal dominant early-onset Alzheimer disease. Molecular psychiatry *17*, 875-879.
Raghavan, N.S., Brickman, A.M., Andrews, H., Manly, J.J., Schupf, N., Lantigua, R., Wolock, C.J., Kamalakaran, S., Petrovski, S., Tosto, G.*, et al.* (2018). Whole-exome sequencing in 20,197 persons for rare variants in Alzheimer's disease. Ann Clin Transl Neurol *5*, 832-842.
Raja, W.K., Mungenast, A.E., Lin, Y.T., Ko, T., Abdurrob, F., Seo, J., and Tsai, L.H. (2016). Self-Organizing 3D Human Neural Tissue Derived from Induced Pluripotent Stem Cells Recapitulate Alzheimer's Disease Phenotypes. PLoS One *11*, e0161969.
Reitz, C., Cheng, R., Rogaeva, E., Lee, J.H., Tokuhiro, S., Zou, F., Bettens, K., Sleegers, K., Tan, E.K., Kimura, R.*, et al.* (2011). Meta-analysis of the association between variants in SORL1 and Alzheimer disease. Arch Neurol *68*, 99-106.
Rogaeva, E., Meng, Y., Lee, J.H., Gu, Y., Kawarai, T., Zou, F., Katayama, T., Baldwin, C.T., Cheng, R., Hasegawa, H.*, et al.* (2007). The neuronal sortilin-related receptor SORL1 is genetically associated with Alzheimer disease. Nat Genet *39*, 168-177.
Rose, S.E., Frankowski, H., Knupp, A., Berry, B.J., Martinez, R., Dinh, S.Q., Bruner, L.T., Willis, S.L., Crane, P.K., Larson, E.B.*, et al.* (2018). Leptomeninges-Derived Induced Pluripotent Stem Cells and Directly Converted Neurons From Autopsy Cases With Varying Neuropathologic Backgrounds. J Neuropathol Exp Neurol.
Sager, K.L., Wuu, J., Leurgans, S.E., Rees, H.D., Gearing, M., Mufson, E.J., Levey, A.I., and Lah, J.J. (2007). Neuronal LR11/sorLA expression is reduced in mild cognitive impairment. Ann Neurol *62*, 640-647.
Schindelin, J., Arganda-Carreras, I., Frise, E., Kaynig, V., Longair, M., Pietzsch, T., Preibisch, S., Rueden, C., Saalfeld, S., Schmid, B.*, et al.* (2012). Fiji: an open-source platform for biological-image analysis. Nat Methods *9*, 676-682.
Skovronsky, D.M., Moore, D.B., Milla, M.E., Doms, R.W., and Lee, V.M. (2000). Protein kinase C-dependent alpha-secretase competes with beta-secretase for cleavage of amyloid-beta precursor protein in the trans-golgi network. J Biol Chem *275*, 2568-2575.
Small, S.A., and Gandy, S. (2006). Sorting through the cell biology of Alzheimer's disease: intracellular pathways to pathogenesis. Neuron *52*, 15-31.
Sole-Domenech, S., Cruz, D.L., Capetillo-Zarate, E., and Maxfield, F.R. (2016). The endocytic pathway in microglia during health, aging and Alzheimer's disease. Ageing Res Rev *32*, 89-103.
Vagnozzi, A.N., and Pratico, D. (2019). Endosomal sorting and trafficking, the retromer complex and neurodegeneration. Molecular psychiatry *24*, 857-868.

Van Acker, Z.P., Bretou, M., and Annaert, W. (2019). Endo-lysosomal dysregulations and late-onset Alzheimer's disease: impact of genetic risk factors. Mol Neurodegener *14*, 20.
Ventura, A., Meissner, A., Dillon, C.P., McManus, M., Sharp, P.A., Van Parijs, L., Jaenisch, R., and Jacks, T. (2004). Cre-lox-regulated conditional RNA interference from transgenes. Proc Natl Acad Sci U S A *101*, 10380-10385.
Wang, C., Najm, R., Xu, Q., Jeong, D.E., Walker, D., Balestra, M.E., Yoon, S.Y., Yuan, H., Li, G., Miller, Z.A.*, et al.* (2018). Gain of toxic apolipoprotein E4 effects in human iPSC-derived neurons is ameliorated by a small-molecule structure corrector. Nat Med *24*, 647-657.
Xu, W., Weissmiller, A.M., White, J.A., 2nd, Fang, F., Wang, X., Wu, Y., Pearn, M.L., Zhao, X., Sawa, M., Chen, S.*, et al.* (2016). Amyloid precursor protein-mediated endocytic pathway disruption induces axonal dysfunction and neurodegeneration. J Clin Invest *126*, 1815-1833.
Young, J.E., Boulanger-Weill, J., Williams, D.A., Woodruff, G., Buen, F., Revilla, A.C., Herrera, C., Israel, M.A., Yuan, S.H., Edland, S.D.*, et al.* (2015). Elucidating Molecular Phenotypes Caused by the SORL1 Alzheimer's Disease Genetic Risk Factor Using Human Induced Pluripotent Stem Cells. Cell stem cell *16*, 373-385.
Young, J.E., Fong, L.K., Frankowski, H., Petsko, G.A., Small, S.A., and Goldstein, L.S.B. (2018). Stabilizing the Retromer Complex in a Human Stem Cell Model of Alzheimer's Disease Reduces TAU Phosphorylation Independently of Amyloid Precursor Protein. Stem Cell Reports *10*, 1046-1058.
Yuan, S.H., Martin, J., Elia, J., Flippin, J., Paramban, R.I., Hefferan, M.P., Vidal, J.G., Mu, Y., Killian, R.L., Israel, M.A.*, et al.* (2011). Cell-surface marker signatures for the isolation of neural stem cells, glia and neurons derived from human pluripotent stem cells. PLoS One *6*, e17540.
Zhang, Y., Chen, K., Sloan, S.A., Bennett, M.L., Scholze, A.R., O'Keeffe, S., Phatnani, H.P., Guarnieri, P., Caneda, C., Ruderisch, N.*, et al.* (2014). An RNA-sequencing transcriptome and splicing database of glia, neurons, and vascular cells of the cerebral cortex. J Neurosci *34*, 11929-11947.

Chapter 3. THE ALZHEIMER'S GENE *SORL1* IS A KEY REGULATOR OF ENDOSOMAL RECYCLING IN HUMAN NEURONS

3.1 INTRODUCTION

Alzheimer's disease (AD) is a progressive neurodegenerative disorder and the most common cause of dementia. The underlying contributors to AD pathology encompass several biological pathways, including endosomal function, amyloid precursor protein (APP) processing, immune function, synaptic function, and lipid metabolism(Karch and Goate, 2015). Among these, endosomal dysfunction in neurons is emerging as a potential causal mechanism(Small and Petsko, 2020). Mutations in the amyloid precursor protein (*APP*) and the two presenilins (*PSEN1* and *PSEN2*) lead to early-onset autosomal dominant AD. When these mutations are modelled in human neurons and other systems they cause endosomal swelling, indicative of traffic jams, a phenotype that is a cytopathological hallmark of AD(Cataldo et al., 2000; Choi et al., 2013; Kwart et al., 2019). Recent genetic studies have identified a fourth gene, the trafficking receptor 'sortilin related receptor 1' (*SORL1*), which, when harboring frame-shift mutations leading to premature stop codons, is described as causal for AD(Holstege et al., 2017; Raghavan et al., 2018; Scheltens et al., 2021). Interestingly, *SORL1* is also linked to the more common, late-onset form of AD(Lambert et al., 2013; Rogaeva et al., 2007b) and its expression is lost in sporadic AD brains (Dodson et al., 2006; Thonberg et al., 2017). When modelled in human neurons, *SORL1* depletion phenocopies *APP* and *PSEN* mutations by causing endosomal swelling(Hung et al., 2021; Knupp et al., 2020).

The *SORL1* gene codes for the protein SORLA, which functions as part of the retromer trafficking complex (Fjorback et al., 2012; Rogaeva et al., 2007a; Small and Gandy, 2006).

Retromer recycles cargo out of the early endosome, either from the endosome to the trans-Golgi network or, with greater importance for neurons, back to the cell surface(Fjorback et al., 2012; Seaman, 2012). To date, the best evidence for *SORL1*'s role in retromer-dependent endosomal recycling comes from studies investigating APP trafficking(Fjorback et al., 2012; Schmidt et al., 2007; Willnow and Andersen, 2013). Our previous work demonstrated that *SORL1* depletion retains APP in early endosomes, which may contribute to endosomal swelling by blocking recycling(Knupp et al., 2020).

Retromer-dependent trafficking in neurons, however, also recycles cargo other than APP. For example, retromer is required for the normal recycling of glutamate receptors, a trafficking event that mediates synaptic plasticity and synaptic health, and this dependency occurs independent of retromer's role in APP recycling(Park et al., 2004; Temkin et al., 2017). Neurotrophin receptors are also trafficked through the endosomal system, in a retromer-dependent manner, and are important for synaptic health(Klinger et al., 2015; Patapoutian and Reichardt, 2001; Rohe et al., 2013).

Here we used human induced pluripotent stem cell derived-neurons (hiPSC-Ns) to test the hypothesis that *SORL1* plays a broader role in neuronal endosomal recycling. We use our previously described *SORL1*-depleted hiPSC lines to generate hiPSC-Ns, which model the loss of *SORL1* expression that occurs in AD(Knupp et al., 2020). Furthermore, we used previously established cell lines engineered to overexpress *SORL1* 2-3-fold over wild-type levels(Young et al., 2015) to test the effects of enhanced *SORL1* expression in hiPSC-Ns on these trafficking pathways. Importantly, all cell lines are isogenic. We map the trafficking effects these manipulations have on three specific receptors, APP, the GLUA1 subunit of the AMPA receptor, and neurotrophin receptor TRKB, all of which are implicated in AD (Devi and Ohno, 2015;

Dewar et al., 1991; Ginsberg et al., 2019; Martin-Belmonte et al., 2020; Wakabayashi et al., 1999; Yasuda et al., 1995).

Finally, we performed RNA-sequencing on the *SORL1* depleted cell lines to explore an unbiased transcriptomics analysis induced by *SORL1* depletion. The results generally confirmed our hypothesis, showing that *SORL1* is a key and broad regulator of endosomal recycling in neurons, a conclusion that has both pathogenic and therapeutic implications.

3.2 RESULTS

3.2.1 *SORL1 Depletion Increases Neuronal Cargo Localization in Early Endosomes*

Using CRISPR/Cas9 genome editing techniques, we previously generated hiPSC-derived neurons (hiPSC-Ns) deficient in *SORL1* expression due to indels introduced in exon 6. We demonstrated that loss of *SORL1* expression in these neurons leads to enlarged early endosomes and an increased colocalization of APP within early endosomes, indicative of endosomal traffic jams(Knupp et al., 2020). We utilized these same cell lines (hereafter referred to as *SORL1*KO and their guide-matched isogenic wild-type clones referred to as WT) to examine localization of the BDNF receptor TRKB and the GLUA1 subunit of the neuronal AMPA receptor. TRKB has been shown to bind to SORLA and this interaction mediates trafficking of TRKB to synaptic plasma membranes(Rohe et al., 2013). GLUA1 is trafficked via the retromer complex, of which SORLA is an adaptor protein(Fjorback et al., 2012; Temkin et al., 2017) and both of these cargo are important in maintaining healthy neuronal function. Because we previously observed an increase in APP localization in early endosomes, resulting in a decrease in localization in downstream vesicles such as Ras-related protein (Rab)7+ late endosomes with *SORL1* depletion(Knupp et al., 2020), we performed an immunocytochemical analysis of both TRKB and GLUA1 localization with the early endosome marker EEA1. Similar to our previous

observations for APP, we documented significantly increased localization of both TRKB (**Figure 3.1A**) and GLUA1 (**Figure 3.1B**) in early endosomes in *SORL1*KO neurons as compared to isogenic WT control neurons. Accumulation of neuronal cargo in early endosomes is indicative of endosomal traffic jams, which are thought to impact the transit of cellular cargo through other arms of the endolysosomal network.

3.2.2 *SORL1 Depletion Mis-traffics Cargo Throughout the Endolysosomal Network*

The early endosome serves as a hub in which internalized cargo can be retrogradely transported to the trans-Golgi, recycled back to the cell surface or degraded as endosomes mature into late endosomes and lysosomes(Mayle et al., 2012). We have previously observed that APP localization within the trans-Golgi network was decreased in *SORL1*KO neurons(Knupp et al., 2020). Here we tested whether trafficking to the degradative arm of the endo-lysosomal network was affected in our *SORL1*KO neurons. Trafficking of substrates out of the early endosome to late endosomes and, subsequently, lysosomes is important for protein degradation and SORLA has been previously implicated in promoting Aβ degradation via lysosomes(Caglayan et al., 2014). We treated *SORL1* deficient neurons with DQ Red BSA, a proteolysis sensitive fluorogenic substrate that generates fluorescence only when enzymatically cleaved in intracellular lysosomal compartments. Since substrate degradation primarily occurs in lysosomes, altered fluorescence intensity of this reagent is a readout of altered lysosomal degradation(Marwaha and Sharma, 2017). We analyzed DQ Red BSA treated neurons for fluorescence intensity using confocal microscopy. Consistent with loss of *SORL1* leading to endosomal traffic jams, we observed a significant reduction of DQ Red BSA fluorescence intensity in *SORL1*KO neurons compared to isogenic WT controls (**Figure 3.2A**). We next performed immunocytochemical staining to quantify the colocalization of our selected neuronal

cargo with Rab7, a marker of late endosomes, and LAMP1 (Lysosomal Associated Membrane Protein 1), a lysosome marker. We show a significant decrease in co-localization of TRKB (**Figure 3.2B**) and GLUA1 (**Figure 3.2C**) with Rab7. This result is consistent with our previous observation for APP (Knupp et al., 2020). We analyzed colocalization of these cargo with LAMP1 and we observed a significant decrease with APP (**Figure 3.2D**) and TRKB (**Figure 3.2E**) and a trend of a decrease with GLUA1 (**Figure 3.2F**). These data indicate some fluidity in the network but suggest that trafficking of APP, TRKB and GLUA1 to late endosomes/lysosomes is all decreased by *SORL1*KO, although GLUA1 may be more likely to be trafficked to cell surface pathways or utilizes other adaptor proteins for late endosome to lysosomal trafficking.

Lysosome size can influence lysosome function and is altered in AD(de Araujo et al., 2020; Hwang et al., 2019). Similarly, location and number of lysosomes within neurons can alter degradative activity (Cheng et al., 2018; Farfel-Becker et al., 2019; Gowrishankar et al., 2015; Yap et al., 2018) and in some cases, altered lysosomal distribution may represent an early neuropathological defect(Zigdon et al., 2017). Recently, loss of *SORL1* in hiPSC neurons was shown to contribute to lysosome dysfunction as indicated by both increased lysosome size and number as well as decreased cathepsin-D activity(Hung et al., 2021). Therefore, we first analyzed LAMP1-immunopositive puncta and also documented a significant increase in lysosome size and number in our *SORL1*KO neurons (**Figure 3.7A**).

Retromer trafficking is required to deliver one of the most abundant lysosomal proteases, pro-cathepsin D, to lysosomes via the mannose-6-phosphate receptor (M6PR)(Qureshi et al., 2018; Seaman, 2004). The SORLA protein has GGA domains similar to that of M6PR(Spoelgen et al., 2006), and mis-trafficking of Cathepsin-D to lysosomes could affect the maturation and

degradative capacity of these organelles. Therefore, we analyzed co-localization of Cathepsin-D and LAMP1 to determine if loss of *SORL1* expression leads to altered Cathepsin-D trafficking in neurons. However, we did not observe a change in Cathepsin-D colocalization between WT and *SORL*1KO (**Figure 3.7B**). Taken together, our data suggest that *SORL1* loss in neurons reduces trafficking of cargo out of the early endosome to the late endosome and lysosome, contributing to lysosome stress as evidenced by an increase in size and number in these conditions while the decreased cathepsin-D activity observed upon *SORL1* loss(Hung et al., 2021) may not be due to impairment of lysosomal trafficking of the enzyme.

3.2.3 *SORL1 Depletion Targets the Endosomal Recycling Pathway*

Another route out of the early endosome is via the endocytic recycling complex (ERC) which can send cargo either to the cell surface or to the trans-Golgi network(Grant and Donaldson, 2009; Mallard et al., 1998; Marsh et al., 1995; Maxfield and McGraw, 2004). To directly examine if *SORL1* expression alters recycling function, we performed a transferrin recycling assay using confocal microscopy. Transferrin can be recycled via a fast pathway within approximately 5-10 minutes after being internalized or via a slower pathway involving the ERC over longer periods of time(Ouellette and Carabeo, 2010; Sonnichsen et al., 2000). We examined the fluorescence intensity of Alexa Fluor 647-conjugated transferrin over a 40-minute time course in WT and *SORL1*KO neurons and observed that a higher percentage of intracellular fluorescent transferrin persisted in *SORL1*KO neurons at both early and later time points as compared to WT neurons, indicating reduced recycling pathway function (**Figure 3.3A**). Cargo destined for the cell surface can transit to the ERC via Rab11+ recycling endosomes (Ren et al., 1998). Altered size of recycling endosomes can be indicative of dysfunctional recycling of cargo through these compartments. We tested whether loss of *SORL1* expression affected the size of

Rab11+ recycling endosomes. Interestingly, we observed a significant increase in the size of Rab11+ recycling endosomes in the *SORL1*KO neurons (**Figure 3.3B**), suggesting that this endosomal compartment is also under stress. To test if increased size is due to abnormal cargo trafficking through recycling endosomes, we assessed colocalization of APP, TRKB and GLUA1 with Rab11 and observed increased co-localization of all three cargo with Rab11+ structures in *SORL1*KO neurons compared to WT neurons (**Figure 3.3C-E**). Together, these data demonstrate that loss of *SORL1* impacts neuronal recycling endosome pathways by causing traffic jams in the recycling endosomes, similar to the effect that *SORL1* loss has on early endosomes.

3.2.4 *SORL1 Depletion Reduces Cell Surface Levels of Cargo*

Together, our data indicate that *SORL1*KO neurons have impaired cargo recycling with increased retention of cargo in recycling endosomes. These observations led us to test whether this cargo was indeed trafficked to the cell surface. A portion of APP has been shown to return to the cell surface via recycling endosomes(Das et al., 2016) and SORLA can interact with the sorting nexin SNX27 to return APP to the cell surface(Das et al., 2016; Huang et al., 2016), although in that study the exact compartment was not described. Furthermore, recycling endosomes are the source for AMPA receptors during long-term potentiation(Park et al., 2004). We therefore examined cell surface levels of APP and GLUA1 using immunofluorescence and confocal microscopy. We documented a significant decrease in cell surface staining of both APP (**Figure 3.4A**) and GLUA1 (**Figure 3.4B**) in *SORL1*KO neurons as compared to WT, consistent with our hypothesis that SORLA is involved in regulating traffic from recycling endosomes.

3.2.5 *SORL1 Overexpression Enhances Endosomal Recycling*

Defects in cell surface recycling have severe consequences in neurons, especially as these processes are necessary for healthy neuronal function. Synapse loss is a main component of AD neurodegeneration and enhancing pathways that support healthy synaptic function may be beneficial. We utilized previously generated cell lines that overexpress *SORL1* cDNA using the piggybac transposon system(Young et al., 2015) to test whether increased *SORL1* expression may enhance the trafficking pathways that are impaired in the *SORL1*KO neurons. Importantly, the *SORL1* overexpressing (*SORL1*OE) cell line and control were generated in the same genetic background as our *SORL1*KO and isogenic WT cell lines. While we found no effect of enhanced *SORL1* expression on DQ Red BSA signal in *SORL1*OE neurons (**Figure 3.8A**), we did observe increased localization of the three tested cargo (APP, TRKB, and GLUA1) in late endosomes and lysosomes in these cells (**Figure 3.8B-D and 3.8E-G**), suggesting that increased *SORL1* expression may enhance cargo trafficking to the degradative pathway.

We analyzed recycling function using the transferrin recycling assay and observed that *SORL1*OE neurons showed significantly faster transferrin recycling (**Figure 3.5A**). We next tested whether colocalization of cargo with recycling endosomes and cell surface recycling was altered between *SORL1*OE and WT neurons. Interestingly, the size of Rab11+ recycling endosomes was significantly smaller in *SORL1*OE neurons (**Figure 3.5B**) possibly indicating that increased *SORL1* expression is clearing cargo more rapidly from this compartment. We observed a significant increase in localization of cargo with Rab11+ recycling endosomes (**Figure 3.5C-E**). While this result was initially surprising, as we also saw increased colocalization with Rab11+recycling endosomes in our *SORL1*KO neurons (**Figure 3.3C-E**), we further documented a significant increase of APP and GLUA1 on the cell surface compared to

WT neurons with only endogenous *SORL1* expression (**Figure 3.5F and 3.5G**), as opposed to decreased APP and GLUA1 localization on the cell surface in *SORL1*KO neurons (**Figure 3.4A and 3.4B**). These results suggest that cell surface trafficking via a Rab11 pathway is enhanced by increased *SORL1* expression and that a crucial action of SORLA is the trafficking out of recycling endosomes. Thus, our data support a critical role for SORLA for trafficking cargo from recycling endosomes to the cell surface. In addition, we show for the first time that SORLA levels may regulate cell surface recycling of AMPA receptor subunits in human neurons.

3.2.6 *SORL1 Depletion Affects Gene Expression*

To determine a more global effect of chronic *SORL1* loss in human neurons, we performed bulk RNA sequencing of *SORL1*KO neurons compared to WT neurons. Interestingly, we observed that there were significantly more down-regulated genes in *SORL1*KO neurons than upregulated ones (**Figure 3.9B**). While none of the cargo we explicitly studied in this work was differentially expressed, GO analysis showed that the top downregulated molecular function pathways in the *SORL1*KO cells were related to receptor-ligand activity and extracellular matrix organization (**Figure 3.6A**). The top upregulated molecular function pathways were related to ion channel activity (**Figure 3.6B**). To understand these data in the context of an integrated network, we used an analysis method that infers ligand receptor interactions from bulk RNA-seq data(Ramilowski et al., 2015; Wang et al., 2020). We observed several nodes of altered receptor-ligand interactions that indicate altered cell surface recycling and neurotrophic activity (**Figure 3.6C**). These include alterations in b-integrin signaling, which is consistent with previous work showing reduced b-integrin on the cell surface in *SORL1*KO cancer cells(Pietila et al., 2019), and altered interactions in ephrins/ephrin receptors, also corroborating previous work implicating *SORL1* expression in ephrin signaling and synapse regulation(Huang et al., 2017). Our analysis

also showed nodes with alterations in nerve growth factor/nerve growth factor receptor (NGF/NGFR) and fibroblast growth factor/fibroblast growth factor receptor (FGF/FGFR) signaling, indicating alterations in neurotrophin and growth factor signaling and suggesting that the presence of endosomal traffic jams in *SORL1*KO neurons may ultimately impact multiple pathways important for neuronal health and development.

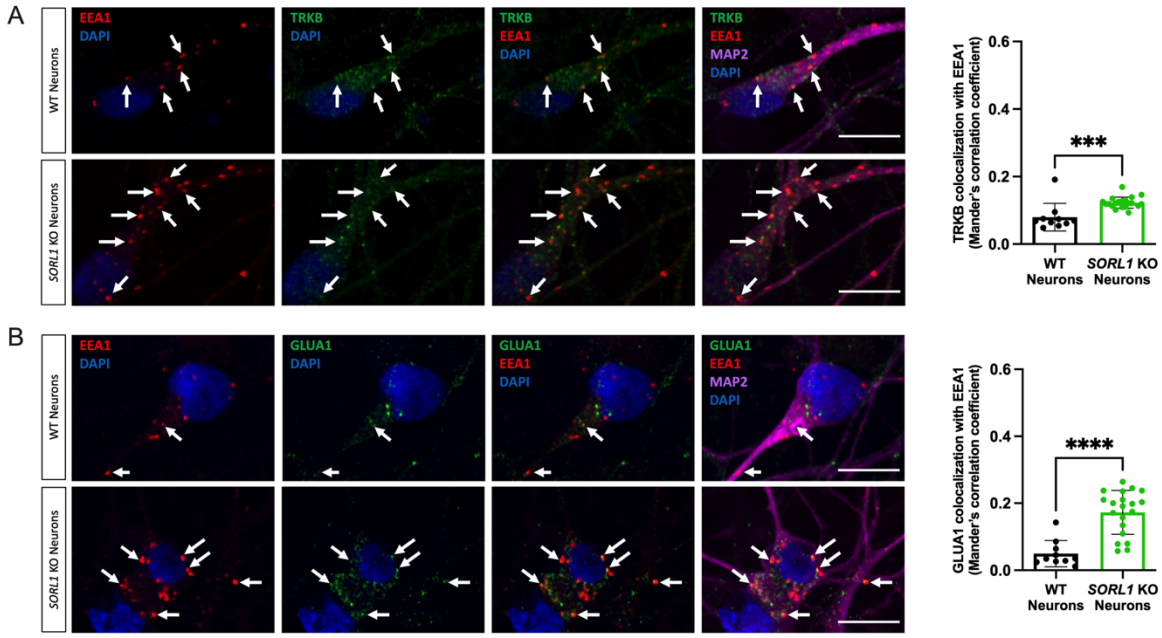

Figure 3.1. **Loss of *SORL1* expression leads to increased TRKB and GLUA1 localization in early endosomes**. Representative immunofluorescent images of WT and *SORL1*KO neurons showing increased colocalization of **(a)** TRKB (green) and **(b)** GLUA1 (green) with EEA1 (red). All neurons were immunolabeled with MAP2 (far-red) and counterstained with DAPI (blue). Scale bar: 10μm. In all cases, quantification of colocalization was represented as Mander's correlation co-efficient (MCC). 10-20 images were analyzed per genotype. Two isogenic clones of each genotype were used in all experiments. Data represented as mean ± SD. Normally distributed data was analyzed using parametric two-tailed unpaired t test and non-normally distributed data was analyzed by non-parametric Mann Whitney test. Significance was defined as a value of *$p < 0.05$, **$p < 0.01$, ***$p < 0.001$, and ****$p < 0.0001$

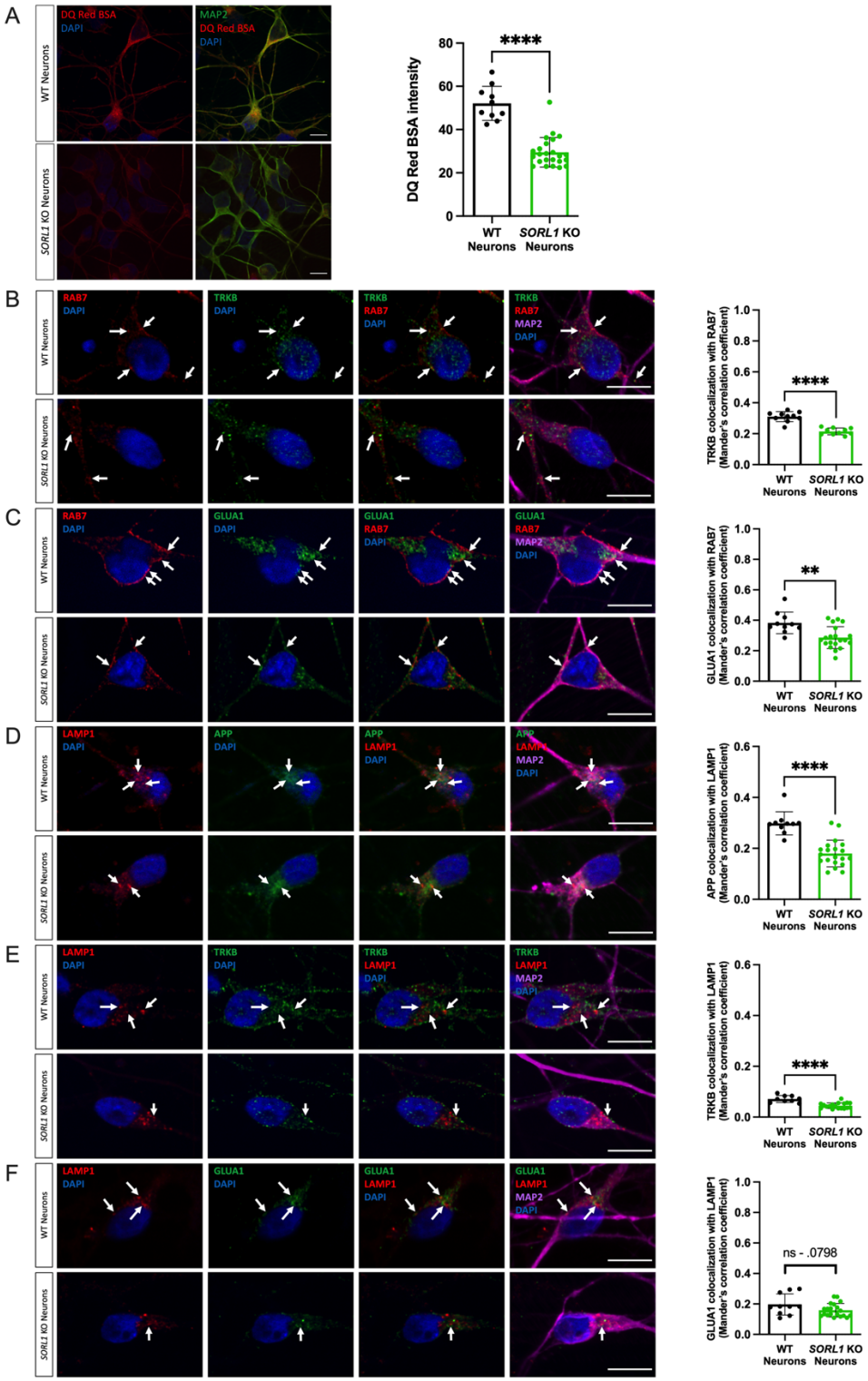

Figure 3.2. **Loss of *SORL1* expression impairs trafficking to late endosomes and lysosomes**.

(a) *SORL1*KO neurons show reduced lysosomal proteolytic activity as measured by DQ Red BSA. Representative immunofluorescent images of WT and *SORL1*KO neurons showing double

immunolabeling for MAP2 (green) and DQ Red BSA (red). Scale bar: 10μm Quantification of fluorescence intensity of DQ Red BSA using ImageJ software. **(b-f)** *SORL1*KO neurons show reduced colocalization of cargo with late endosomes and lysosomes. Representative immunofluorescent images of WT and *SORL1*KO neurons showing reduced colocalization of **(b)** TRKB (green) and **(c)** GLUA1 (green) with Rab7 positive late endosomes (red) in *SORL1*KO neurons. Representative immunofluorescent images of WT and *SORL1*KO neurons showing reduced colocalization of **(d)** APP (green) and **(e)** TRKB (green) and **(f)** GLUA1 (green) with LAMP1 positive lysosomes (red) in *SORL1*KO neurons. Scale bar: 10μm. In all cases, quantification of colocalization was represented as Mander's correlation co-efficient (MCC). 10-20 images were analyzed per genotype. Two isogenic clones of each genotype were used in all experiments. Data represented as mean ± SD. Normally distributed data was analyzed using parametric two-tailed unpaired t test and non-normally distributed data was analyzed by non-parametric Mann Whitney test. Significance was defined as a value of *$p < 0.05$, **$p < 0.01$, ***$p < 0.001$, and ****$p < 0.0001$.

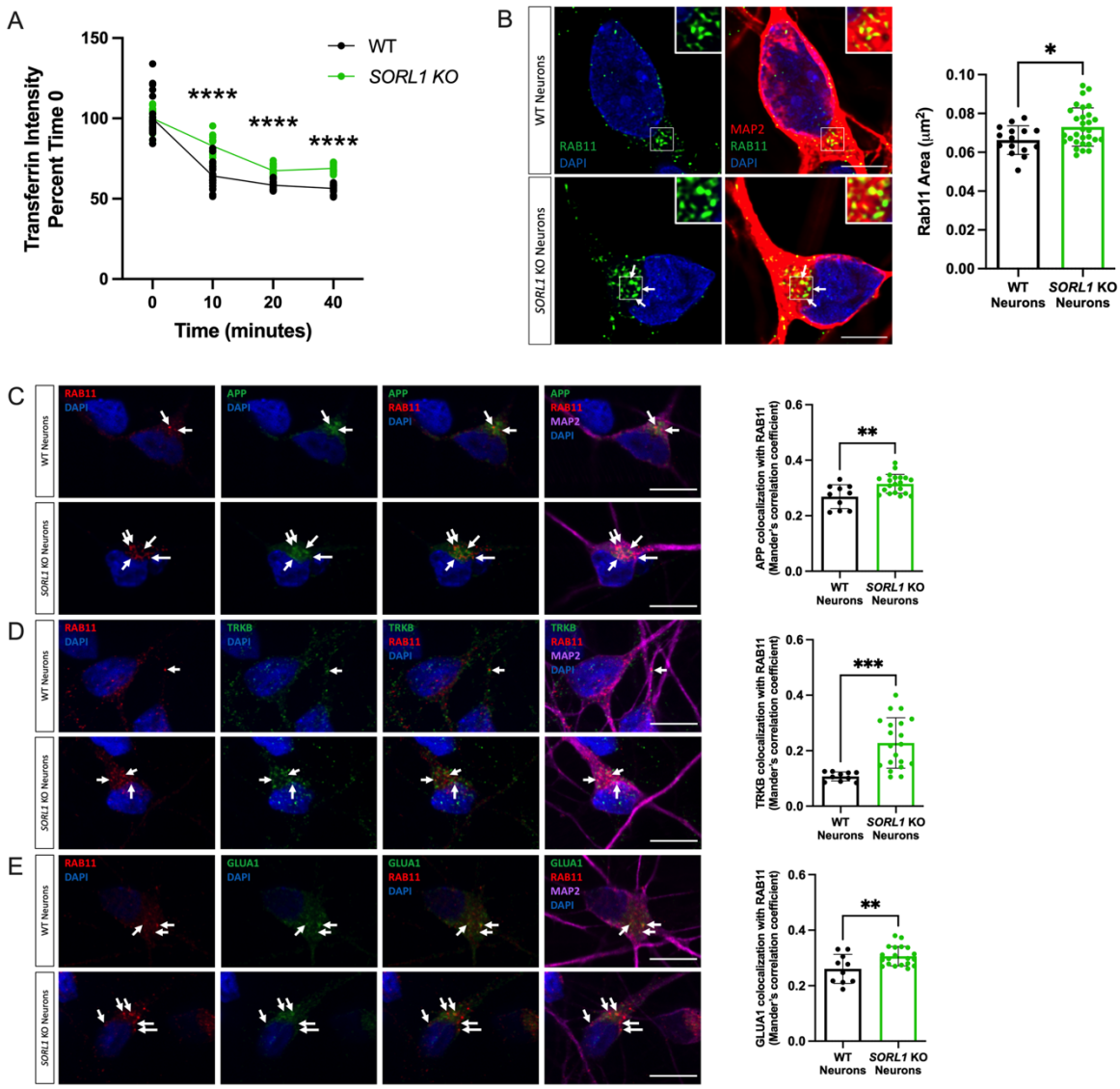

Figure 3.3. **Loss of *SORL1* impacts the cell surface recycling pathway. (a)** *SORL1*KO neurons show slower rate of transferrin recycling. Quantification of fluorescence intensity of intracellular transferrin at different time points after treating cells with Alexa Fluor 647-conjugated transferrin for 15 mins, using ImageJ software. Data represented as percent of time 0 fluorescence intensity. **(b)** *SORL1*KO neurons show larger recycling endosomes. Representative immunofluorescent images of WT and *SORL1*KO neurons labeled with antibodies for MAP2 (red) and Rab11 (green). Nuclei were counterstained with DAPI (blue). Scale bar: 5µm. Quantification of size of Rab11 labeled recycling endosomes using CellProfiler software. Representative immunofluorescent images of WT and *SORL1*KO neurons showing increased colocalization of **(c)** APP (green), **(d)** TRKB (green) and **(e)** GLUA1 (green) with Rab11 positive recycling

endosomes (red) in *SORL1*KO neurons. Scale bar:10μm In all cases, quantification of colocalization was represented as Mander's correlation co-efficient (MCC). 10-20 images were analyzed per genotype. Two isogenic clones of each genotype were used in all experiments. Data represented as mean ± SD. Normally distributed data was analyzed using parametric two-tailed unpaired t test and non-normally distributed data was analyzed by non-parametric Mann Whitney test. Significance was defined as a value of *$p < 0.05$, **$p < 0.01$, ***$p < 0.001$, and ****$p < 0.0001$.

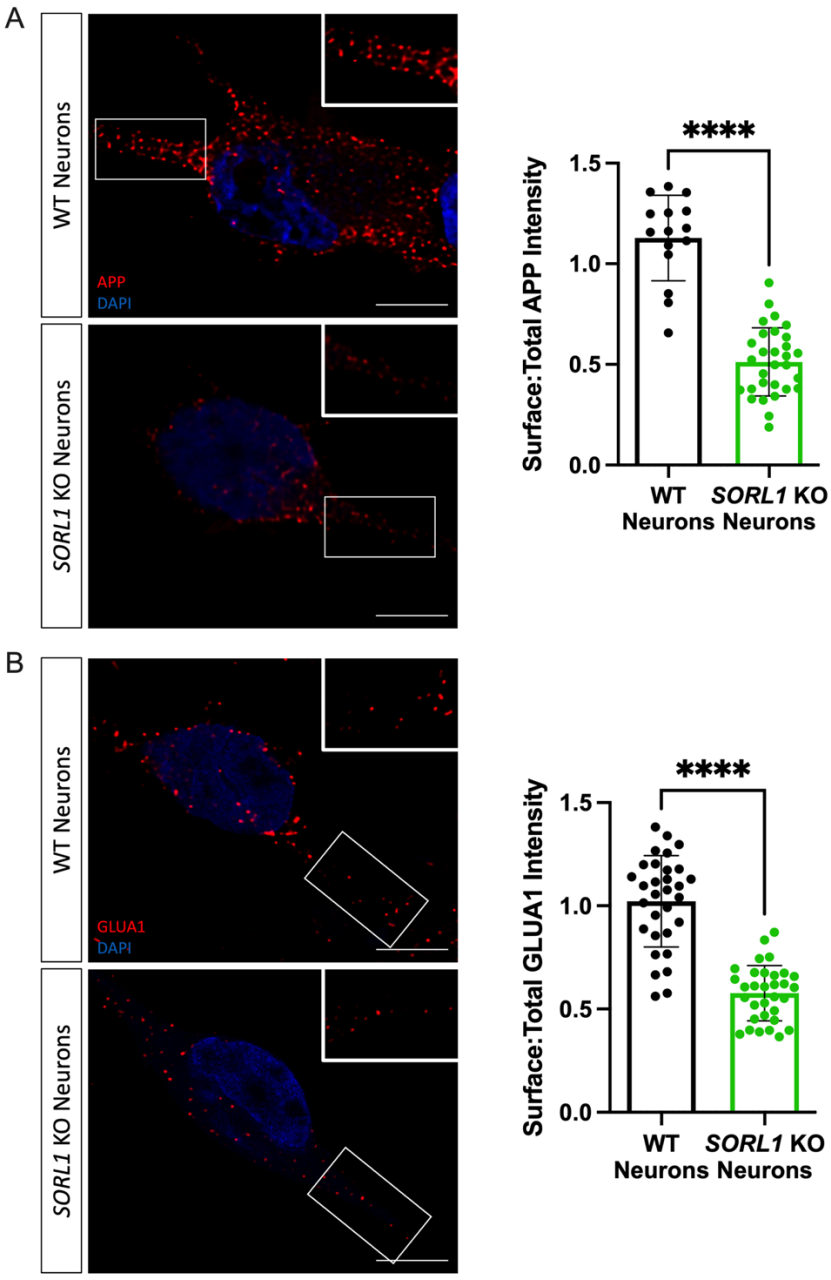

Figure 3.4. **Loss of *SORL1* expression impairs recycling to the cell surface**. **(a-b)** *SORL1*KO neurons show reduced cell surface expression of APP **(a)** and GLUA1 **(b)**. Representative immunofluorescent images of WT and *SORL1*KO neurons labeled with antibodies for APP **(a)** (red) and GLUA1 **(b)** (red). Scale bar: 5µm. Intensity of APP and GLUA1 measured using ImageJ software. Data is presented as a ratio of surface intensity to total intensity. Two isogenic clones of each genotype were used in all experiments. Data represented as mean ± SD. Normally distributed data was analyzed using parametric two-tailed unpaired t test. Significance was defined as a value of *$p < 0.05$, **$p < 0.01$, ***$p < 0.001$, and ****$p < 0.0001$

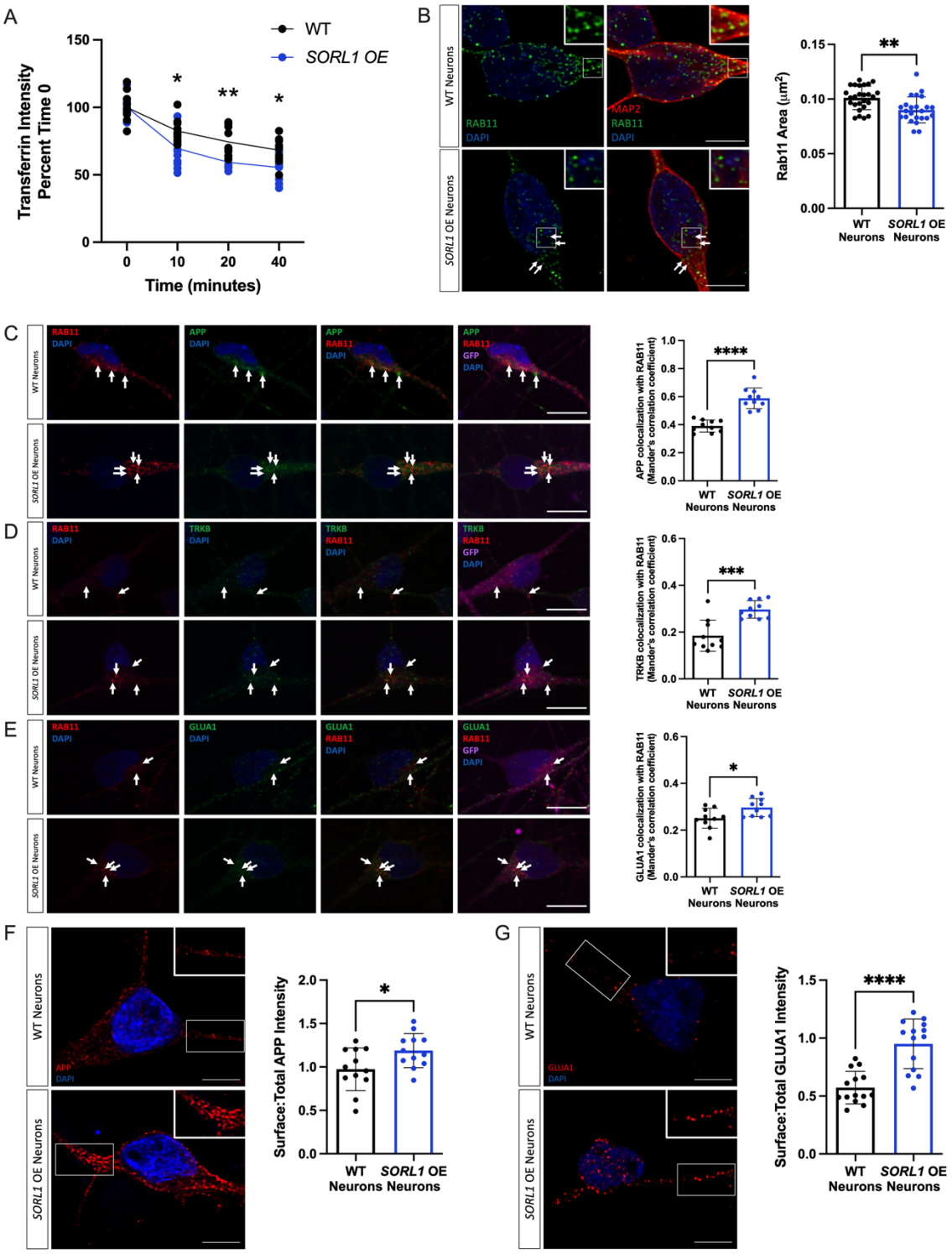

Figure 3.5. **Overexpression of *SORL1* enhances endosomal recycling. (a)** *SORL1*OE neurons show faster rate of transferrin recycling. Quantification of fluorescence intensity of intracellular transferrin at different time points after treating cells with Alexa Fluor 647-conjugated transferrin for 15 mins, using ImageJ software. Data represented as percent of time 0 fluorescence intensity.

(b) *SORL1*OE neurons show reduced size of recycling endosomes. Representative immunofluorescent images of WT and *SORL1*OE neurons labeled with Rab11 (green) and MAP2 (red) showing smaller Rab11 positive recycling endosomes in *SORL1*OE neurons. Nuclei counterstained with DAPI (blue). Quantification of Rab11+ recycling endosome size performed using Cell Profiler software and represented as area of Rab11+ vesicles. Scale bar: 5μm. Representative immunofluorescent images of WT and *SORL1*OE neurons showing increased colocalization of **(c)** APP (green), **(d)** TRKB (green) and **(e)** GLUA1 (green) with Rab11 (red) positive recycling endosomes. *SORL1*OE neurons and controls have endogenous GFP expression due to the piggybac vector system. GFP fluorescence is pseudo-colored (Far-red) and was used to outline cell bodies. Quantification of colocalization with Rab11 represented as Mander's Correlation Co-efficient (MCC). Scale bar: 10μm. Representative immunofluorescent images of WT and *SORL1*OE neurons showing increased cell surface expression of **(f)** APP (red) and **(g)** GLUA1 (red) in *SORL1*OE neurons. Scale bar: 5μm Fluorescence intensity of APP and GLUA1 measured using ImageJ software. Data is presented as a ratio of surface intensity to total intensity. Nuclei counterstained with DAPI. Two isogenic clones of each genotype were used in all experiments. Data represented as mean ± SD. Normally distributed data was analyzed using parametric two-tailed unpaired t test. Significance defined as a value of $*p < 0.05$, $**p < 0.01$, $***p < 0.001$, and $****p < 0.0001$

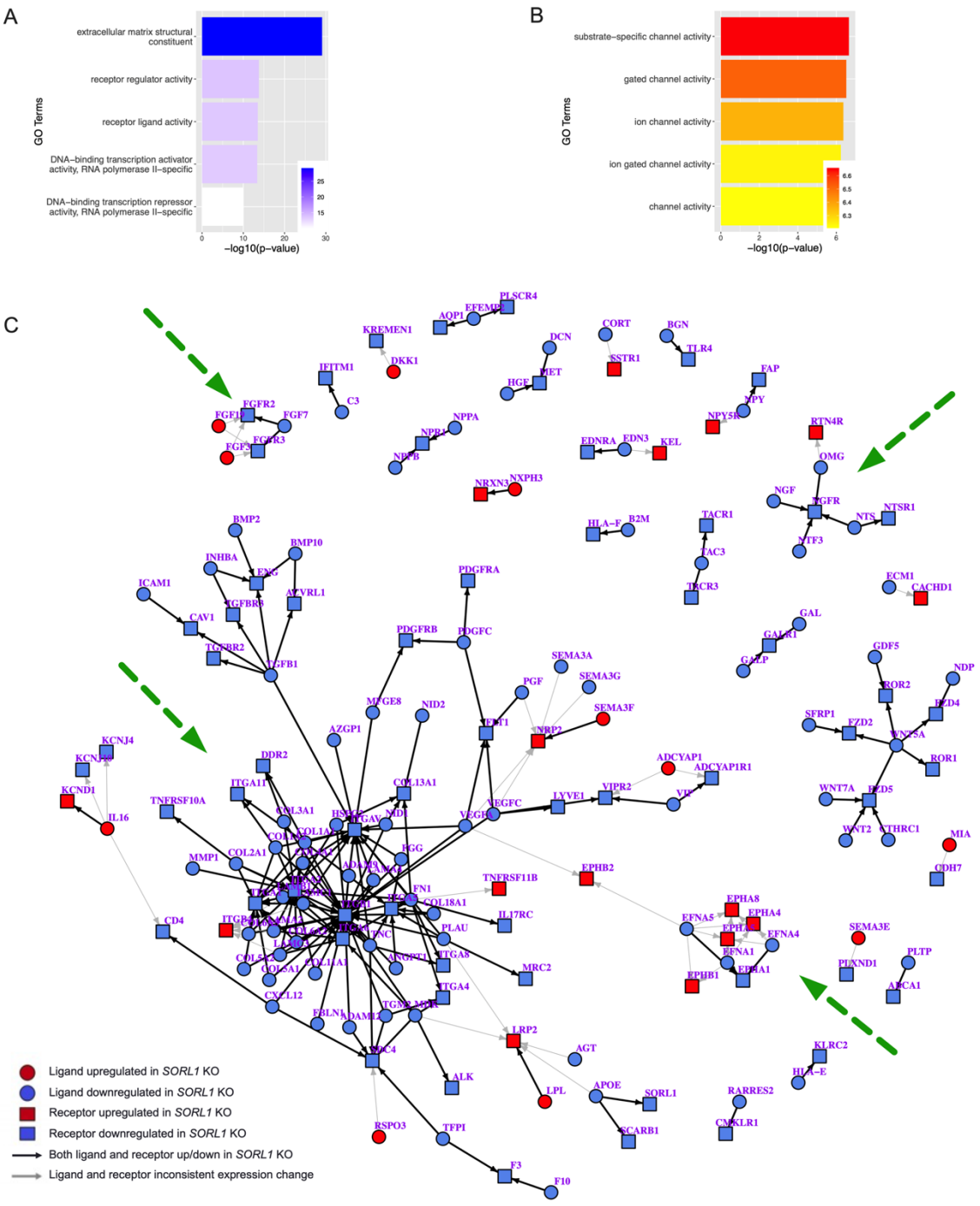

Figure 3.6. **Analysis of bulk RNA-sequencing data indicates alterations in cell surface and extracellular trafficking, receptor-ligand and channel activity**. Gene ontology analysis of DEGs in WT and *SORL1*KO neurons. Shown here are the top upregulated **(a)** and downregulated **(b)** molecular function terms in *SORL1*KO neurons. GO annotation terms are listed on the y-axis, adjusted p-value is shown on the x-axis. **(c)** Ligand-receptor network changes in *SORL1*KO

neurons, identified if genes are more than 1.5-fold increased or decreased in *SORL1*KO neurons with an adjusted p-value less than 0.05. Circles denote ligands, squares denote receptors, blue indicates genes expressed significantly lower in *SORL1*KO neurons, red indicates genes expressed significantly higher in *SORL1*KO neurons. Arrows point from ligand to receptor, denoting receptor-ligand interactions. Black arrows denote consistent expression changes between ligand and receptor, indicating that both genes in the pair are either upregulated or downregulated. Gray arrows denote inconsistent changes between ligand and receptor. Clusters impacted by cell surface recycling (b-integrins, ephrins) or neurotrophic signaling (FGF/FGFR, NGF/NGFR) are indicated by green dotted arrows.

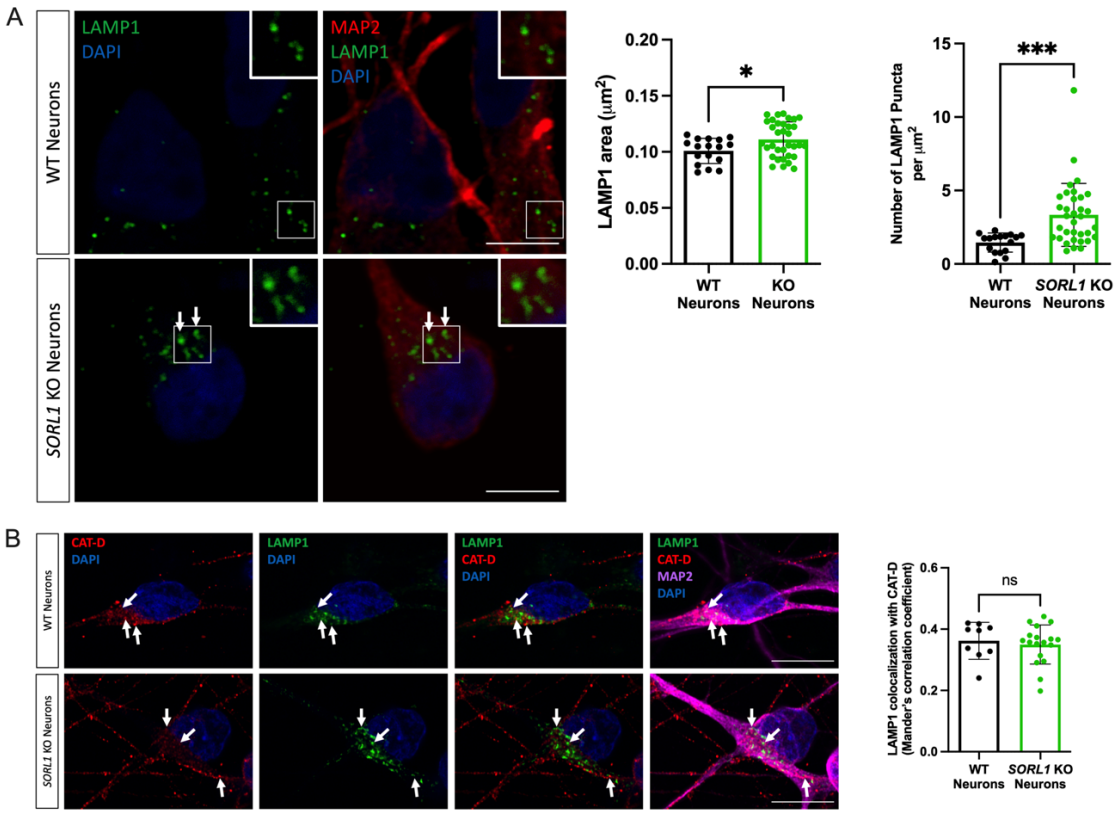

Figure 3.7. **Loss of *SORL1* alters lysosome size. (a)** *SORL1*KO neurons show larger lysosome size and increased lysosome number. Representative immunofluorescent images of WT and *SORL1*KO neurons labeled with LAMP1 (green) and MAP2 (red) showing increased LAMP1 positive vesicle size in *SORL1*KO neurons. Quantification of LAMP1 size and number was performed using Cell Profiler software. LAMP1 size is represented as area of LAMP1 positive vesicles, and LAMP1 number is represented as number of LAMP1 positive vesicles per square micron of cell area. Scale bar: 5µm **(b)** *SORL1*KO neurons show no change in colocalization of lysosomes with the lysosomal enzyme Cathepsin D. Representative immunofluorescent images of WT and *SORL1*KO neurons labeled with antibodies for LAMP1 (green), Cathepsin D (red) and MAP2 (Far-red) showing no alteration in colocalization of Cathepsin-D with LAMP1 in *SORL1*KO neurons. Nuclei counterstained with DAPI (blue). Scale bar: 10µm Quantification of colocalization of LAMP1 with Cathepsin-D represented as Mander's correlation coefficient (MCC). 10-20 images were analyzed per genotype. Two isogenic clones of each genotype were used in all experiments. Data represented as mean ± SD. Significance was determined using two-tailed unpaired Student's t-test and defined as a value of *$p < 0.05$, **$p < 0.01$, ***$p < 0.001$, and ****$p < 0.0001$.

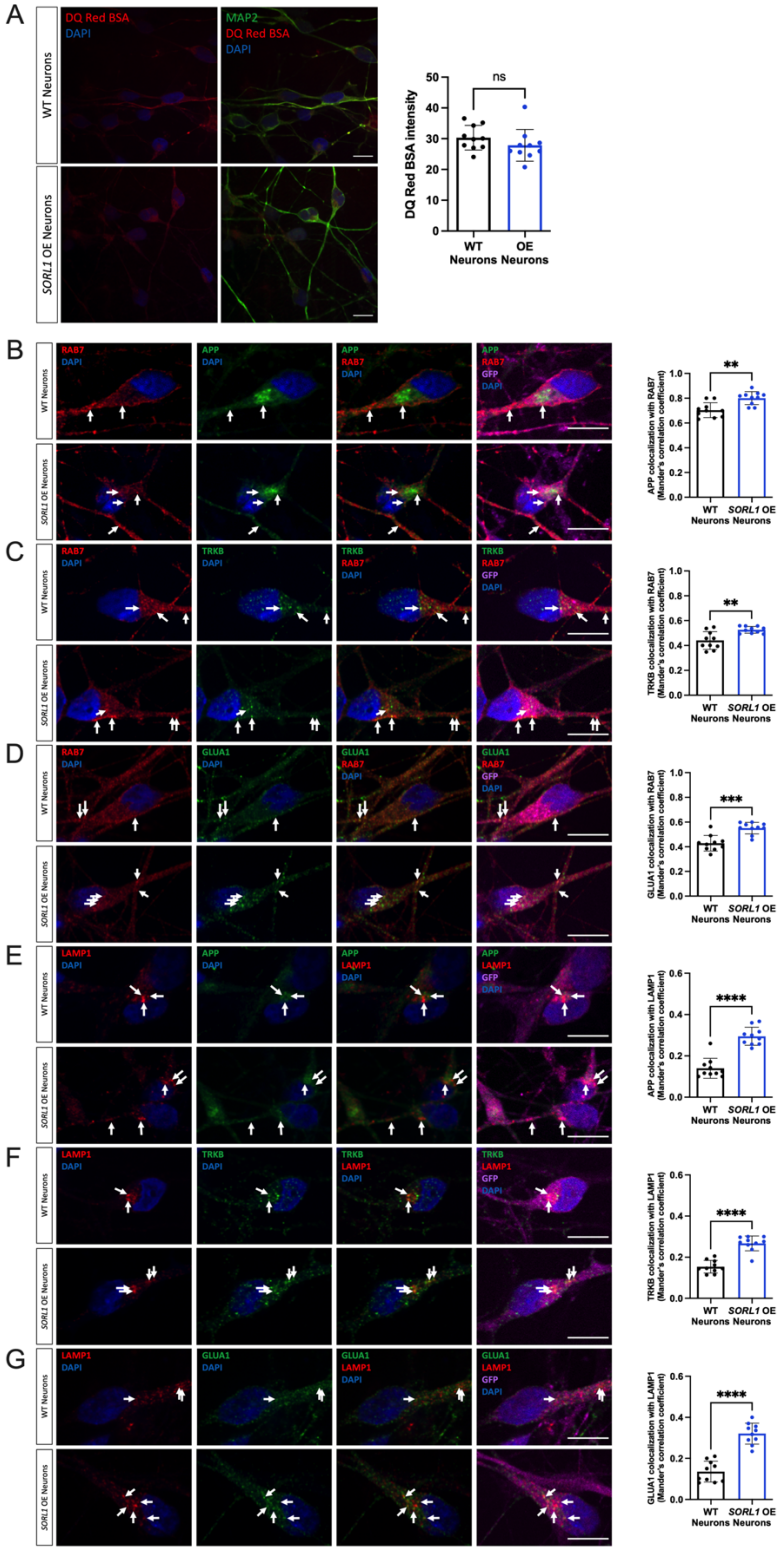

Figure 3.8. ***SORL1* overexpression alters degradative pathway trafficking**. **(a)** *SORL1*OE neurons show no change in lysosomal proteolytic activity as measured using DQ Red BSA. Representative immunofluorescent images of WT and *SORL1*OE neurons showing double

immunolabeling for MAP2 (green) and DQ Red BSA (red). Scale bar: 10μm. Quantification of fluorescence intensity of DQ Red BSA using ImageJ software. Representative immunofluorescent images of WT and *SORL1*OE neurons showing increased colocalization of APP, TRKB and GLUA1 (green) with Rab7 (red) **(b-d)** and LAMP1 (red) **(e-g)** in *SORL1*OE neurons. *SORL1*OE neurons and controls have endogenous GFP expression due to the piggybac vector system. GFP fluorescence is pseudo-colored (Far-red) and was used to outline cell bodies. Scale bar: 10μm. Nuclei are counterstained with DAPI (blue). In all cases, quantification of colocalization was represented as Mander's correlation co-efficient (MCC). 10-20 images were analyzed per genotype. Two isogenic clones of each genotype were used in all experiments. Data represented as mean ± SD. Significance was determined using two-tailed unpaired Student's t-test and was defined as a value of *$p < 0.05$, **$p < 0.01$, ***$p < 0.001$, and ****$p < 0.0001$.

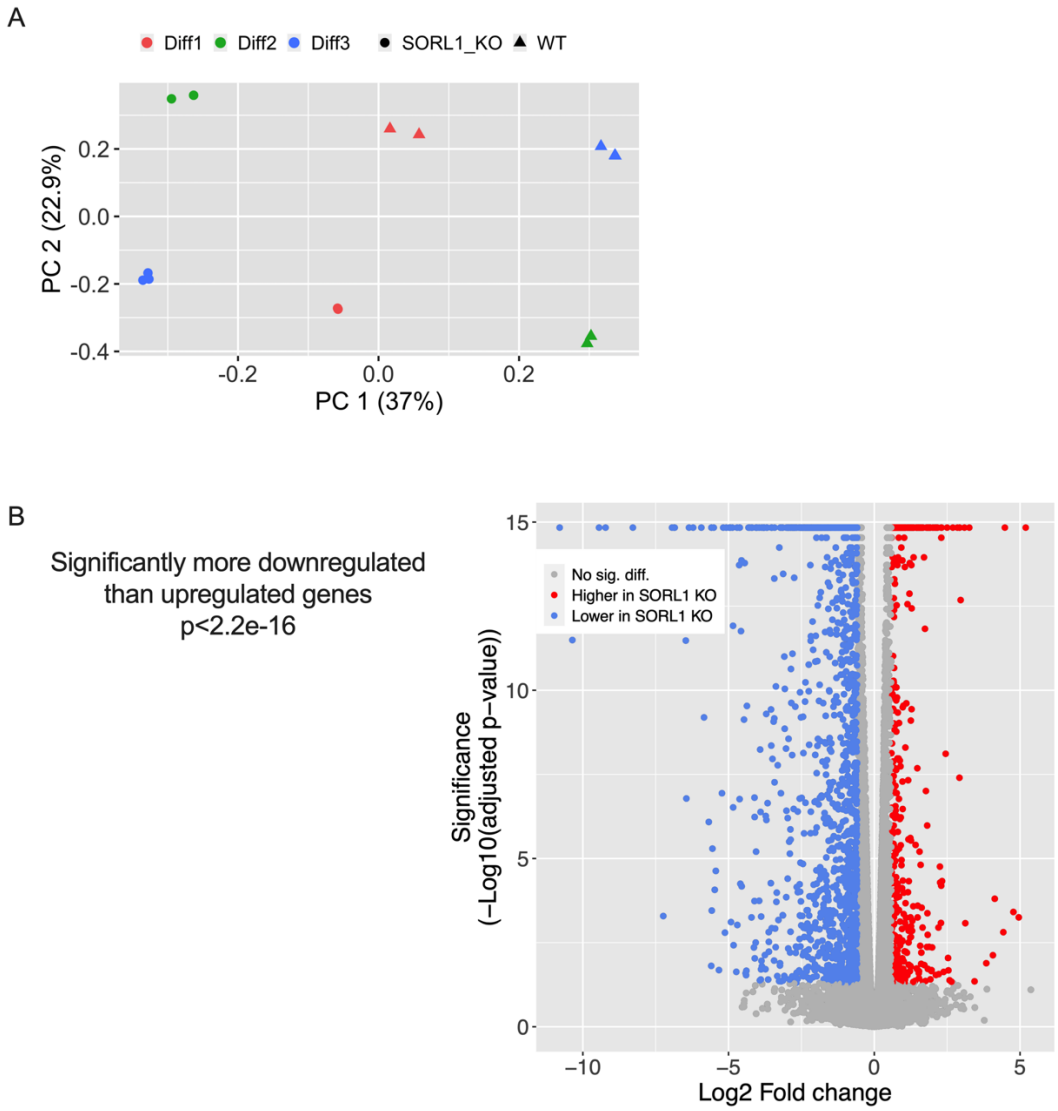

Figure 3.9. **Analysis of bulk RNAseq data from *SORL1*KO neurons**. **(a)** Principle component analysis (PCA) plot of all RNAseq samples using all expressed genes. Samples are color coded by differentiation batch. Triangles represent WT samples, circles represent *SORL1*KO. Genotype accounts for the highest variance (37%, PC1, x-axis). **b)** Volcano plot. Log2 fold change between *SORL1*KO and WT is shown along the x-axis. Statistical significance is shown along the y-axis and is measured by adjusted p-value. Genes upregulated in *SORL1*KO neurons are shown by red circles, genes downregulated in *SORL1*KO neurons are shown by blue circles. We observed 6643 DEGs, with 2819 upregulated and 3824 downregulated. There are significantly more down regulated genes than upregulated genes (p<2.2e-16). Grey circles represent genes that are not significantly differentially expressed.

3.3 DISCUSSION

Trafficking through the endo-lysosomal network regulates intra-cellular location of proteins, dictating their homeostasis, function and influence on cellular physiology. Functional studies by our group and others document endosomal abnormalities in hiPSC-derived neuronal models of AD(Hung et al., 2021; Knupp et al., 2020; Kwart et al., 2019). Emerging from this evidence is the role of *SORL1* as an endosomal gene that plays essential roles in mediating cargo trafficking. Recent work has implicated *SORL1* as AD's fourth causal gene(Olav M. Andersen, 2021; Scheltens et al., 2021), and of these genes it is the only one linked to the common late-onset form of the disease. Understanding *SORL1*'s function is paramount for understanding AD's pathogenic mechanisms and for potential therapeutic interventions.

Acting as a receptor of the retromer trafficking complex, SORLA has already been pathogenically linked to AD by its role in recycling APP out of endosomes(Andersen et al., 2005; Herskowitz et al., 2012; Offe et al., 2006). This current work and our previous study(Knupp et al., 2020) shows that *SORL1* depletion leads to increased APP localization in early and recycling endosomes. By lengthening the residence time of APP in these endosomal compartments, accelerated amyloidogenic cleavage of APP occurs due to the close proximity of APP and BACE1(Sun and Roy, 2018). Indeed, loss of *SORL1* leads to the accumulation of Ab peptides, an antecedent of 'amyloid pathology' (Andersen et al., 2005; Knupp et al., 2020; Rogaeva et al., 2007b). We hypothesized that loss of *SORL1* in neurons would impact other cargo important for healthy neuronal function. To test this hypothesis, in addition to APP, we examined localization of the neurotrophin receptor TRKB and the GLUA1 subunit of the AMPA receptor. These cargo link to another key pathology of AD: neurodegeneration, a slowly progressive process that begins with synaptic dysfunction characterized by glutamate receptor

loss, which then progresses to synaptic loss before ultimately, over years, leading to widespread neuronal cell death (Selkoe, 2002).

Our experiments point to *SORL1*'s key role in cell surface recycling. By using a prototypical cargo, transferrin, we demonstrate a reciprocal role between loss and enhancement of *SORL1* expression in cell surface recycling. Specifically, by showing that *SORL1* plays a role in recycling glutamate receptors, a trafficking event critical for preventing synaptic dysfunction and synaptic loss, our results link *SORL1* to AD's early-stage neurodegenerative process. Since retromer-dependent glutamate receptor recycling has been shown to occur independent of APP(Temkin et al., 2017), our results suggest that *SORL1* mutations can, at least in principle, drive two key AD pathologies, amyloid pathology and synaptic pathology, through parallel mechanisms(Small and Petsko, 2020).

Interestingly, AD's defining cytopathology, swollen endosomes, also seems to occur independent of Aβ peptides. In the case of early-onset causal genes, studies have shown that APP and PSEN mutations lead to endosomal swelling even when the production of Aβ peptides are arrested, but is driven instead by an APP intermediate, the β -C-terminal fragment produced by BACE1 cleavage(Kwart et al., 2019). We previously demonstrated that endosomal swelling occurs in *SORL1*KO neurons even when BACE1 is inhibited(Knupp et al., 2020). However, a recent study showed that there is a reduction in endosomal swelling when total APP expression is reduced(Hung et al., 2021). One interpretation that reconciles these findings is that reduction of cargo in general, especially one as abundant as APP, may relieve some of the stress on neuronal endosomes induced by *SORL1* deficiency. Collectively, however, our data suggest that AD's core histopathology, amyloid plaques, and cytopathology, swollen endosomes, occur through parallel events.

To test the hypothesis that *SORL1* functions more broadly in neuronal endosomal recycling, we measured recycling endosome size and showed that, in addition to APP and GLUA1, the neurotrophin receptor TRKB, is dependent on *SORL1* for normal endosomal trafficking. TRKB is part of a different family of proteins that depend on retromer-dependent endosomal recycling for its normal trafficking, and one that has been linked to synaptic health(Klinger et al., 2015; Rohe et al., 2013) (Patapoutian and Reichardt, 2001).

Our unbiased transcriptomic screen further supported that neurotrophic signaling and cell surface recycling pathways are impacted by *SORL1* deficiency. Our goal for this analysis was to determine the global effect of *SORL1* loss on neuronal networks. Indeed, our analysis does not show that the specific cargo proteins described here are differentially expressed. However, the analysis does indicate that loss of *SORL1* in human neurons impacts cell surface networks, including receptor ligand interactions in neurotrophic and growth factor pathways, b-integrin signaling, and ephrin signaling. Our analysis corroborates previous work and the altered networks we observe impact neuronal health, axonal guidance, and synapse formation(Huang et al., 2017; Huang et al., 2006; Pietila et al., 2019).

The early endosome is considered the central station in the sorting and trafficking of cargo throughout the many stations of the endo-lysosomal system. While the early endosome is the station that is affected first and foremost in AD, it is not surprising that a primary dysfunction in this central station will secondarily influence trafficking throughout the system. Our work, along with other recent work(Hung et al., 2021) also supports a role for *SORL1* in lysosomal trafficking in neurons. We observed an increase in lysosome size and altered localization of APP, TRKB, and GLUA1 in late endosomes and lysosomes in *SORL1*KO neurons. Hung et al., also reported decreased Cathepsin-D activity in *SORL1* deficient neurons, suggesting that *SORL1*

loss directly impacts lysosome function. We interpret our functional and colocalization data to suggest that loss of *SORL1* expression mainly affects trafficking of cargo to lysosomes, but our data does not rule out a role of SORLA in neuronal lysosome function. While we did not observe a difference in Cathepsin-D localization to lysosomes, it is important to note that that LAMP1 only partially colocalizes with Cathepsin-D in neurons (Cheng et al., 2018). Furthermore, the loss of proteolytic activity evidenced by decreased intensity of DQ Red BSA in *SORL1*KO neurons may not be completely due to reduced trafficking to lysosomes but could be a result of abnormal lysosomal function as DQ Red BSA is internalized by a process called macropinocytosis wherein macropinosomes can be directly trafficked to lysosomes (Hamasaki et al., 2004; Lorenzen et al., 2010; Racoosin and Swanson, 1993). Thus, the loss of proteolytic activity evidenced by decreased intensity of DQ Red BSA in *SORL1*KO neurons may not be completely due to reduced trafficking to lysosomes but could also be a result of abnormal lysosomal function.

In this work, we report that *SORL1* depletion affects endosomal trafficking by retaining cargo in early and recycling endosomes and impacts cell surface recycling and lysosomal trafficking of neuronal cargo. In particular, we demonstrate that *SORL1* expression in neurons affects cell surface localization of GLUA1, a phenotype that may ultimately impact synaptic dysfunction and neurodegeneration in AD. Interestingly, increasing SORL1 expression enhances endosomal recycling and increases cell surface GLUA1. While the secondary downstream effects induced by *SORL1* depletion in the endo-lysosomal system are interesting and likely relevant to AD's ultimate pathogenesis, from a therapeutic perspective it is best to target *SORL1*'s primary defect, which seems to localize to the endosomal recycling pathway. Interestingly, recent biomarker studies suggest that defects in retromer-dependent endosomal

recycling occur in a majority of patients with 'sporadic' AD(Simoes et al., 2020), suggesting that the observed *SORL1*-induced defects may generalize across early and late onset forms of the disorder. Collectively, our results support the conclusion that *SORL1*, and the retromer-dependent pathway in which it functions, is a valid therapeutic target and interventions directed at this pathway may ameliorate endosomal recycling defects that seem to act as, at least, one primary driver of AD.

3.4 METHODS

3.4.1 *Cell Lines Generated by CRISPR/Cas9 Gene Editing Technology*

The generation of the cell lines used in this paper is described in our previously published work(Knupp et al., 2020) and consists of four clones: Two wild-type clones, designated clone A6 and clone A7, and two *SORL1*KO clones, designated clone E1 and clone E4. Cell lines were generated from our previously published and characterized CV background human induced pluripotent stem cell line(Young et al., 2015). This cell line is male and has a APOE ε3/ε4 genotype(Levy et al., 2007). All four clones were shown to have normal karyotypes and are routinely tested for mycoplasma (MycoAlert).

3.4.2 *CRISPR/Cas9 gRNA, ssODN, and Primer Sequences*

gRNA: ATTGAACGACATGAACCCTC

ssODN:

GGGAATTGATCCCTATGACAAACCAAATACCATCTACATTGAACGACATGAACCCTC

TGGCTACTCCACGTCTTCCGA

AGTACAGATTTCTTCCAGTCCCGGGAAAACCAGGAAG

Forward primer: ctctatcctgagtcaaggagtaac

Reverse primer: ccttccaattcctgtgtatgc

PCR amplifies 458 bp sequence. These sequences have been previously published in (Knupp et al., 2020)

3.4.3 *SORL1 Overexpression Cell Lines*

Isogenic cell lines with overexpression of *SORL1* were generated as previously described(Young et al., 2015). These lines are generated from the CV parental line, the same parental line as the *SORL1*KO cell lines were made from. Briefly, stable integration of *SORL1* cDNA into the genome was achieved by using piggybac transposon system (Systems Biosciences). Vector alone (WT) or vector with *SORL1* cDNA (*SORL1*OE) constructs were introduced into iPSCs by electroporation and stable cell lines were selected with puromycin (2μg/ml) treatment. For all overexpression experiments *SORL1*OE cells were compared to the vector alone controls.

3.4.4 *hiPSC Neuronal Differentiation*

hiPSCs were differentiated to neurons using dual-SMAD inhibition(Chambers et al., 2009; Shi et al., 2012). Briefly, hiPSCs were plated on Matrigel coated 6-well plates at a density of 3.5 million cells per well and fed with Basal Neural Maintenance Media (1:1 DMEM/F12 + glutamine media/neurobasal media, 0.5% N2 supplement, 1% B27 supplement, 0.5% GlutaMax, 0.5% insulin-transferrin-selenium, 0.5% NEAA, 0.2% β-mercaptoethanol; Gibco, Waltham, MA) + 10mM SB-431542 + 0.5mM LDN-193189 (Biogems, Westlake Village, CA). Cells were fed daily for seven days. On day eight, cells were incubated with Versene, gently dissociated using cell scrapers, and passaged at a ratio of 1:3. On day nine, media was switched to Basal Neural Maintenance Media and fed daily. On day 13, media was switched to Basal Neural

Maintenance Media with 20 ng/mL FGF (R&D Systems, Minneapolis, MN) and fed daily. On day sixteen, cells were passaged again at a ratio of 1:3. Cells were fed until approximately day twenty-three. At this time, cells were FACS sorted to obtain the CD184/CD24 positive, CD44/CD271 negative neural precursor cell (NPC) population. Following sorting, NPCs were expanded for neural differentiation. For cortical neuronal differentiation, NPCs were plated out in 10cm cell culture dishes at a density of 6 million cells/10cm plate. After 24 hours, cells were switched to Neural Differentiation media (DMEM-F12 + glutamine, 0.5% N2 supplement, 1% B27 supplement, 0.5% GlutaMax) + 0.02ug/mL brain-derived neurotrophic factor (PeproTech, Rocky Hill, NJ) + 0.02ug/mL glial-cell-derived neurotrophic factor (PeproTech) + 0.5mM dbcAMP (Sigma Aldrich, St Louis, MO). Media was refreshed twice a week for three weeks. After three weeks, neurons were selected for CD184/CD44/CD271 negative population by MACS sorting and plated for experiments.

3.4.5 *Purification of Neurons*

Following three weeks of differentiation, neurons were dissociated with accutase and resuspended in Magnet Activated Cell Sorting (MACS) buffer (PBS + 0.5% bovine serum albumin [Sigma Aldrich, St Louis, MO] + 2mM ethylenediaminetetraacetic acid [Thermo Fisher Scientific, Waltham, MA]). Following a modification of (Yuan et al., 2011), cells were incubated with PE-conjugated mouse anti-Human CD44 and mouse anti-Human CD184 antibodies (BD Biosciences, San Jose, CA) at a concentration of 5µl/10 million cells. Following antibody incubation, cells were washed with MACS buffer and incubated with anti-PE magnetic beads (BD Biosciences, San Jose, CA) at a concentration of 25µl/10 million cells. Bead-antibody complexes were pulled down using a rare earth magnet, supernatants were selected, washed, and plated at an appropriate density.

3.4.6 *DQ Red BSA Assay for Visualization of Lysosomal Degradation*

Lysosomal proteolytic degradation was evaluated using DQ Red BSA (#D-12051; Thermo Fisher Scientific), a fluorogenic substrate for lysosomal proteases, that generates fluorescence only when enzymatically cleaved in intracellular lysosomal compartments. hiPSC-derived neurons were seeded at a density of 400,000 cells/well of a matrigel coated 48 well plate. After 24 hours, cells were washed once with DPBS, treated with complete media containing either 10µg/ml DQ Red BSA or vehicle (PBS) and incubated for 5 hours at 37°C in a 5% CO_2 incubator as described in(Marwaha and Sharma, 2017). At the end of 5 hours, cells were washed with PBS, fixed with 4% PFA and immunocytochemistry was performed as described in methods. Cells were imaged using a Leica SP8 confocal microscope and all image processing was completed with ImageJ software. Cell bodies were identified by MAP2 labeling, and fluorescence intensity of DQ Red BSA was measured in regions of the images containing the MAP2 label.

3.4.7 *Immunocytochemistry*

For immunocytochemistry, cells were fixed with 4% PFA for 20 minutes. Fixed cells were washed three times with PBST (PBS with 0.05% tween 20), permeabilized with Triton X-100 in PBS for 15 minutes, washed twice again with PBST, blocked with 5% BSA in PBS at room temperature for 1h and incubated with appropriate primary antibodies overnight at 4°C. The next day, cells were incubated with appropriate secondary antibodies and 1µg/ml DAPI for 1 hour at RT, washed three times with PBST and mounted on glass slides with Prolong Gold Antifade mountant (#P36930; Thermo Fisher Scientific).

3.4.8 *Colocalization Analysis*

To investigate colocalization with endo-lysosomal compartments, hiPSC-derived neurons were labeled with markers specific for each intra-cellular compartment (EEA1 for early endosomes, Rab7 for late endosomes, LAMP1 for lysosomes and Rab11 for recycling endosomes) using immunocytochemistry. A minimum of 10 fields of confocal z-stack images were captured under blinded conditions using a Yokogawa W1 spinning disk confocal microscope (Nikon) and a 100X plan apochromat oil immersion objective. Median filtering was used to remove noise from images and Otsu thresholding was applied to all images. Colocalization was quantified using the JACOP plugin(Bolte and Cordelieres, 2006) in Image J software(Schindelin et al., 2012) and presented as Mander's correlation coefficient(Dunn et al., 2011; Manders et al., 1993).

3.4.9 *Cell Surface Staining*

Cell surface expression of GLUA1 and APP was determined using immunocytochemistry and confocal microscopy. To label proteins at the cell surface, cells were fixed with 4% PFA, washed and treated with primary and secondary antibodies as described in the '*Immunocytochemistry*' section of methods. Permeabilization with 0.1% Triton X-100 was not performed for this experiment. To label total protein levels, cells were fixed with 4% PFA, washed, permeabilized with 0.1% Triton X-100 and treated with primary and secondary antibodies as described in the 'immunocytochemistry' section of methods. Analysis of fluorescence intensity was done using Image J software. Cell surface expression was represented as ratio of fluorescence intensity measured under non-permeabilized conditions and fluorescence intensity measured under permeabilized conditions.

3.4.10 *Antibodies*

The following primary antibodies were used: Early endosome antigen 1 (EEA1) at 1:500 (#610456; BD Biosciences); amyloid precursor protein (APP) at 1:500 (#ab32136; Abcam); microtubule-associated protein 2 (MAP2) at 1:1000 (ab92434; Abcam); Ras-related protein Rab-7a (Rab7) at 1:1000 (ab50533; Abcam); Ras-related protein Rab-11 (Rab11) at 1:250 (#610656; BD Biosciences); Lysosome associated membrane protein-1 (LAMP1) at 1:250 (#sc 2011; Santa Cruz); Tropomyosin receptor kinase B (TRKB; # ab18987; abcam) and GLUA1(# MAB2263; Millipore sigma) at 1:500(DAPI at 1 mg/mL final (Alfa Aesar).

3.4.11 *Transferrin Recycling Assay*

To measure recycling pathway function, we utilized transferrin recycling assay as previously described(Rapaport et al., 2010). Purified neurons were seeded at 400,000 cells/well of a 24 well plate containing matrigel coated 12 mm glass coverslip/well. After 5 DIV, cells were washed once with DMEM-F12 medium and incubated with starving medium (DMEM-F12 medium+25mM HEPES+ 0.5% BSA) for 30 minutes at 37°C in a 5% CO_2 incubator to remove any residual transferrin. Thereafter, cells were pulsed with either 100µg/ml transferrin from human serum conjugated with Alexa Fluor™ 647(#T23366; Thermo Fisher Scientific) or vehicle (PBS) in 'starving medium'. At the end of 10 mins, cells were washed twice with ice-cold PBS to remove any external transferrin and stop internalization of transferrin and washed once with acid stripping buffer (25mM citric acid+24.5mM sodium citrate+280mM sucrose+0.01mM Deferoxamine) to remove any membrane bound transferrin. Next, cells were either fixed in 4% PFA or 'Chase medium' (DMEM-F12+50µM Deferoxamine+20mM HEPES+500µg/ml Holo-transferrin) was added for different time points. Immunocytochemistry was done using MAP2 antibody to label neurons, confocal images were captured using Leica SP8 confocal microscope

under blinded conditions. Fluorescence intensity of transferrin was measured using ImageJ software. Recycling function was presented as transferrin fluorescence intensity as a percentage of the fluorescence intensity measured at time zero.

3.4.12 *Measurement of Lysosome and Recycling Endosome Size*

Immunocytochemistry using antibodies for LAMP1 and MAP2 or RAB11 and MAP2 was performed as described above. Using a Leica SP8 confocal microscope with an apochromatic 63X oil immersion lens, z-stack images were obtained under blinded conditions. For the LAMP1 analysis, 17-34 fields were analyzed for a total of 45 – 76 cells analyzed. For the RAB11 analysis, 15-30 fields were analyzed for a total of 59 – 124 cells analyzed. Vesicle size measurements were performed using Cell Profiler software as previously described (Knupp et al., 2020) (McQuin et al., 2018). Briefly, the vesicle channel was masked using the MAP2 channel and automated segmentation algorithms were used to identify individual puncta. The pixel area of each puncta was measured and is presented as mean area of all puncta per field.

3.4.13 *Statistical Analysis*

For all the experiments, at least two independent clones of each genotype were used. For all imaging experiments the data was analyzed in a blinded manner. Experimental data was tested for normal distributions using the ShapiroWilk normality test. Normally distributed data was analyzed using parametric two-tailed unpaired t tests. Non-normally distributed data was analyzed by non-parametric Mann-Whitney test. Significance was defined as a value of $p > 0.05$. All statistical analysis was completed using GraphPad Prism software. Statistical details of individual experiments, including biological and technical replicate information, can be found in the figure legends.

3.4.14 *RNA Extraction*

RNA was collected from 3 separate differentiations including a combination of two WT clones and two *SORL1*KO clones. Each sample includes 2-3 technical replicates. RNA was collected from 2 million purified neurons for each sample. Purification of total RNA was completed using the PureLink RNA Mini Kit (Thermo Fisher 12183018A). Assessment of purified RNA was completed using a NanoDrop. Final RNA quantification was completed using the Quant-iT RNA assay (Invitrogen) and RNA integrity analysis was completed using a fragment analyzer (Advanced Analytical).

3.4.15 *RNA Library Prep and Sequencing*

Library preparation was completed using the TruSeq Stranded mRNA kit (Illumina RS-122-2103) per manufacturer instructions. Sequencing was performed on a NovaSeq 6000 instrument.

3.4.16 *RNAseq Data Analysis*

Raw reads were aligned to GRCh38 with reference transcriptome GENCODE release 29 using STAR v2.6.1d (Dobin et al. 2013). Gene-level expression quantification is generated by RSEM v1.3.1(Li and Dewey, 2011). Genes with fewer than 20 normalized reads across all samples were omitted from further analysis. We did observe variation in the transcriptome based on differentiation (**Figure 3.9A**), however this was corrected for using the sva package(Leek et al., 2012).

To identify differentially expressed genes (DEGs), we used DESeq (Anders and Huber 2010). Briefly, we fit two models: a null model where gene expression only depends on batch effects (i.e., differentiation), and an alternative model where gene expression depends on both

genotype (*SORL1*KO vs. WT) and batch effects. Chi-squared tests were performed to compare both fits, and we declare a gene as differentially expressed only when the alternative model fits the expression data better. DEGs are defined as genes with false discovery rate less than 0.05 and fold change greater than 1.5. The top gene ontology (GO) package (Alexa and Rahnenfuhrer 2021) was used to identify GO terms that were enriched. GO terms were tested according to the Fisher's exact test. Finally, we mapped DEGs onto receptor-ligand interaction diagrams generated by Ramilowski et al(Ramilowski et al., 2015) using the igraph plugin (Csardi and Nepusz, 2006). To compare the amount of down-regulated vs. up-regulated genes we used a 2-sample test for equality of proportions with continuity correction in R.

3.5 REFERENCES

Andersen, O.M., Reiche, J., Schmidt, V., Gotthardt, M., Spoelgen, R., Behlke, J., von Arnim, C.A., Breiderhoff, T., Jansen, P., Wu, X.*, et al.* (2005). Neuronal sorting protein-related receptor sorLA/LR11 regulates processing of the amyloid precursor protein. Proc Natl Acad Sci U S A *102*, 13461-13466.

Bolte, S., and Cordelieres, F.P. (2006). A guided tour into subcellular colocalization analysis in light microscopy. J Microsc *224*, 213-232.

Caglayan, S., Takagi-Niidome, S., Liao, F., Carlo, A.S., Schmidt, V., Burgert, T., Kitago, Y., Fuchtbauer, E.M., Fuchtbauer, A., Holtzman, D.M.*, et al.* (2014). Lysosomal sorting of amyloid-beta by the SORLA receptor is impaired by a familial Alzheimer's disease mutation. Science translational medicine *6*, 223ra220.

Cataldo, A.M., Peterhoff, C.M., Troncoso, J.C., Gomez-Isla, T., Hyman, B.T., and Nixon, R.A. (2000). Endocytic pathway abnormalities precede amyloid beta deposition in sporadic Alzheimer's disease and Down syndrome: differential effects of APOE genotype and presenilin mutations. Am J Pathol *157*, 277-286.

Chambers, S.M., Fasano, C.A., Papapetrou, E.P., Tomishima, M., Sadelain, M., and Studer, L. (2009). Highly efficient neural conversion of human ES and iPS cells by dual inhibition of SMAD signaling. Nat Biotechnol *27*, 275-280.

Cheng, X.-T., Xie, Y.-X., Zhou, B., Huang, N., Farfel-Becker, T., and Sheng, Z.-H. (2018). Characterization of LAMP1-labeled nondegradative lysosomal and endocytic compartments in neurons. J Cell Biol *217*, 3127-3139.

Choi, J.H., Kaur, G., Mazzella, M.J., Morales-Corraliza, J., Levy, E., and Mathews, P.M. (2013). Early endosomal abnormalities and cholinergic neuron degeneration in amyloid-beta protein precursor transgenic mice. J Alzheimers Dis *34*, 691-700.

Das, U., Wang, L., Ganguly, A., Saikia, J.M., Wagner, S.L., Koo, E.H., and Roy, S. (2016). Visualizing APP and BACE-1 approximation in neurons yields insight into the amyloidogenic pathway. Nat Neurosci *19*, 55-64.

de Araujo, M.E.G., Liebscher, G., Hess, M.W., and Huber, L.A. (2020). Lysosomal size matters. Traffic *21*, 60-75.

Devi, L., and Ohno, M. (2015). TrkB reduction exacerbates Alzheimer's disease-like signaling aberrations and memory deficits without affecting β-amyloidosis in 5XFAD mice. Translational psychiatry *5*, e562-e562.

Dewar, D., Chalmers, D.T., Graham, D.I., and McCulloch, J. (1991). Glutamate metabotropic and AMPA binding sites are reduced in Alzheimer's disease: an autoradiographic study of the hippocampus. Brain Res *553*, 58-64.

Dodson, S.E., Gearing, M., Lippa, C.F., Montine, T.J., Levey, A.I., and Lah, J.J. (2006). LR11/SorLA expression is reduced in sporadic Alzheimer disease but not in familial Alzheimer disease. J Neuropathol Exp Neurol *65*, 866-872.

Dunn, K.W., Kamocka, M.M., and McDonald, J.H. (2011). A practical guide to evaluating colocalization in biological microscopy. Am J Physiol Cell Physiol *300*, C723-C742.

Farfel-Becker, T., Roney, J.C., Cheng, X.T., Li, S., Cuddy, S.R., and Sheng, Z.H. (2019). Neuronal Soma-Derived Degradative Lysosomes Are Continuously Delivered to Distal Axons to Maintain Local Degradation Capacity. Cell Rep *28*, 51-64.e54.

Fjorback, A.W., Seaman, M., Gustafsen, C., Mehmedbasic, A., Gokool, S., Wu, C., Militz, D., Schmidt, V., Madsen, P., Nyengaard, J.R.*, et al.* (2012). Retromer binds the FANSHY sorting

motif in SorLA to regulate amyloid precursor protein sorting and processing. The Journal of neuroscience : the official journal of the Society for Neuroscience *32*, 1467-1480.
Ginsberg, S.D., Malek-Ahmadi, M.H., Alldred, M.J., Chen, Y., Chen, K., Chao, M.V., Counts, S.E., and Mufson, E.J. (2019). Brain-derived neurotrophic factor (BDNF) and TrkB hippocampal gene expression are putative predictors of neuritic plaque and neurofibrillary tangle pathology. Neurobiology of Disease *132*, 104540.
Gowrishankar, S., Yuan, P., Wu, Y., Schrag, M., Paradise, S., Grutzendler, J., De Camilli, P., and Ferguson, S.M. (2015). Massive accumulation of luminal protease-deficient axonal lysosomes at Alzheimer's disease amyloid plaques. Proceedings of the National Academy of Sciences *112*, E3699-E3708.
Grant, B.D., and Donaldson, J.G. (2009). Pathways and mechanisms of endocytic recycling. Nat Rev Mol Cell Biol *10*, 597-608.
Hamasaki, M., Araki, N., and Hatae, T. (2004). Association of early endosomal autoantigen 1 with macropinocytosis in EGF-stimulated A431 cells. Anat Rec A Discov Mol Cell Evol Biol *277*, 298-306.
Herskowitz, J.H., Offe, K., Deshpande, A., Kahn, R.A., Levey, A.I., and Lah, J.J. (2012). GGA1-mediated endocytic traffic of LR11/SorLA alters APP intracellular distribution and amyloid-beta production. Mol Biol Cell *23*, 2645-2657.
Holstege, H., van der Lee, S.J., Hulsman, M., Wong, T.H., van Rooij, J.G., Weiss, M., Louwersheimer, E., Wolters, F.J., Amin, N., Uitterlinden, A.G.*, et al.* (2017). Characterization of pathogenic SORL1 genetic variants for association with Alzheimer's disease: a clinical interpretation strategy. Eur J Hum Genet *25*, 973-981.
Huang, T.Y., Zhao, Y., Jiang, L.L., Li, X., Liu, Y., Sun, Y., Pina-Crespo, J.C., Zhu, B., Masliah, E., Willnow, T.E.*, et al.* (2017). SORLA attenuates EphA4 signaling and amyloid beta-induced neurodegeneration. J Exp Med *214*, 3669-3685.
Huang, T.Y., Zhao, Y., Li, X., Wang, X., Tseng, I.C., Thompson, R., Tu, S., Willnow, T.E., Zhang, Y.W., and Xu, H. (2016). SNX27 and SORLA Interact to Reduce Amyloidogenic Subcellular Distribution and Processing of Amyloid Precursor Protein. The Journal of neuroscience : the official journal of the Society for Neuroscience *36*, 7996-8011.
Huang, Z., Shimazu, K., Woo, N.H., Zang, K., Muller, U., Lu, B., and Reichardt, L.F. (2006). Distinct roles of the beta 1-class integrins at the developing and the mature hippocampal excitatory synapse. The Journal of neuroscience : the official journal of the Society for Neuroscience *26*, 11208-11219.
Hung, C., Tuck, E., Stubbs, V., van der Lee, S.J., Aalfs, C., van Spaendonk, R., Scheltens, P., Hardy, J., Holstege, H., and Livesey, F.J. (2021). SORL1 deficiency in human excitatory neurons causes APP-dependent defects in the endolysosome-autophagy network. Cell Rep *35*, 109259.
Hwang, J., Estick, C.M., Ikonne, U.S., Butler, D., Pait, M.C., Elliott, L.H., Ruiz, S., Smith, K., Rentschler, K.M., Mundell, C.*, et al.* (2019). The Role of Lysosomes in a Broad Disease-Modifying Approach Evaluated across Transgenic Mouse Models of Alzheimer's Disease and Parkinson's Disease and Models of Mild Cognitive Impairment. Int J Mol Sci *20*.
Karch, C.M., and Goate, A.M. (2015). Alzheimer's disease risk genes and mechanisms of disease pathogenesis. Biol Psychiatry *77*, 43-51.
Klinger, S.C., Siupka, P., and Nielsen, M.S. (2015). Retromer-Mediated Trafficking of Transmembrane Receptors and Transporters. Membranes (Basel) *5*, 288-306.

Knupp, A., Mishra, S., Martinez, R., Braggin, J.E., Szabo, M., Kinoshita, C., Hailey, D.W., Small, S.A., Jayadev, S., and Young, J.E. (2020). Depletion of the AD Risk Gene SORL1 Selectively Impairs Neuronal Endosomal Traffic Independent of Amyloidogenic APP Processing. Cell Rep *31*, 107719.
Kwart, D., Gregg, A., Scheckel, C., Murphy, E.A., Paquet, D., Duffield, M., Fak, J., Olsen, O., Darnell, R.B., and Tessier-Lavigne, M. (2019). A Large Panel of Isogenic APP and PSEN1 Mutant Human iPSC Neurons Reveals Shared Endosomal Abnormalities Mediated by APP beta-CTFs, Not Abeta. Neuron *104*, 256-270 e255.
Lambert, J.C., Ibrahim-Verbaas, C.A., Harold, D., Naj, A.C., Sims, R., Bellenguez, C., Jun, G., Destefano, A.L., Bis, J.C., Beecham, G.W.*, et al.* (2013). Meta-analysis of 74,046 individuals identifies 11 new susceptibility loci for Alzheimer's disease. Nat Genet *45*, 1452-1458.
Leek, J.T., Johnson, W.E., Parker, H.S., Jaffe, A.E., and Storey, J.D. (2012). The sva package for removing batch effects and other unwanted variation in high-throughput experiments. Bioinformatics *28*, 882-883.
Levy, S., Sutton, G., Ng, P.C., Feuk, L., Halpern, A.L., Walenz, B.P., Axelrod, N., Huang, J., Kirkness, E.F., Denisov, G.*, et al.* (2007). The diploid genome sequence of an individual human. PLoS Biol *5*, e254.
Li, B., and Dewey, C.N. (2011). RSEM: accurate transcript quantification from RNA-Seq data with or without a reference genome. BMC Bioinformatics *12*, 323.
Lorenzen, A., Samosh, J., Vandewark, K., Anborgh, P.H., Seah, C., Magalhaes, A.C., Cregan, S.P., Ferguson, S.S.G., and Pasternak, S.H. (2010). Rapid and Direct Transport of Cell Surface APP to the Lysosome defines a novel selective pathway. Molecular Brain *3*, 11.
Mallard, F., Antony, C., Tenza, D., Salamero, J., Goud, B., and Johannes, L. (1998). Direct pathway from early/recycling endosomes to the Golgi apparatus revealed through the study of shiga toxin B-fragment transport. J Cell Biol *143*, 973-990.
Manders, E., Verbeek, F., and Aten, J. (1993). Measurement of co-localization of objects in dual-colour confocal images. Journal of microscopy *169*, 375-382.
Marsh, E.W., Leopold, P.L., Jones, N.L., and Maxfield, F.R. (1995). Oligomerized transferrin receptors are selectively retained by a lumenal sorting signal in a long-lived endocytic recycling compartment. J Cell Biol *129*, 1509-1522.
Martin-Belmonte, A., Aguado, C., Alfaro-Ruiz, R., Itakura, M., Moreno-Martinez, A.E., de la Ossa, L., Molnar, E., Fukazawa, Y., and Lujan, R. (2020). Age-Dependent Shift of AMPA Receptors From Synapses to Intracellular Compartments in Alzheimer's Disease: Immunocytochemical Analysis of the CA1 Hippocampal Region in APP/PS1 Transgenic Mouse Model. Front Aging Neurosci *12*, 577996.
Marwaha, R., and Sharma, M. (2017). DQ-Red BSA Trafficking Assay in Cultured Cells to Assess Cargo Delivery to Lysosomes. Bio Protoc *7*.
Maxfield, F.R., and McGraw, T.E. (2004). Endocytic recycling. Nature reviews Molecular cell biology *5*, 121-132.
Mayle, K.M., Le, A.M., and Kamei, D.T. (2012). The intracellular trafficking pathway of transferrin. Biochim Biophys Acta *1820*, 264-281.
McQuin, C., Goodman, A., Chernyshev, V., Kamentsky, L., Cimini, B.A., Karhohs, K.W., Doan, M., Ding, L., Rafelski, S.M., Thirstrup, D.*, et al.* (2018). CellProfiler 3.0: Next-generation image processing for biology. PLOS Biology *16*, e2005970.
Offe, K., Dodson, S.E., Shoemaker, J.T., Fritz, J.J., Gearing, M., Levey, A.I., and Lah, J.J. (2006). The lipoprotein receptor LR11 regulates amyloid beta production and amyloid precursor

protein traffic in endosomal compartments. The Journal of neuroscience : the official journal of the Society for Neuroscience *26*, 1596-1603.
Olav M. Andersen, N.B., Anne M. Landau, Gro Grunnet Pløen, Anne Mette G. Jensen, Giulia Monti, Benedicte Parm Ulhøi, Jens Randel Nyengaard, Kirsten Rosenmay Jacobsen, Margarita Melnikova Jørgensen, Ida E. Holm, Marianne L. Kristensen, Esben Søvsø Szocska Hansen, Charlotte E. Teunissen, Laura Breidenbach, Mathias Droescher, Ying Liu, Hanne Skovsgaard Pedersen, Henrik Callesen, Yonglun Luo, Lars Bolund, David J. Brooks, Christoffer Laustsen, Scott A. Small, Lars F. Mikkelsen, Charlotte B. Sørensen (2021). In vivo evidence that SORL1, encoding the endosomal recycling receptor SORLA, can function as a causal gene in Alzheimer's Disease. bioRxiv *doi: https://doi.org/10.1101/2021.07.13.452149*.
Ouellette, S.P., and Carabeo, R.A. (2010). A Functional Slow Recycling Pathway of Transferrin is Required for Growth of Chlamydia. Front Microbiol *1*, 112.
Park, M., Penick, E.C., Edwards, J.G., Kauer, J.A., and Ehlers, M.D. (2004). Recycling endosomes supply AMPA receptors for LTP. Science *305*, 1972-1975.
Patapoutian, A., and Reichardt, L.F. (2001). Trk receptors: mediators of neurotrophin action. Curr Opin Neurobiol *11*, 272-280.
Pietila, M., Sahgal, P., Peuhu, E., Jantti, N.Z., Paatero, I., Narva, E., Al-Akhrass, H., Lilja, J., Georgiadou, M., Andersen, O.M.*, et al.* (2019). SORLA regulates endosomal trafficking and oncogenic fitness of HER2. Nat Commun *10*, 2340.
Qureshi, Y.H., Patel, V.M., Berman, D.E., Kothiya, M.J., Neufeld, J.L., Vardarajan, B., Tang, M., Reyes-Dumeyer, D., Lantigua, R., Medrano, M.*, et al.* (2018). An Alzheimer's Disease-Linked Loss-of-Function CLN5 Variant Impairs Cathepsin D Maturation, Consistent with a Retromer Trafficking Defect. Mol Cell Biol *38*.
Racoosin, E.L., and Swanson, J.A. (1993). Macropinosome maturation and fusion with tubular lysosomes in macrophages. J Cell Biol *121*, 1011-1020.
Raghavan, N.S., Brickman, A.M., Andrews, H., Manly, J.J., Schupf, N., Lantigua, R., Wolock, C.J., Kamalakaran, S., Petrovski, S., Tosto, G.*, et al.* (2018). Whole-exome sequencing in 20,197 persons for rare variants in Alzheimer's disease. Ann Clin Transl Neurol *5*, 832-842.
Ramilowski, J.A., Goldberg, T., Harshbarger, J., Kloppmann, E., Lizio, M., Satagopam, V.P., Itoh, M., Kawaji, H., Carninci, P., Rost, B.*, et al.* (2015). A draft network of ligand-receptor-mediated multicellular signalling in human. Nat Commun *6*, 7866.
Rapaport, D., Lugassy, Y., Sprecher, E., and Horowitz, M. (2010). Loss of SNAP29 Impairs Endocytic Recycling and Cell Motility. PLOS ONE *5*, e9759.
Ren, M., Xu, G., Zeng, J., De Lemos-Chiarandini, C., Adesnik, M., and Sabatini, D.D. (1998). Hydrolysis of GTP on rab11 is required for the direct delivery of transferrin from the pericentriolar recycling compartment to the cell surface but not from sorting endosomes. Proc Natl Acad Sci U S A *95*, 6187-6192.
Rogaeva, E., Meng, Y., Lee, J.H., Gu, Y., Kawarai, T., Zou, F., Katayama, T., Baldwin, C.T., Cheng, R., Hasegawa, H.*, et al.* (2007a). The neuronal sortilin-related receptor SORL1 is genetically associated with Alzheimer disease. Nat Genet.
Rogaeva, E., Meng, Y., Lee, J.H., Gu, Y., Kawarai, T., Zou, F., Katayama, T., Baldwin, C.T., Cheng, R., Hasegawa, H.*, et al.* (2007b). The neuronal sortilin-related receptor SORL1 is genetically associated with Alzheimer disease. Nat Genet *39*, 168-177.
Rohe, M., Hartl, D., Fjorback, A.N., Klose, J., and Willnow, T.E. (2013). SORLA-mediated trafficking of TrkB enhances the response of neurons to BDNF. PLoS One *8*, e72164.

Scheltens, P., De Strooper, B., Kivipelto, M., Holstege, H., Chetelat, G., Teunissen, C.E., Cummings, J., and van der Flier, W.M. (2021). Alzheimer's disease. Lancet *397*, 1577-1590.
Schindelin, J., Arganda-Carreras, I., Frise, E., Kaynig, V., Longair, M., Pietzsch, T., Preibisch, S., Rueden, C., Saalfeld, S., Schmid, B.*, et al.* (2012). Fiji: an open-source platform for biological-image analysis. Nat Methods *9*, 676-682.
Schmidt, V., Sporbert, A., Rohe, M., Reimer, T., Rehm, A., Andersen, O.M., and Willnow, T.E. (2007). SorLA/LR11 regulates processing of amyloid precursor protein via interaction with adaptors GGA and PACS-1. J Biol Chem *282*, 32956-32964.
Seaman, M.N. (2004). Cargo-selective endosomal sorting for retrieval to the Golgi requires retromer. J Cell Biol *165*, 111-122.
Seaman, M.N. (2012). The retromer complex - endosomal protein recycling and beyond. J Cell Sci *125*, 4693-4702.
Selkoe, D.J. (2002). Alzheimer's disease is a synaptic failure. Science *298*, 789-791.
Shi, Y., Kirwan, P., Smith, J., Robinson, H.P., and Livesey, F.J. (2012). Human cerebral cortex development from pluripotent stem cells to functional excitatory synapses. Nat Neurosci *15*, 477-486, S471.
Simoes, S., Neufeld, J.L., Triana-Baltzer, G., Moughadam, S., Chen, E.I., Kothiya, M., Qureshi, Y.H., Patel, V., Honig, L.S., Kolb, H.*, et al.* (2020). Tau and other proteins found in Alzheimer's disease spinal fluid are linked to retromer-mediated endosomal traffic in mice and humans. Science translational medicine *12*.
Small, S.A., and Gandy, S. (2006). Sorting through the cell biology of Alzheimer's disease: intracellular pathways to pathogenesis. Neuron *52*, 15-31.
Small, S.A., and Petsko, G.A. (2020). Endosomal recycling reconciles the Alzheimer's disease paradox. Science translational medicine *12*.
Sonnichsen, B., De Renzis, S., Nielsen, E., Rietdorf, J., and Zerial, M. (2000). Distinct membrane domains on endosomes in the recycling pathway visualized by multicolor imaging of Rab4, Rab5, and Rab11. J Cell Biol *149*, 901-914.
Spoelgen, R., von Arnim, C.A., Thomas, A.V., Peltan, I.D., Koker, M., Deng, A., Irizarry, M.C., Andersen, O.M., Willnow, T.E., and Hyman, B.T. (2006). Interaction of the cytosolic domains of sorLA/LR11 with the amyloid precursor protein (APP) and beta-secretase beta-site APP-cleaving enzyme. The Journal of neuroscience : the official journal of the Society for Neuroscience *26*, 418-428.
Sun, J., and Roy, S. (2018). The physical approximation of APP and BACE-1: A key event in alzheimer's disease pathogenesis. Dev Neurobiol *78*, 340-347.
Temkin, P., Morishita, W., Goswami, D., Arendt, K., Chen, L., and Malenka, R. (2017). The Retromer Supports AMPA Receptor Trafficking During LTP. Neuron *94*, 74-82 e75.
Thonberg, H., Chiang, H.H., Lilius, L., Forsell, C., Lindstrom, A.K., Johansson, C., Bjorkstrom, J., Thordardottir, S., Sleegers, K., Van Broeckhoven, C.*, et al.* (2017). Identification and description of three families with familial Alzheimer disease that segregate variants in the SORL1 gene. Acta Neuropathol Commun *5*, 43.
Wakabayashi, K., Narisawa-Saito, M., Iwakura, Y., Arai, T., Ikeda, K., Takahashi, H., and Nawa, H. (1999). Phenotypic down-regulation of glutamate receptor subunit GluR1 in Alzheimer's disease. Neurobiol Aging *20*, 287-295.
Wang, Y., Eng, D.G., Kaverina, N.V., Loretz, C.J., Koirala, A., Akilesh, S., Pippin, J.W., and Shankland, S.J. (2020). Global transcriptomic changes occur in aged mouse podocytes. Kidney Int *98*, 1160-1173.

Willnow, T.E., and Andersen, O.M. (2013). Sorting receptor SORLA--a trafficking path to avoid Alzheimer disease. J Cell Sci *126*, 2751-2760.
Yap, C.C., Digilio, L., McMahon, L.P., Garcia, A.D.R., and Winckler, B. (2018). Degradation of dendritic cargos requires Rab7-dependent transport to somatic lysosomes. Journal of Cell Biology *217*, 3141-3159.
Yasuda, R.P., Ikonomovic, M.D., Sheffield, R., Rubin, R.T., Wolfe, B.B., and Armstrong, D.M. (1995). Reduction of AMPA-selective glutamate receptor subunits in the entorhinal cortex of patients with Alzheimer's disease pathology: a biochemical study. Brain Res *678*, 161-167.
Young, J.E., Boulanger-Weill, J., Williams, D.A., Woodruff, G., Buen, F., Revilla, A.C., Herrera, C., Israel, M.A., Yuan, S.H., Edland, S.D.*, et al.* (2015). Elucidating Molecular Phenotypes Caused by the SORL1 Alzheimer's Disease Genetic Risk Factor Using Human Induced Pluripotent Stem Cells. Cell stem cell *16*, 373-385.
Yuan, S.H., Martin, J., Elia, J., Flippin, J., Paramban, R.I., Hefferan, M.P., Vidal, J.G., Mu, Y., Killian, R.L., Israel, M.A.*, et al.* (2011). Cell-surface marker signatures for the isolation of neural stem cells, glia and neurons derived from human pluripotent stem cells. PLoS One *6*, e17540.
Zigdon, H., Meshcheriakova, A., Farfel-Becker, T., Volpert, G., Sabanay, H., and Futerman, A.H. (2017). Altered lysosome distribution is an early neuropathological event in neurological forms of Gaucher disease. FEBS Lett *591*, 774-783.

Chapter 4. PHARMACOLOGIC STABILIZATION OF RETROMER RESCUES ENDOSOME ENLARGEMENT IN HUMAN NEURONAL MODELS OF ALZHEIMER'S DISEASE

4.1 INTRODUCTION

Alzheimer's disease is a devastating neurodegenerative disorder that affects a growing population of older adults. There are currently very few medications that alleviate symptoms of AD and no treatment that effectively modifies the course of the disorder for more than several months. Most of the available drugs for AD target amyloid beta (Aβ), the main component of senile plaques which are a hallmark AD neuropathology. However, recent genetic studies have implicated genes associated with increased AD risk in distinct cellular pathways, including vesicular trafficking, inflammation, and lipid metabolism(Karch and Goate, 2015). Defects in trafficking through the endo-lysosomal network (ELN) are apparent in AD and enlarged or swollen endosomes are a hallmark cytopathology of the disorder. Probing ELN dysfunction in more detail may provide the opportunity to develop more precise therapeutic options for AD.

The well-established AD risk gene *SORL1* encodes the sorting receptor SORLA, which functions in retromer-dependent trafficking of cargo through the ELN. *SORL1* is a large gene with a significant amount of genetic variation(Holstege et al., 2017; Rogaeva et al., 2007). Non-coding variants of low-effect have been implicated by GWAS and candidate-based gene studies(Lambert et al., 2013; Rogaeva et al., 2007; Scheltens et al., 2016) and coding variants of high effect size are found throughout the protein(Holstege et al., 2017; Nicolas et al., 2016; Pottier et al., 2012; Scheltens et al., 2021). Variants that lead to premature stop codons, and thus haploinsufficiency of *SORL1*, are considered causative for AD(Holstege et al., 2017; Raghavan

et al., 2018; Scheltens et al., 2021). Studies have shown that loss of *SORL1* results in ELN dysfunction, including APP mislocalization and enlarged early endosomes(Hung et al., 2021; Knupp et al., 2020).

SORLA engages with retromer as an adaptor protein for various cargo, including APP(Andersen et al., 2005). The retromer protein complex is critical to proper ELN function, sorting proteins out of the early endosome to the trans-Golgi network (TGN) or out to the cell surface(Fjorback et al., 2012; Seaman, 2012). Retromer consists of two major components, the trimeric cargo recognition complex (VPS35, VPS29 and VPS26) and a membrane-targeting component consisting of sorting nexins (SNX1, SNX3, SNX5, SNX27). Mutations in retromer or loss or of retromer expression is documented in several neurodegenerative diseases including Alzheimer's disease and Parkinson's disease(Berman et al., 2015; Muhammad et al., 2008).

Small molecules that stabilize retromer may be a viable therapeutic strategy for mitigating ELN defects that occur in AD(Berman et al., 2015). These small molecules, termed retromer chaperones, have been shown to increase transport of APP out of early endosomes and reduce Aβ secretion in mouse and human hiPSC-derived cells(Mecozzi et al., 2014; Young et al., 2018). Retromer chaperones have further been shown to reduce tau phosphorylation independently of Aβ in iPSC-derived neurons(Young et al., 2018), as well as reducing Aβ and tau pathology and improving memory in AD transgenic mice(Li et al., 2020). However, the effect of these chaperones on endosomal morphology and ELN trafficking, pathogenic events that may occur prior to accumulation of Aβ, has not been analyzed.

In this work we used the small molecule TPT260, a pharmacologic chaperone which stabilizes and increases levels of the VPS35 subunit of retromer, to test whether endosomal phenotypes induced by depletion of *SORL1* or by AD-associated variants in *SORL1* can be

rescued by retromer enhancement. We selected three coding variants identified in AD patients and located in the VPS10 domain of SORL1 for further study, the E270K variant, the G511R variant, and the Y141C variant, all of which have been suggested to be potentially pathogenic(Pottier et al., 2012; Vardarajan et al., 2015). Using CRISPR/Cas9 genome editing, we generated isogenic stem cell lines containing these heterozygous variants (*SORL1*^{Var}) **(Figure 4.5)** to determine if variants in the VPS10 domain result in loss of certain SORLA functions. We also generated a heterozygous *SORL1* knockout line (*SORL1*$^{+/-}$) **(Figure 4.6)** and included previously published homozygous *SORL1* knockout lines (*SORL1*KO) for comparison. In all cell lines we analyzed endosome size, Aβ secretion and tau phosphorylation and investigated whether treatment with retromer chaperones might mitigate those phenotypes.

4.2 RESULTS

4.2.1 *SORL1*^{Var} *Neurons Show Altered APP Processing*

Some *SORL1* variants in the VPS10 domain have been shown to alter APP processing. When expressed in HEK293T cells, the E270K variant has been shown to increase both Aβ secretion and sAPP secretion(Vardarajan et al., 2015), and the G511R variant has been shown to disrupt Aβ targeting to lysosomes(Caglayan et al., 2014). While the Y141C variant has not been previously studied, it is similarly located within the VPS10 domain. To investigate whether *SORL1*^{Var} neurons have altered APP processing, we measured levels of Aβ secreted from hiPSC-derived neurons. We confirmed that neurons from all three VPS10 domain variant lines secreted increased levels of $A\beta_{40}$ (**Figure 4.1A**) and $A\beta_{42}$ (**Figure 4.1B**) as compared to WT neurons although the ratio of these two peptides did not change **(Figure 4.1C)**. We did not expect a change in the $A\beta_{42}$:$A\beta_{40}$ ratio, as we have previously observed that homozygous loss of *SORL1*

(*SORL1*KO) does not alter Aβ peptide ratios(Knupp et al., 2020). Increases in Aβ secretion in all three *SORL1*^{Var} lines were similar in magnitude those observed in the *SORL1*$^{+/-}$, but less than the increase in Aβ observed in the full *SORL1*KO neurons **(Figure 4.1A-B)**. We additionally assessed the effects of *SORL1*^{Var} lines on intracellular tau. It is known that tau is trafficked through the ELN to the lysosome for degradation(Vaz-Silva et al., 2018), and it is unknown if SORLA contributes to tau sorting. We did not observe any significant differences in the ratio of phosphorylated:total tau (pTau:tTau) (**Figure 4.1D**) in *SORL1*^{Var}, *SORL1*$^{+/-}$, or *SORL1*KO neurons when the Thr 231 phospho-epitope was analyzed.

4.2.2 *SORL1 Haploinsufficient and SORL1*^{Var} *Neurons Exhibit Enlarged Early Endosomes*

Enlarged early endosomes have become one of the defining cytopathologies of AD, indicative of endosomal "traffic jams"(Small et al., 2017). We and others have previously observed enlarged early endosomes in homozygous *SORL1*KO hiPSC-derived neurons(Hung et al., 2021; Knupp et al., 2020). We hypothesized that *SORL1*^{Var} neurons would similarly contain enlarged early endosomes, although we predicted that due to the single copy of WT *SORL1*, the phenotype could be more subtle. We analyzed confocal images of early endosomes in hiPSC-derived neurons using CellProfiler software (**Figure 4.2A**), as described previously(Knupp et al., 2020). Analyzing early-endosome antigen 1 (EEA1) marked puncta, we quantified puncta properties including mean size (**Figure 4.2B**) and mean intensity (**Figure 4.2C**) per field. *SORL1*^{Var} and *SORL1*$^{+/-}$ neurons contained significantly larger and more intense EEA1 puncta than WT. We also confirmed previous findings that *SORL1*KO neurons contain significantly enlarged early endosomes (**Figure 4.2B**). Interestingly, *SORL1*KO neurons had significantly enlarged and more intense EEA1 puncta as compared to the *SORL1*^{Var} neurons. Taken together,

this data indicates that loss of SORLA function is contributing to endosome enlargement in a gene dose-dependent manner and that harboring one copy of an AD-associated variant in *SORL1* is sufficient to induce early endosome enlargement in neurons.

4.2.3 *Pharmacologic Stabilization of Retromer Reduces Pathogenic Aβ and pTau and Enlarged Early Endosomes in SORL1^{Var} and SORL1 Deficient Neurons*

The retromer complex is critical for the proper function of retrograde sorting pathways. As a retromer adaptor, SORLA can transport APP from endosomal compartments to the TGN, reducing amyloidogenic cleavage(Andersen et al., 2016). Retromer stabilizing small molecules have been identified that increase steady-state concentrations of retromer and prevent its degradation. These retromer chaperones have also been shown to limit APP processing and reduce secreted Aβ in mouse and hiPSC-derived cells(Mecozzi et al., 2014; Young et al., 2018). We hypothesized retromer chaperones might reduce Aβ secretion in *SORL1*^{Var} and *SORL1* deficient neurons.

We treated hiPSC-derived neurons with retromer chaperone TPT260 at a 15 μM concentration or DMSO control. To confirm that TPT260 treatment was effective, we measured the expression of vacuolar protein sorting-associated protein 35 (VPS35), a core retromer protein **(Figure 4.7)**, and verified that it was significantly increased. We measured significantly less secreted $A\beta_{40}$ (**Figure 4.3A**) and $A\beta_{42}$ (**Figure 4.3B**) in media collected from TPT260-treated WT, *SORL1*^{Var}, and *SORL1*$^{+/-}$ neurons as compared to their DMSO controls. This indicates that TPT260 enhances retrograde trafficking of APP in cell lines with at least one WT copy of *SORL1*.

SORLA is the main adaptor protein for retromer-dependent trafficking of APP(Andersen et al., 2005). In the *SORL1*KO neurons, we expected that there would be a smaller effect on Aβ

secretion than in cell lines with one functional copy of *SORL1* and this is what we observed. *SORL1*KO neurons show only slightly reduced $A\beta_{40}$ secretion, and no change in $A\beta_{42}$ secretion with TPT260 treatment **(Figure 4.3A-B)**. The slight decrease in $A\beta_{40}$ secretion could indicate that another adaptor protein is also capable of retromer-dependent retrograde transport of APP or Aβ in addition to SORLA. Retromer chaperones have also been shown to reduce phosphorylated:total tau ratios in hiPSC-derived neurons(Young et al., 2018). We analyzed tau levels following TPT260 treatment and found that TPT260 reduced phosphorylated:total tau ratios in all cell lines (**Figure 4.3C**), indicating that enhancement of retromer expression may facilitate pathogenic tau clearance.

Both SORLA and retromer core components have been shown to be reduced in AD patient brains(Muhammad et al., 2008; Scherzer et al., 2004), indicating that reduced function of endolysosomal sorting components may be contributing to enlarged early endosomes. We hypothesized that treating *SORL1*^{Var} neurons with retromer chaperones might increase retrograde sorting of cargo out of early endosomes and reduce the size of enlarged endosomes. Following TPT260 treatment, we performed immunocytochemistry to identify early endosomes by EEA1 and analyzed confocal images of EEA1 puncta as above (**Figure 4.4A**). We observed reductions in puncta size **(Figure 4.4B)** and intensity **(Figure 4.4C)** in TPT260-treated *SORL1*^{Var} neurons, *SORL1*$^{+/-}$ neurons, and *SORL1*KO neurons as compared to their DMSO controls, suggesting that the retromer chaperone reduces enlarged early endosome size. We did not observe any changes in EEA1 puncta size or intensity in WT neurons treated with TPT260, indicating that the retromer chaperone does not alter the size of endosomes that are not enlarged.

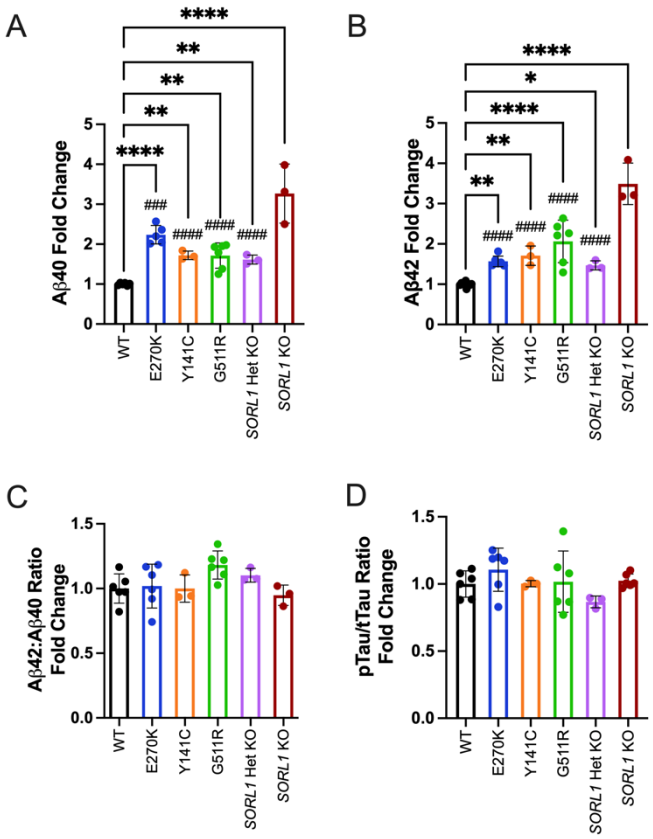

Figure 4.1. ***SORL1* VPS10 domain variants alter APP processing, but not tau.** Heterozygous *SORL1* E270K, Y141C, and G511R variant, *SORL1*$^{+/-,}$ and *SORL1*KO hiPSC-derived neurons secrete significantly increased levels of **(a)**$A\beta_{40}$ and **(b)**$A\beta_{42}$ as compared to WT controls, indicated by asterisks. *SORL1*KO neurons secrete significantly increased levels of **(a)**$A\beta_{40}$ and **(b)**$A\beta_{42}$ as compared to *SORL1*^{Var} and *SORL1*$^{+/-}$ neurons, indicated by hash marks. *SORL1* variants in the VPS10 domain do not alter **(c)**$A\beta_{42}$: $A\beta_{40}$ ratios or **(d)**pTau:tTau ratios. Data represented as mean ± SD. Normally distributed data was analyzed using parametric one-way ANOVA. Significance was defined as a value of *$p < 0.05$, **$p < 0.01$, ***$p < 0.001$, and ****$p < 0.0001$.

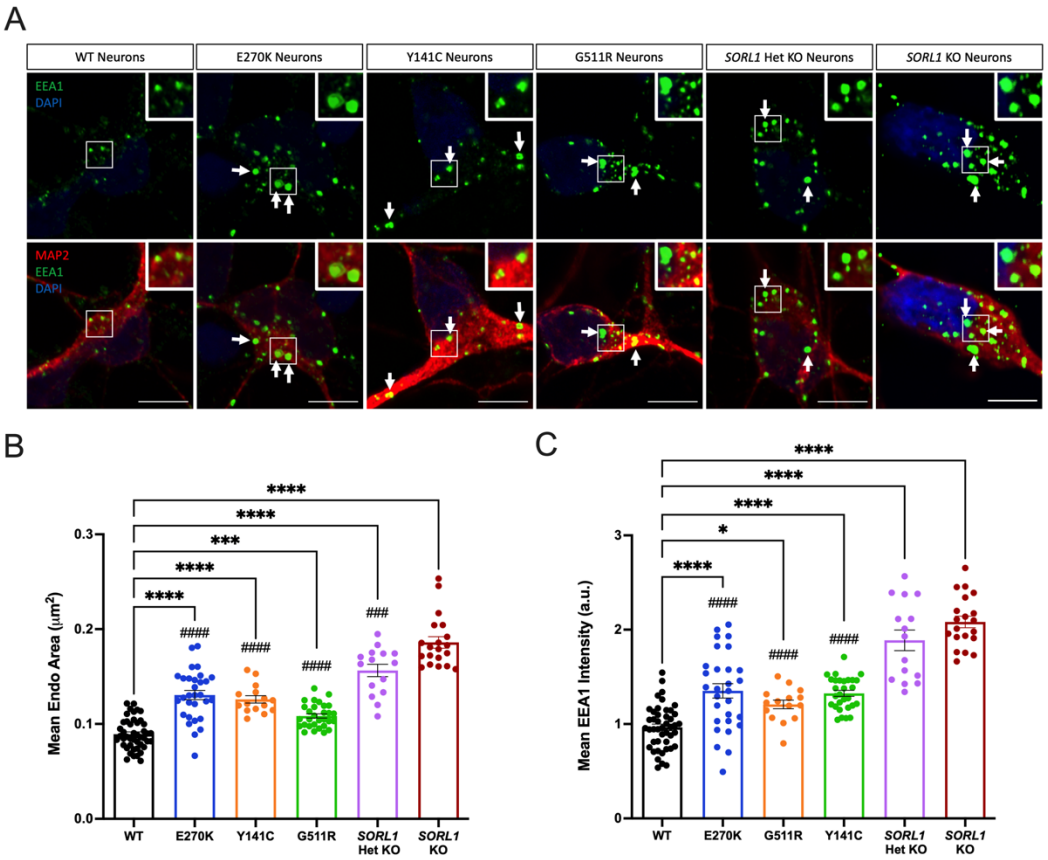

Figure 4.2. **hiPSC-derived neurons containing *SORL1* VPS10 domain variants have enlarged early endosomes. (a)** Representative immunofluorescent images of WT, heterozygous *SORL1* VPS10 domain variant, *SORL1* Het KO, and *SORL1* KO hiPSC-derived neurons. Neurons are stained with EEA1 (green) to mark early endosomes, MAP2 (red) to mark cell bodies, and DAPI (blue) to mark nuclei. Scale bar: 5 µm. *SORL1*^{Var}, *SORL1*$^{+/-}$, and *SORL1*KO neurons have **(b)** larger and **(c)**more intense early endosomes than WT, indicated by asterisks. *SORL1*KO neurons have **(b)** larger early endosomes than *SORL1*^{Var} and *SORL1*$^{+/-}$ neurons, indicated by hash marks. 10-20 images were analyzed per genotype. Data represented as mean ± SEM. Normally distributed data was analyzed using parametric one-way ANOVA. Significance was defined as a value of *p < 0.05, **p < 0.01, ***p < 0.001, and ****p < 0.0001.

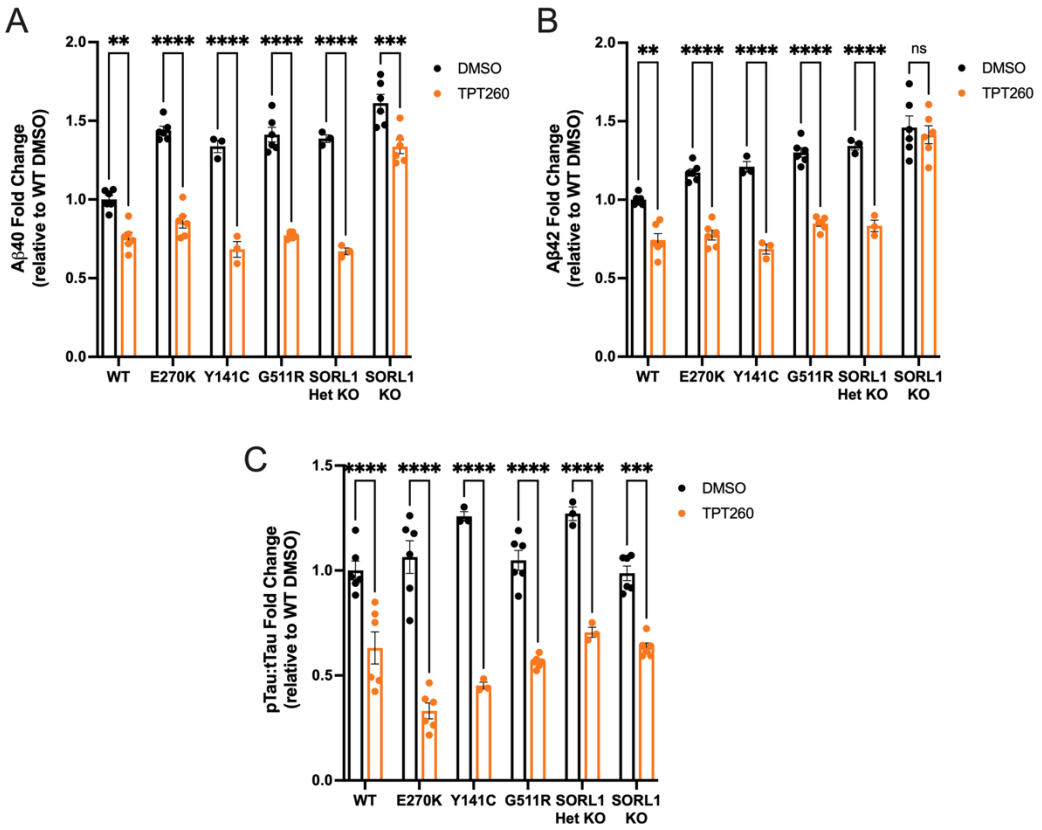

Figure 4.3. **Retromer chaperone reduces Aβ secretion and pTau:tTau ratios in hiPSC-derived neurons containing *SORL1* VPS10 variants.** Retromer chaperone TPT260 significantly reduces **(a)**$A\beta_{40}$ and **(b)**$A\beta_{42}$ in WT, heterozygous *SORL1* E270K, Y141C, and G511R variant, and *SORL1* Het KO hiPSC-derived neurons as compared to DMSO controls. TPT260 significantly reduces $A\beta_{40}$, but not $A\beta_{42}$ in *SORL1* KO neurons. Retromer chaperone TPT260 significantly reduces **(c)**pTau:tTau ratios in WT, heterozygous *SORL1* E270K, Y141C, and G511R variant, *SORL1* Het KO, and *SORL1* KO hiPSC-derived neurons as compared to DMSO controls. Data represented as mean ± SD. Normally distributed data was analyzed using parametric two-way ANOVA. Significance was defined as a value of $*p < 0.05$, $**p < 0.01$, $***p < 0.001$, and $****p < 0.0001$.

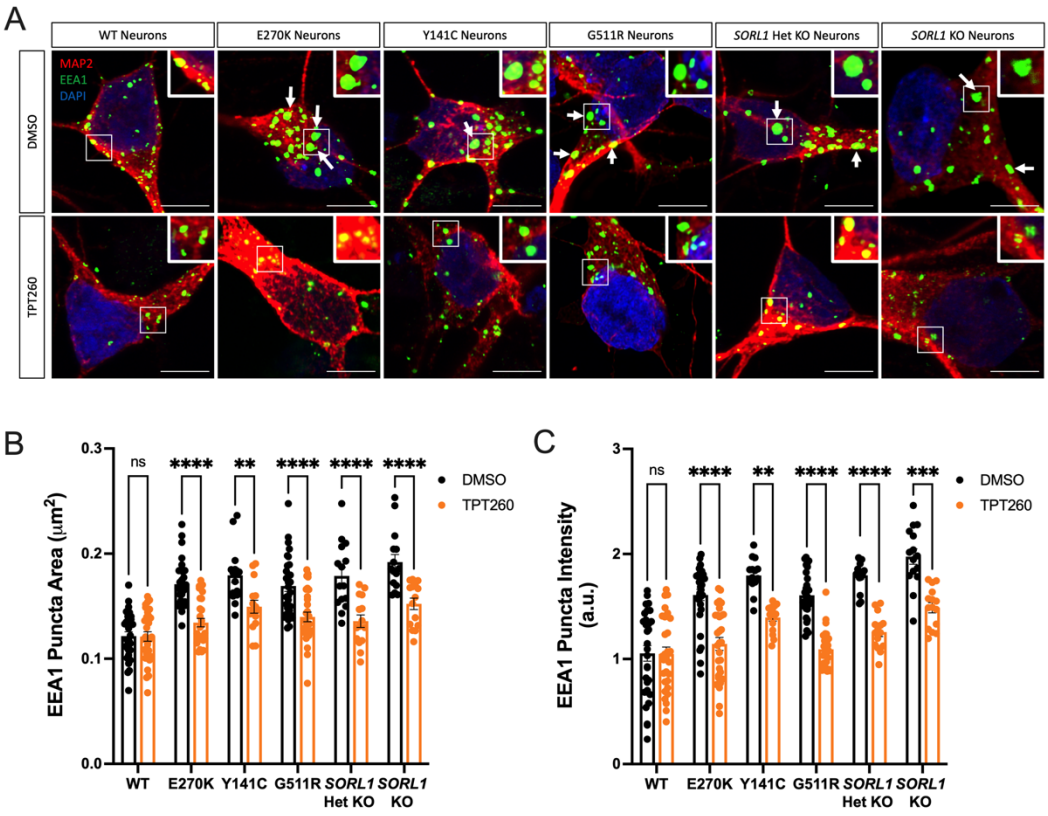

Figure 4.4. **Retromer chaperone reduces endosome size in hiPSC-derived neurons containing *SORL1* VPS10 variants. (a)** Representative immunofluorescent images of TPT260- and DMSO-treated WT, heterozygous *SORL1* VPS10 domain variant, *SORL1* Het KO, and *SORL1* KO hiPSC-derived neurons. Neurons are stained with EEA1 (green) to mark early endosomes, MAP2 (red) to mark cell bodies, and DAPI (blue) to mark nuclei. Scale bar: 5 μm. All TPT260-treated neurons have early endosomes that are **(b)** smaller and **(b)**less intense than the DMSO-treated controls. 10-20 images were analyzed per genotype. Data represented as mean ± SEM. Normally distributed data was analyzed using parametric two-way ANOVA. Significance was defined as a value of *$p < 0.05$, **$p < 0.01$, ***$p < 0.001$, and ****$p < 0.0001$.

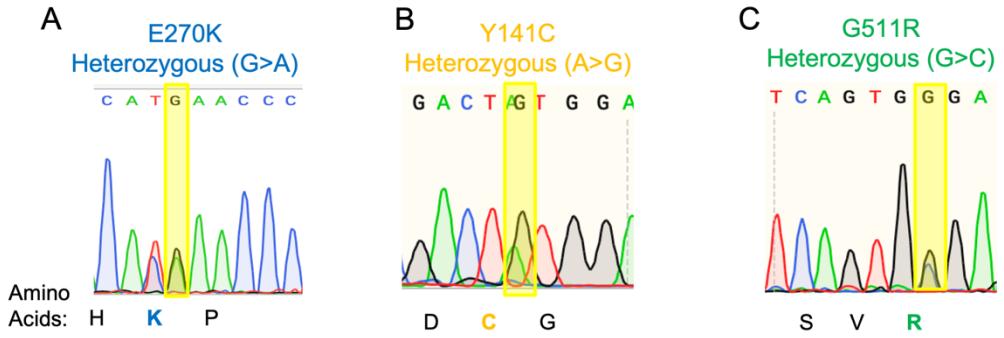

Figure 4.5. **Genomic sequence of cell lines containing *SORL1* VPS10 domain variants.** Sequencing of cell lines containing heterozygous *SORL1* variants **(a)** E270K, **(b)** Y141C, and **(c)** G511R.

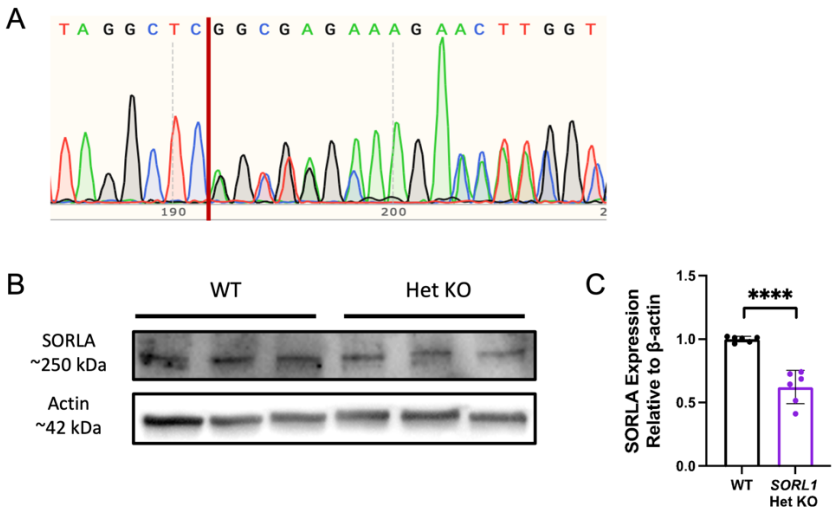

Figure 4.6. **Genomic sequence of heterozygous *SORL1* KO (*SORL1* Het KO) cell lines.** **(a)**Sequencing of *SORL1*$^{+/-}$ cell line shows a heterozygous deletion resulting in a premature stop codon. **(b)** Representative western blot of *SORL1*$^{+/-}$ hiPSC-derived neurons showing reduced expression of SORLA as compared to WT. **(c)** Quantification of western blots of *SORL1*$^{+/-}$ hiPSC-derived neurons confirms significantly reduced expression of SORLA protein as compared to WT neurons. n=6 biological replicates per genotype. Data is presented as mean ± SD. Normally distributed data was analyzed using parametric unpaired two-tailed t-test. Significance was defined as a value of *$p < 0.05$, **$p < 0.01$, ***$p < 0.001$, and ****$p < 0.0001$.

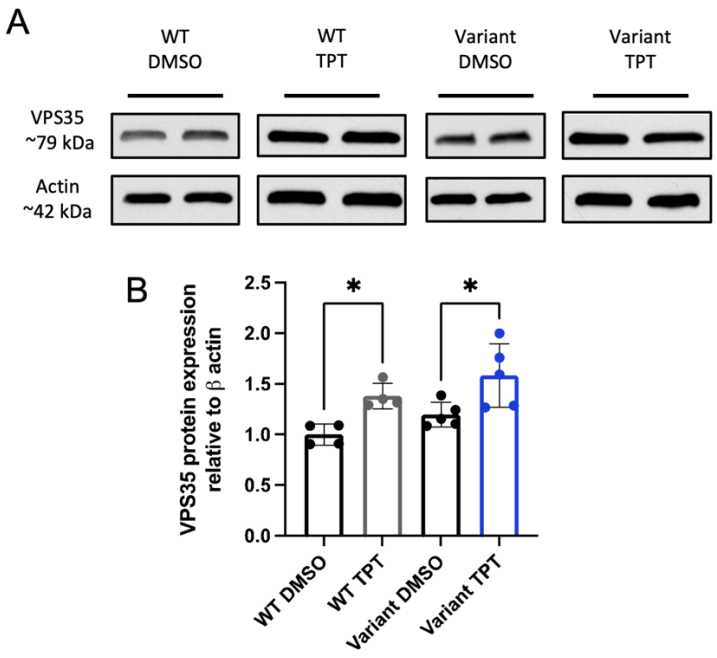

Figure 4.7. **Retromer chaperone increases expression of retromer component VPS35.** **(a)**Representative western blot of TPT260- and DMSO-treated WT and heterozygous *SORL1*^{Var} neurons. **(b)** Quantification of western blots of TPT260- and DMSO-treated WT and heterozygous *SORL1*^{Var} neurons. TPT260-treated neurons have significantly increased expression of retromer component VPS35. n=4-5 biological replicates per genotype. Data is presented as mean ± SD. Normally distributed data was analyzed using parametric one-way ANOVA. Significance was defined as a value of *p < 0.05, **p < 0.01, ***p < 0.001, and ****p < 0.0001.

4.3 DISCUSSION

When considering the development of novel therapeutics for Alzheimer's disease, it is critical to examine biologically relevant pathways such as protein trafficking through the ELN in neurons. In particular, trafficking of APP directly affects its processing into amyloidogenic forms, such as Ab. Furthermore, indicators of ELN dysfunction, such as enlarged endosomes, are early cytopathological phenotypes in AD, evident before substantial accumulation of other neuropathologic hallmarks and thus a potentially attractive therapeutic target(Cataldo et al., 2000). We examined hiPSC-derived neurons containing heterozygous *SORL1* VPS10 domain variants for cellular phenotypes associated with AD. It has been previously reported that heterozygous and homozygous loss of *SORL1* result in increased secretion of Aβ and enlarged early endosomes(Hung et al., 2021; Knupp et al., 2020). We observed similar phenotypes in the *SORL1* VPS10 domain variant lines **(Figure 4.1, Figure 4.2)**. Both secreted Aβ and enlarged early endosome phenotypes seem to be gene dose-dependent, which aligns with previous reports(Dodson et al., 2008; Hung et al., 2021). This data is also consistent with indications that *SORL1* haploinsufficiency is causative for AD(Andersen et al., 2021; Holstege et al., 2017), and suggests that certain rare variants in the VPS10 domain of *SORL1* may result in haploinsufficiency leading to AD.

Deficiency of the multi-protein sorting complex, retromer, is implicated in multiple neurodegenerative disorders(Carosi et al., 2021). Of relevance to AD, SORLA is a major adaptor protein for retromer-dependent retrograde trafficking of APP(Andersen et al., 2016). Both loss of SORLA and loss of retromer subunits increases secretion of Aβ(Knupp et al., 2020; Young et al., 2018). We previously reported that treatment with retromer chaperones decrease Aβ in cell lines derived from SAD and FAD patients(Young et al., 2018). Here we directly tested the effect of

retromer chaperones on the increased Aβ we observe in neurons with loss of *SORL1* expression or that harbor *SORL1* VPS10 domain variants. We show that in all cell lines with at least one WT copy of *SORL1*, chaperone treatment reduces levels of amyloidogenic Aβ **(Figure 4.3**). In *SORL1*KO lines, the retromer chaperone provides a slight reduction in $A\beta_{40}$, of a much smaller magnitude that those seen in cell lines with one WT copy of *SORL1*, and no significant reduction in $A\beta_{42}$. This data corroborates previous work showing that SORLA is that main retromer adaptor responsible for sorting APP. With no WT copies of SORLA, the effects of the retromer chaperone on Aβ secretion are strongly blunted. However, our data does not rule out and independent effect of TPT260 on Aβ secretion that is independent of SORLA.

The early endosome is the sorting hub for cargo in the ELN, and enlarged early endosomes are indicative of traffic jams in the ELN(Small et al., 2017). Importantly, enlarged early endosomes are a very early cellular pathology in AD, arising before Aβ and pTau pathology(Cataldo et al., 2000). Enlarged early endosomes are also apparent in FAD cell lines, where altered APP processing is a main disease driver. In these conditions, reducing amyloidogenic processing by treatment with a β-secretase inhibitor (BACEi) was able to rescue endosome enlargement(Kwart et al., 2019). In contrast, enlarged endosomes due to loss of *SORL1* expression were not rescued by treatment with BACEi(Knupp et al., 2020) but were rescued by total reduction of APP using anti-sense oligos(Hung et al., 2021). Together this set of data indicates endosome enlargement in SORL1 deficient cells is directly due to loss of a sorting protein which impacts the flow of proteins through the ELN. Strategies that reduce the total amount of cargo within early endosomes (such as reduction of total APP) may thus help to alleviate endosome enlargement. Because SORLA traffics cargo other than APP through the ELN in a retromer-dependent manner(Rohe et al., 2013), we hypothesized that enhancing

retromer trafficking might be another effective strategy to reduce cargo in early endosomes. We show here that the retromer chaperone partially rescues the enlarged endosome phenotype, reducing mean endosome size in all *SORL1*^{Var}, *SORL1*$^{+/-}$, and *SORL1*KO neurons (**Figure 4.4)**. We hypothesize that this small molecule enhances retrograde sorting of most retromer cargo, not just those that rely on SORLA as an adaptor, out of the early endosome. This is one explanation for why the retromer chaperone reduces endosome size in the *SORL1*KO line, which contains no wild-type SORLA. Importantly for therapeutic implications, the retromer chaperone does not appear to affect endosome size in the WT cell lines at the concentrations we tested.

Loss of SORLA and ELN dysfunction have been shown to be one driver of AD pathogenesis(Holstege et al., 2017; Hung et al., 2021; Knupp et al., 2020). In this work we show that *SORL1* VPS10 domain variants result in neuronal phenotypes similar to those resulting from loss of *SORL1*, including enlarged early endosomes and increased Aβ secretion. We further show that treatment with the retromer chaperone TPT260 can improve these cellular phenotypes. Collectively, our data confirm that ELN dysfunction that occurs early in the course of AD is a viable therapeutic target worth further study.

4.4 METHODS

4.4.1 *CRISPR/Cas9 Genome Editing*

All genome editing was completed in the previously published and characterized CV background human induced pluripotent stem cell line(Young et al., 2015), which is male with an APOE e3/e4 genotype(Levy et al., 2007). Genome editing was performed according to published protocols(Young et al., 2018). Briefly, the Zhang Lab CRISPR Design website (crispr.mit.edu) was used to generate guide RNAs (gRNAs) with minimal off-target effects. gRNAs were cloned

into the px458 vector that also expresses GFP and the Cas-9 nuclease. hiPSCs were electroporated with plasmids, sorted by flow cytometry for GFP expression, and plated at a clonal density of ~1x10^4 cells per 10cm plate. After approximately two weeks of growth, colonies were picked and split into identical sets. One set was analyzed by Sanger sequencing and one set was expanded to generate isogenic cell lines. A total of 6 previously unpublished clones were chosen for experiments contained in this publication: 2 clones containing the heterozygous *SORL1* E270K variant (**Figure 4.5A**), 1 clone containing the heterozygous *SORL1* Y141C variant (**Figure 4.5B**), 2 clones containing the heterozygous *SORL1* G511R variant (**Figure 4.5C**), and 1 clone containing a deletion resulting in a heterozygous *SORL1* KO (*SORL1*$^{+/-}$) (**Figure 4.6**). Also included in this publication are four previously published clones including 2 WT clones and 2 homozygous *SORL1* KO clones (*SORL1*KO)(Knupp et al., 2020). All clones were shown to have normal karyotypes and verified to be free of mycoplasma (MycoAlert).

4.4.2 *CRISPR/Cas9 gRNA, ssODN, and Primer Sequences*

E270K gRNA: ATTGAACGACATGAACCCTC

E270K ssODN

GGGAATTGATCCCTATGACAAACCAAATACCATCTACATTGAACGACATGAACCCTC

TGGCTACTCCACGTCTTCCGAAGTACAGATTTCTTCCAGTCCCGGGAAAACCAGGAA

G

E270K Forward primer: ctctatcctgagtcaaggagtaac

E270K Reverse primer: ccttccaattcctgtgtatgc

PCR amplifies 458 bp sequence

Y141C gRNA: GTACGTGTCTTACGACTA

Y141C ssODN:

GAAAGATCTTTCTGCCAGTTTCTCACCAACTCTTTCTTTTTCATCTCCTTTTCTCTGTA

TTCCAGGTGTACGTGTCTTACGACTGTGGAAAATCATTCAAGAAAATTTCAGACAAG

TTAAACTTTGGCTTGGGAAATAGGAGTGAAGCTG

Y141C Forward primer: gtggcaggtgcctgtaatcc

Y141C Reverse primer: cacagagagcgccatctcc

PCR amplifies 445 bp sequence

G511R gRNA: CTCTTGCATTTTAGGCTCAG

G511R ssODN:

CTGACATATTCTTGAAATTAAAAATAATTATTTCTCTTGCATTTTAGGCTCAGTGCGA

AAGAACTTGGCTAGCAAGACAAACGTGTACATCTCTAGCAGTGCTGGAGCCAGGTG

GCG

G511R Forward primer: cgccactggtaagtgtgcttgc

G511R Reverse primer: ctggcattactggtctctgccatg

PCR amplifies 413 bp sequence

4.4.3 *hiPSC Neuronal Differentiation*

hiPSCs were cultured and differentiated into neurons using previously published methods(Knupp et al., 2020; Rose et al., 2018). Briefly, cortical neurons were differentiated from hiPSCs using the dual-SMAD inhibition technique. hiPSCs were plated on 1:20 Matrigel-coated (Growth factor reduced basement membrane matrix; # 356231; Corning) 6-well plates at a density of 3.5 million cells per well. Cells were fed with Basal Neural Maintenance Media

(BNMM) (1:1 DMEM/F12 (#11039047 Life Technologies) + glutamine media/neurobasal media (#21103049, Gibco), 0.5% N2 supplement (# 17502-048; Thermo Fisher Scientific,) 1% B27 supplement (# 17504-044; Thermo Fisher Scientific), 0.5% GlutaMax (# 35050061; Thermo Fisher Scientific), 0.5% insulin-transferrin-selenium (#41400045; Thermo Fisher Scientific), 0.5% NEAA (# 11140050; Thermo Fisher Scientific), 0.2% β-mercaptoethanol (#21985023, Life Technologies)) supplemented with 10 μM SB-431542 and 0.5 μM LDN-193189 (#1062443, Biogems) for seven days. On day 8, cells were incubated with Versene (#15640066, Gibco), dissociated with cell scrapers, and passaged 1:3. From days 9-13, cells were fed daily with BNMM containing no supplements. On day 13, media was switched to BNMM containing 20 ng/mL FGF (R&D Systems, Minneapolis, MN). On day 16, cells were passaged 1:3. Cells were fed daily until approximately day 23, when cells were FACS sorted to enrich a stable population of CD184/CD24 (#557145/561646 BD Pharmingen) positive, CD44/CD271 (#555479/557196 BD Pharmingen) negative neural progenitor cells(Yuan et al., 2011). After sorting, cells were expanded for cortical neuronal differentiation. Neural progenitor cells were plated on Matrigel at a density of 5 million cells per 10cm plate. Media was switched to BNMM supplemented with 0.02 μg/mL brain-derived neurotrophic factor (#450-02 PeproTech) + 0.02 μg/mL glial-cell-derived neurotrophic factor (#450-10 PeproTech) + 0.5 mM dbcAMP (#D0260 Sigma Aldrich). Cells were fed twice a week for three weeks. After three weeks, neurons were sorted by magnetic activated techniques to enrich the population of CD184/CD44/CD271 negative cells and plated out for experiments. All cell culture was maintained at 37C and 5% CO_2.

4.4.4 *Cortical Neuron Purification*

After three weeks of differentiation, neurons were purified to enrich the cortical neuron population using previously published methods(Knupp et al., 2020; Young et al., 2015). In brief,

cells were dissociated using Accutase (#AT104-500 Innovative Cell Tech) and resuspended in IMAG solution (PBS + 0.5% bovine serum albumin [Sigma Aldrich] + 2 mM ethylenediaminetetraacetic acid [ThermoFisher]). Cells were incubated with PE-conjugated mouse anti-human antibodies to CD184, CD44, and CD271 (BD Pharmingen) at concentrations of 5 μL/10 million cells. After antibody incubation, cells were washed using IMAG solution and incubated with anti-PE magnetic beads (BD Pharmingen) at a concentration of 25 μL/10 million cells. Complexes of antibodies and beads were pulled down using a rare earth magnet, and the supernatant containing cells of interested was collected. Cells were counted and plated at appropriate experimental densities.

4.4.5 *Western Blotting*

Cell lysates we separated on 4-20% Mini-PROTEAN TGX Precast Protein Gels (#4561096; Biorad). Proteins were then transferred to PVDF membranes and membranes were incubated with antibodies to Sortilin-related receptor 1 (SORLA) at 1:1000 (BD 611860 and abcam ab190684), β-actin (ACTB) at 1:2000 (EMD Millipore Corp MAB1501), early endosome antigen 1 (EEA1) at 1:5000 (BD 610456), and vacuolar protein sorting-associated protein 35 (VPS35) at 1:1000 (abcam ab97545). All images of blots were quantified using ImageJ software.

4.4.6 *Amyloid Beta and Phosphorylated Tau Measurements*

Aβ peptides and phosphorylated tau protein were measured as previously described(Knupp et al., 2020; Young et al., 2015). Briefly, purified neurons were plated in 96well plates at a density of 200,000 cells per well. Cell lysates and media were harvested from triplicate wells. To measure Aβ peptides, an Aβ Triplex ELISA plate (Meso Scale Discovery #151200E-2) was used to assess media. To measure phosphorylated and total tau, a

Phospho(Thr231)/Total Tau ELISA plate (Meso Scale Discovery K15121D-2) was used to assess cell lysates.

4.4.7 *TPT260 Treatment*

Purified neurons from all cell lines were plated either in Matrigel-coated 96-well plates at a density of 2x10e5 or on Matrigel coated coverslips at a density of 5x10e5. After five days, cells were treated with media containing 15 μM TPT260 (Cayman Chemical 16079) or DMSO control. All experiments were performed after 72hrs of treatment. At this time point, media was harvested for quantification of $A\beta_{40}$ and $A\beta_{42}$ by ELISA. Cell lysates were harvested for western blotting and tau quantification by ELISA. Additionally, cells on coverslips were fixed in 4% paraformaldehyde (PFA, Alfa Aesar, Reston, VA) in preparation for immunocytochemistry.

4.4.8 *Immunocytochemistry*

Immunocytochemistry was performed as previously described(Knupp et al., 2020). Glass coverslips were plated in a 24-well plate and coated with Matrigel. Neurons were purified, seeded at a density of 500,000 per well, and maintained in culture for 5 days prior to experiments. Neurons were fixed for 15 minutes in 4% paraformaldehyde (PFA, Alfa Aesar, Reston, VA). Following fixation, neurons were incubated for 30 minutes in blocking buffer containing 2.5% bovine serum albumin and 0.1% Triton-X (Sigma Aldrich, St Louis, MO) in PBS. Primary antibodies were diluted in blocking buffer and incubated for 2 hours at room temperature. Neurons were then washed three times in buffer containing 0.1% Triton-X in PBS and incubated for 1 hour at room temperature with secondary antibodies diluted in blocking buffer. Finally, neurons were rinsed three times with PBS. Glass coverslips were mounted on slides using ProLong Gold Antifade mountant (ThermoFisher, Waltham, MA). The following

primary antibodies were used: early endosome antigen 1 (EEA1) at 1:500 (BD 610456); microtubule-associated protein 2 (MAP2) at 1:1000 (Abcam ab92434); DAPI at 1 μg/mL final (Alfa Aesar).

4.4.9 *Confocal Microscopy and Image Processing*

All microscopy, image processing, and image analyses were performed under blinded conditions. Confocal z-stack images were obtained using a Leica SP8 confocal microscope with x63 apochromat oil immersion lens. Image processing was completed using ImageJ software(Schindelin et al., 2012). Endosome size analysis was performed as previously described(Knupp et al., 2020). Briefly, maximum intensity projections of confocal z-stacks were generated. The rolling ball algorithm was used to subtract background in endosome channel images. Cell body stains were used to mask endosome channels, and size and intensity measurements were made using CellProfiler software(McQuin et al., 2018). Automated segmentation algorithms were used to identify individual puncta, and puncta properties including area and intensity were calculated. Mean intensity and mean puncta area are presented as a mean value over all puncta per field.

4.4.10 *Quantification and Statistical Analysis*

For all experiments, we used two independent clones containing the heterozygous E270K variant, one clone containing the Y141C variant, two independent clones containing the G511R variant, one *SORL1* heterozygous KO clone, and three independent clones of isogenic WT cell lines (cells that underwent the CRISPR/Cas9 transfection and sub-cloning process, but in which editing events did not occur). In addition, we used two independent clones of *SORL1* homozygous KO cell lines that were previously published(Knupp et al., 2020). Data was tested

for normality using the Schapiro-Wilk normality test. Normally distributed data was analyzed using parametric one-way ANOVA or two-way ANOVA tests. Significance was defined as $p<0.05$. All statistical analysis was performed using Graphpad Prism software. Details of individual experiments, including biological and technical replicates, can be found in figure legends.

4.5 REFERENCES

Andersen, O.M., Reiche, J., Schmidt, V., Gotthardt, M., Spoelgen, R., Behlke, J., von Arnim, C.A., Breiderhoff, T., Jansen, P., Wu, X.*, et al.* (2005). Neuronal sorting protein-related receptor sorLA/LR11 regulates processing of the amyloid precursor protein. Proc Natl Acad Sci U S A *102*, 13461-13466.

Berman, D.E., Ringe, D., Petsko, G.A., and Small, S.A. (2015). The use of pharmacological retromer chaperones in Alzheimer's disease and other endosomal-related disorders. Neurotherapeutics *12*, 12-18.

Carosi, J.M., Denton, D., Kumar, S., and Sargeant, T.J. (2021). Retromer dysfunction at the nexus of tauopathies. Cell Death Differ *28*, 884-899.

Cataldo, A.M., Peterhoff, C.M., Troncoso, J.C., Gomez-Isla, T., Hyman, B.T., and Nixon, R.A. (2000). Endocytic pathway abnormalities precede amyloid beta deposition in sporadic Alzheimer's disease and Down syndrome: differential effects of APOE genotype and presenilin mutations. Am J Pathol *157*, 277-286.

Fjorback, A.W., Seaman, M., Gustafsen, C., Mehmedbasic, A., Gokool, S., Wu, C., Militz, D., Schmidt, V., Madsen, P., Nyengaard, J.R.*, et al.* (2012). Retromer binds the FANSHY sorting motif in SorLA to regulate amyloid precursor protein sorting and processing. J Neurosci *32*, 1467-1480.

Holstege, H., van der Lee, S.J., Hulsman, M., Wong, T.H., van Rooij, J.G., Weiss, M., Louwersheimer, E., Wolters, F.J., Amin, N., Uitterlinden, A.G.*, et al.* (2017). Characterization of pathogenic SORL1 genetic variants for association with Alzheimer's disease: a clinical interpretation strategy. Eur J Hum Genet *25*, 973-981.

Hung, C., Tuck, E., Stubbs, V., van der Lee, S.J., Aalfs, C., van Spaendonk, R., Scheltens, P., Hardy, J., Holstege, H., and Livesey, F.J. (2021). SORL1 deficiency in human excitatory neurons causes APP-dependent defects in the endolysosome-autophagy network. Cell Rep *35*, 109259.

Karch, C.M., and Goate, A.M. (2015). Alzheimer's disease risk genes and mechanisms of disease pathogenesis. Biol Psychiatry *77*, 43-51.

Knupp, A., Mishra, S., Martinez, R., Braggin, J.E., Szabo, M., Kinoshita, C., Hailey, D.W., Small, S.A., Jayadev, S., and Young, J.E. (2020). Depletion of the AD Risk Gene SORL1 Selectively Impairs Neuronal Endosomal Traffic Independent of Amyloidogenic APP Processing. Cell Rep *31*, 107719.

Kwart, D., Gregg, A., Scheckel, C., Murphy, E.A., Paquet, D., Duffield, M., Fak, J., Olsen, O., Darnell, R.B., and Tessier-Lavigne, M. (2019). A Large Panel of Isogenic APP and PSEN1 Mutant Human iPSC Neurons Reveals Shared Endosomal Abnormalities Mediated by APP beta-CTFs, Not Abeta. Neuron *104*, 1022.

Lambert, J.C., Ibrahim-Verbaas, C.A., Harold, D., Naj, A.C., Sims, R., Bellenguez, C., DeStafano, A.L., Bis, J.C., Beecham, G.W., Grenier-Boley, B.*, et al.* (2013). Meta-analysis of 74,046 individuals identifies 11 new susceptibility loci for Alzheimer's disease. Nat Genet *45*, 1452-1458.

Levy, S., Sutton, G., Ng, P.C., Feuk, L., Halpern, A.L., Walenz, B.P., Axelrod, N., Huang, J., Kirkness, E.F., Denisov, G.*, et al.* (2007). The diploid genome sequence of an individual human. PLoS Biol *5*, e254.

Mecozzi, V.J., Berman, D.E., Simoes, S., Vetanovetz, C., Awal, M.R., Patel, V.M., Schneider, R.T., Petsko, G.A., Ringe, D., and Small, S.A. (2014). Pharmacological chaperones stabilize retromer to limit APP processing. Nature chemical biology *10*, 443-449.
Nicolas, G., Charbonnier, C., Wallon, D., Quenez, O., Bellenguez, C., Grenier-Boley, B., Rousseau, S., Richard, A.C., Rovelet-Lecrux, A., Le Guennec, K.*, et al.* (2016). SORL1 rare variants: a major risk factor for familial early-onset Alzheimer's disease. Mol Psychiatry *21*, 831-836.
Pottier, C., Hannequin, D., Coutant, S., Rovelet-Lecrux, A., Wallon, D., Rousseau, S., Legallic, S., Paquet, C., Bombois, S., Pariente, J.*, et al.* (2012). High frequency of potentially pathogenic SORL1 mutations in autosomal dominant early-onset Alzheimer disease. Mol Psychiatry *17*, 875-879.
Raghavan, N.S., Brickman, A.M., Andrews, H., Manly, J.J., Schupf, N., Lantigua, R., Wolock, C.J., Kamalakaran, S., Petrovski, S., Tosto, G.*, et al.* (2018). Whole-exome sequencing in 20,197 persons for rare variants in Alzheimer's disease. Ann Clin Transl Neurol *5*, 832-842.
Rogaeva, E., Meng, Y., Lee, J.H., Gu, Y., Kawarai, T., Zou, F., Katayama, T., Baldwin, C.T., Cheng, R., Hasegawa, H.*, et al.* (2007). The neuronal sortilin-related receptor SORL1 is genetically associated with Alzheimer disease. Nat Genet *39*, 168-177.
Rohe, M., Hartl, D., Fjorback, A.N., Klose, J., and Willnow, T.E. (2013). SORLA-mediated trafficking of TrkB enhances the response of neurons to BDNF. PLoS One *8*, e72164.
Scheltens, P., Blennow, K., Breteler, M.M., de Strooper, B., Frisoni, G.B., Salloway, S., and Van der Flier, W.M. (2016). Alzheimer's disease. Lancet *388*, 505-517.
Scheltens, P., De Strooper, B., Kivipelto, M., Holstege, H., Chételat, G., Teunissen, C.E., Cummings, J., and van der Flier, W.M. (2021). Alzheimer's disease. Lancet *397*, 1577-1590.
Seaman, M.N. (2012). The retromer complex - endosomal protein recycling and beyond. J Cell Sci *125*, 4693-4702.
Vardarajan, B.N., Zhang, Y., Lee, J.H., Cheng, R., Bohm, C., Ghani, M., Reitz, C., Reyes-Dumeyer, D., Shen, Y., Rogaeva, E.*, et al.* (2015). Coding mutations in SORL1 and Alzheimer disease. Ann Neurol *77*, 215-227.
Young, J.E., Boulanger-Weill, J., Williams, D.A., Woodruff, G., Buen, F., Revilla, A.C., Herrera, C., Israel, M.A., Yuan, S.H., Edland, S.D.*, et al.* (2015). Elucidating Molecular Phenotypes Caused by the SORL1 Alzheimer's Disease Genetic Risk Factor Using Human Induced Pluripotent Stem Cells. Cell stem cell *16*, 373-385.
Young, J.E., Fong, L.K., Frankowski, H., Petsko, G.A., Small, S.A., and Goldstein, L.S.B. (2018). Stabilizing the Retromer Complex in a Human Stem Cell Model of Alzheimer's Disease Reduces TAU Phosphorylation Independently of Amyloid Precursor Protein. Stem Cell Reports *10*, 1046-1058.
Yuan, S.H., Martin, J., Elia, J., Flippin, J., Paramban, R.I., Hefferan, M.P., Vidal, J.G., Mu, Y., Killian, R.L., Israel, M.A.*, et al.* (2011). Cell-surface marker signatures for the isolation of neural stem cells, glia and neurons derived from human pluripotent stem cells. PLoS One *6*, e17540.

Chapter 5. CONCLUSION

5.1 INTRODUCTION

AD affects over 5 million adults in the United States(2020), and current therapeutic options do not halt disease progression(Cummings et al., 2019). There have been hundreds of failed treatment options, many of which attempt to reduce production of or facilitate clearance of Aβ. There is an urgent need for new treatment strategies that do not rely on direct modulation of Aβ. ELN dysfunction represents one possible driver of AD pathogenesis upstream from Aβ generation(Small and Petsko, 2020).

ELN dysfunction is an interesting therapeutic target for AD, particularly because modulating the ELN can directly affect multiple AD pathologies. Because APP is cleaved within ELN compartments, Aβ generation can be increased by depletion of SORLA(Knupp et al., 2020) or decreased by overexpression of SORLA(Young et al., 2015). ELN function also affects tau generation, as it has been shown that enhancing retromer traffic can reduce tau phosphorylation(Young et al., 2018). Retromer-dependent recycling is also required for reinsertion of AMPA receptor subunits into the plasma membrane at post-synaptic sites, which directly affects long-term synaptic health(Temkin et al., 2017). Collectively, these studies support the further study of ELN dysfunction as one possible driver of AD pathogenesis and recommend the development of ELN therapeutics.

5.2 Depletion of the AD Risk Gene *SORL1* Selectively Impairs Neuronal Endosomal Traffic Independent of Amyloidogenic APP Processing

ELN dysfunction is known to occur in AD brains. GWAS and sequencing studies have identified many genes in the ELN associated with AD(Lambert et al., 2013; Miyashita et al., 2013; Raghavan et al., 2018), and enlarged early endosomes have been identified in neurons prior to the buildup of Aβ(Cataldo et al., 2000). Because these defects occur early in the course of disease, the ELN represents a viable therapeutic target for AD.

In this work, we show that loss of SORLA results in ELN dysfunction. In hiPSC-derived neurons, loss of SORLA results in enlarged early endosomes, the hallmark cytopathology of AD. EOAD mutations have been similarly shown to result in this phenotype, though interestingly, enlarged early endosomes from EOAD mutations can be rescued through BACE1 inhibition(Kwart et al., 2019). In contrast, we find that enlarged early endosomes from loss of SORLA are amyloid-independent. This suggests that ELN homeostasis is a global event in AD and may be impacted by different factors in the early onset and late onset forms of disease.

We further show that enlarged early endosomes from loss of SORLA are cell-type specific, and do not occur in hiPSC-derived microglial-like cells. As phagocytic cells, microglia are highly reliant on ELN function, but loss of SORLA in microglial-like cells does not alter early endosome size. This emphasizes that cell-type specific differences occur in response to ELN defects, and further study of the effects of loss of SORLA on microglial ELN is necessary.

Collectively, this data confirms a role for SORLA beyond APP trafficking and suggest that SORLA may be critical for normal ELN function in neurons. As enlarged early endosomes due to loss of SORLA are independent from Aβ generation, this data supports the idea that ELN

dysfunction in AD occurs long before Aβ build-up begins(Cataldo et al., 2004; Cataldo et al., 2000). Finally, this work is indicative of the role that hiPSC-derived models can play in determining the cellular mechanisms of AD pathogenesis.

5.3 The Alzheimer's Gene *SORL1* is a Key Regulator of Endosomal Recycling in Human Neurons

SORLA has long been linked to AD for its role in retromer-related trafficking of APP out of early endosomes(Andersen et al., 2006; Offe et al., 2006). We show that loss of SORLA results in APP accumulation in early and recycling endosomes, with a corresponding increase in Aβ secretion. More broadly, we show that loss of SORLA affects the sorting of additional cargo, including the BDNF receptor TRKB and the AMPA receptor subunit GLUA1. Mislocalization of these cargoes links loss of SORLA to synaptic dysfunction, an additional AD pathology.

In this work, we also determine a role for SORLA in retromer-dependent recycling of cargo to the cell surface. Loss of SORLA results in enlarged recycling endosomes and accumulation of cargo within them, suggesting traffic jams similar to those occurring in the early endosome. We also show that loss of SORLA reduces cell surface recycling of GLUA1, which is critical for synaptic plasticity and long-term synaptic health. As GLUA1 recycling has been shown to be independent of APP(Temkin et al., 2017), this work shows that SORLA is able to drive two separate pathologies of AD, APP accumulation and synaptic dysfunction, through parallel mechanisms.

Overall, we show that loss of SORLA results in accumulation of cargo in early and recycling endosomes. As the early endosome serves as a sorting hub for neuronal cargo, downstream trafficking defects are unsurprising. In particular, we report that loss of SORLA reduces recycling of GLUA1 to the cell surface, which may affect long-term synaptic function.

Collectively, our results indicate that SORLA and retromer-dependent trafficking are worth exploring as a therapeutic target for AD.

5.4 Pharmacologic Stabilization of Retromer Rescues Endosome Enlargement in Human Neuronal Models of Alzheimer's Disease

Rare coding variants have been found throughout *SORL1* that are associated with increased risk of AD(Nicolas et al., 2016). Along with truncating variants, variants in the VPS10 domain are thought to be the most pathogenic(Holstege et al., 2017). We show here that variants in the *SORL1* VPS10 domain in hiPSC-derived neurons result in enlarged early endosomes and increased Aβ secretion, similarly to neurons with heterozygous or homozygous loss of *SORL1*. These cellular phenotypes seem to be gene-dose dependent, which aligns with previous reports that *SORL1* haploinsufficiency is causative for AD(Andersen et al., 2021; Scheltens et al., 2021).

SORLA serves as a retromer-dependent receptor, trafficking cargo out of the early endosome(Andersen et al., 2005). Retromer-stabilizing small molecules, termed retromer chaperones, have been shown to increase trafficking of APP out of the early endosome and reduce Aβ secretion(Mecozzi et al., 2014). We show that the classic AD cytopathology of enlarged early endosomes can be mitigated by enhancing retromer expression with chaperones. We hypothesize that retromer chaperones accomplish this by increasing trafficking of all retromer cargo out of the early endosome, not just SORLA-dependent cargo.

Loss of SORLA and ELN dysfunction have been shown to be one driver of AD pathogenesis(Holstege et al., 2017; Hung et al., 2021; Knupp et al., 2020). We show that *SORL1* variants in the VPS10 domain result in neuronal phenotypes similar to loss of *SORL1*, including enlarged early endosomes and increased Aβ secretion. These cellular phenotypes can be ameliorated by treatment with a retromer chaperone. This data confirms that ELN dysfunction

occurring early in disease pathogenesis is a viable and valuable therapeutic target, and requires further study in preclinical models.

5.5 CONCLUSION

SORL1 haploinsufficiency seems to function as a causal event in EOAD(Andersen et al., 2021; Holstege et al., 2017; Scheltens et al., 2021). Of the four known causal genes for AD, *SORL1* is the only one associated with LOAD as well. Understanding the role of *SORL1* in ELN dysfunction is critical for understanding the cellular mechanisms of AD pathogenesis. Here, we determine that ELN defects such as enlarged early endosomes and increased Aβ secretion occur from loss of *SORL1* and from rare AD-associated *SORL1* variants. We additionally show that we can rescue some ELN defects occurring from loss of *SORL1* by enhancing retromer-dependent retrograde trafficking. Collectively, this work shows that *SORL1* and retromer-dependent trafficking are valid therapeutic targets and may ameliorate ELN defects that seem to be a primary driver of AD.

5.6 REFERENCES

(2020). 2020 Alzheimer's disease facts and figures. Alzheimer's & Dementia *16*, 391-460.
Andersen, O.M., Bøgh, N., Landau, A.M., Pløen, G.G., Jensen, A.M.G., Monti, G., Ulhøi, B.P., Nyengaard, J.R., Jacobsen, K.R., Jørgensen, M.M.*, et al.* (2021). In vivo evidence that SORL1, encoding the endosomal recycling receptor SORLA, can function as a causal gene in Alzheimer's Disease. bioRxiv, 2021.2007.2013.452149.
Andersen, O.M., Reiche, J., Schmidt, V., Gotthardt, M., Spoelgen, R., Behlke, J., von Arnim, C.A., Breiderhoff, T., Jansen, P., Wu, X.*, et al.* (2005). Neuronal sorting protein-related receptor sorLA/LR11 regulates processing of the amyloid precursor protein. Proc Natl Acad Sci U S A *102*, 13461-13466.
Andersen, O.M., Schmidt, V., Spoelgen, R., Gliemann, J., Behlke, J., Galatis, D., McKinstry, W.J., Parker, M.W., Masters, C.L., Hyman, B.T.*, et al.* (2006). Molecular dissection of the interaction between amyloid precursor protein and its neuronal trafficking receptor SorLA/LR11. Biochemistry *45*, 2618-2628.
Cataldo, A.M., Petanceska, S., Terio, N.B., Peterhoff, C.M., Durham, R., Mercken, M., Mehta, P.D., Buxbaum, J., Haroutunian, V., and Nixon, R.A. (2004). Abeta localization in abnormal endosomes: association with earliest Abeta elevations in AD and Down syndrome. Neurobiol Aging *25*, 1263-1272.
Cataldo, A.M., Peterhoff, C.M., Troncoso, J.C., Gomez-Isla, T., Hyman, B.T., and Nixon, R.A. (2000). Endocytic pathway abnormalities precede amyloid beta deposition in sporadic Alzheimer's disease and Down syndrome: differential effects of APOE genotype and presenilin mutations. Am J Pathol *157*, 277-286.
Cummings, J.L., Tong, G., and Ballard, C. (2019). Treatment Combinations for Alzheimer's Disease: Current and Future Pharmacotherapy Options. J Alzheimers Dis *67*, 779-794.
Holstege, H., van der Lee, S.J., Hulsman, M., Wong, T.H., van Rooij, J.G., Weiss, M., Louwersheimer, E., Wolters, F.J., Amin, N., Uitterlinden, A.G.*, et al.* (2017). Characterization of pathogenic SORL1 genetic variants for association with Alzheimer's disease: a clinical interpretation strategy. Eur J Hum Genet *25*, 973-981.
Hung, C., Tuck, E., Stubbs, V., van der Lee, S.J., Aalfs, C., van Spaendonk, R., Scheltens, P., Hardy, J., Holstege, H., and Livesey, F.J. (2021). SORL1 deficiency in human excitatory neurons causes APP-dependent defects in the endolysosome-autophagy network. Cell Rep *35*, 109259.
Knupp, A., Mishra, S., Martinez, R., Braggin, J.E., Szabo, M., Kinoshita, C., Hailey, D.W., Small, S.A., Jayadev, S., and Young, J.E. (2020). Depletion of the AD Risk Gene SORL1 Selectively Impairs Neuronal Endosomal Traffic Independent of Amyloidogenic APP Processing. Cell Rep *31*, 107719.
Kwart, D., Gregg, A., Scheckel, C., Murphy, E.A., Paquet, D., Duffield, M., Fak, J., Olsen, O., Darnell, R.B., and Tessier-Lavigne, M. (2019). A Large Panel of Isogenic APP and PSEN1 Mutant Human iPSC Neurons Reveals Shared Endosomal Abnormalities Mediated by APP beta-CTFs, Not Abeta. Neuron *104*, 1022.
Lambert, J.C., Ibrahim-Verbaas, C.A., Harold, D., Naj, A.C., Sims, R., Bellenguez, C., DeStafano, A.L., Bis, J.C., Beecham, G.W., Grenier-Boley, B.*, et al.* (2013). Meta-analysis of 74,046 individuals identifies 11 new susceptibility loci for Alzheimer's disease. Nat Genet *45*, 1452-1458.

Mecozzi, V.J., Berman, D.E., Simoes, S., Vetanovetz, C., Awal, M.R., Patel, V.M., Schneider, R.T., Petsko, G.A., Ringe, D., and Small, S.A. (2014). Pharmacological chaperones stabilize retromer to limit APP processing. Nature chemical biology *10*, 443-449.
Miyashita, A., Koike, A., Jun, G., Wang, L.S., Takahashi, S., Matsubara, E., Kawarabayashi, T., Shoji, M., Tomita, N., Arai, H.*, et al.* (2013). SORL1 is genetically associated with late-onset Alzheimer's disease in Japanese, Koreans and Caucasians. PLoS One *8*, e58618.
Nicolas, G., Charbonnier, C., Wallon, D., Quenez, O., Bellenguez, C., Grenier-Boley, B., Rousseau, S., Richard, A.C., Rovelet-Lecrux, A., Le Guennec, K.*, et al.* (2016). SORL1 rare variants: a major risk factor for familial early-onset Alzheimer's disease. Mol Psychiatry *21*, 831-836.
Offe, K., Dodson, S.E., Shoemaker, J.T., Fritz, J.J., Gearing, M., Levey, A.I., and Lah, J.J. (2006). The lipoprotein receptor LR11 regulates amyloid beta production and amyloid precursor protein traffic in endosomal compartments. J Neurosci *26*, 1596-1603.
Raghavan, N.S., Brickman, A.M., Andrews, H., Manly, J.J., Schupf, N., Lantigua, R., Wolock, C.J., Kamalakaran, S., Petrovski, S., Tosto, G.*, et al.* (2018). Whole-exome sequencing in 20,197 persons for rare variants in Alzheimer's disease. Ann Clin Transl Neurol *5*, 832-842.
Scheltens, P., De Strooper, B., Kivipelto, M., Holstege, H., Chételat, G., Teunissen, C.E., Cummings, J., and van der Flier, W.M. (2021). Alzheimer's disease. Lancet *397*, 1577-1590.
Small, S.A., and Petsko, G.A. (2020). Endosomal recycling reconciles the Alzheimer's disease paradox. Sci Transl Med *12*.
Temkin, P., Morishita, W., Goswami, D., Arendt, K., Chen, L., and Malenka, R. (2017). The Retromer Supports AMPA Receptor Trafficking During LTP. Neuron *94*, 74-82.e75.
Young, J.E., Boulanger-Weill, J., Williams, D.A., Woodruff, G., Buen, F., Revilla, A.C., Herrera, C., Israel, M.A., Yuan, S.H., Edland, S.D.*, et al.* (2015). Elucidating molecular phenotypes caused by the SORL1 Alzheimer's disease genetic risk factor using human induced pluripotent stem cells. Cell Stem Cell *16*, 373-385.
Young, J.E., Fong, L.K., Frankowski, H., Petsko, G.A., Small, S.A., and Goldstein, L.S.B. (2018). Stabilizing the Retromer Complex in a Human Stem Cell Model of Alzheimer's Disease Reduces TAU Phosphorylation Independently of Amyloid Precursor Protein. Stem Cell Reports *10*, 1046-1058.

VITA

Allison E Knupp was born in Bryn Mawr, PA in 1985 and raised in Medway, MA. She earned her Bachelor of Science in Applied Mathematics from the Fu Foundation School of Engineering and Applied Sciences at Columbia University in 2008. Allison obtained a Master of Science in Aeronautics from California Institute of Technology in 2009 and worked as an aerospace engineer for five years. In 2015, Allison joined the lab of Dr. Ian Nicholas "Nick" Crispe at the University of Washington as a research technician. She entered her doctoral program in the fall of 2016 and joined Dr. Jessica Young's lab. Allison completed her Doctor of Philosophy in Molecular Medicine and Mechanisms of Disease from the University of Washington in 2021.